Ph.D. Thesis

DEVELOPMENT OF A TECHNIQUE FOR ESTIMATING RAIN PARAMETERS FROM RAIN NOISE MEASUREMENTS

Submitted to the
Cochin University of Science And Technology

In partial fulfilment of the requirement for the award of the degree of

Doctor of Philosophy

By

T.K. MANI

Under the guidance of

Prof. (Dr.) P.R.S. Pillai

DEPARTMENT OF ELECTRONICS

COCHIN UNIVERSITY OF SCIENCE AND TECHNOLOGY

COCHIN, KERALA, INDIA 682022

FEBRUARY 2006

Development of a Technique for Estimating Rain Parameters from Rain Noise Measurements

Ph. D Thesis in the field of Acoustic Instrumentation

Author

T.K. Mani
Department Of Electronics
Cochin University Of Science And Technology
Cochin,
Kerala,
India 682022
Email: mani_thundiyil@cusat.ac.in

Research Advisor

Dr. P.R.S. Pillai
Professor
Department Of Electronics
Cochin University Of Science And Technology
Cochin,
Kerala,
India 682022
Email: prsp@cusat.ac.in

February 2006

Dedicated to.....

My parents, wife & children

DEPARTMENT OF ELECTRONICS
COCHIN UNIVERSITY OF SCIENCE AND TECHNOLOGY
COCHIN - 22

CERTIFICATE

This is to certify that this Thesis entitled ***Development of a Technique for Estimating Rain Parameters from Rain Noise Measurements*** *is a bonafide record of the research work carried out by Mr. T.K Mani, under my supervision in the Department of Electronics, Cochin University of Science And Technology. The results presented in this thesis or parts of it have not been presented for the award of any other degree.*

Dr. P.R.S. Pillai
(Supervising Guide)
Professor
Department of Electronics
Cochin University Of Science And Technology

Cochin- 22
28-2-2006

DECLRATION

I hereby declare that the Thesis entitled ***Development of a Technique for Estimating Rain Parameters from Rain Noise Measurements*** *is based on the original research work carried out by me under the supervision of the* ***Dr. P.R.S. Pillai*** *in the Department of Electronics, Cochin University of Science And Technology. The results presented in this thesis or parts of it have not been presented for the award of any other degree.*

T.K. Mani

Cochin – 22
28-2-2006

ACKNOWLEDGEMENT

I would like to express my heartfelt gratitude to my research guide Dr. P.R.S. Pillai, Professor, Department of Electronics, Cochin University for his guidance and support. He has been a great source of inspiration for me. I could not have been completed the thesis without his and constant advices and valuable suggestions.

I sincerely thank the Director, IHRD for giving me opportunity to carry out this research work at Cochin University of Science and technology.

Let me express my sincere gratitude to Prof. K. Vasudevan, Head of Department of Electronics, Cochin University of Science And Technology, and also Prof. K.G. Balakrishnan, Dr. C.S. Sridhar, former heads of Department, for extending the facilities in the department for my research work.

My sincere thanks to all the faculty members of the Department of Electronics, especially to Prof. K.T. Mathew, Dr. Mohanan, Dr. C.K. Anandan, Dr. Tessamma Thomas, Dr. Rajaveerappa, Mr. James Kurian and Mrs. M.H. Supriya for their valued support and help.

I am greatly indebted to Dr. K.S.M Panicker, Principal, FISAT for his motivation and encouragement in my research work.

My sincere thanks are due to Dr. C. Madhavan, retired scientist from NPOL for his guidance and suggestions.

All the research scholars in the department, especially Dr. Anilkumar, Mr. Sajith N Pai, Mr. Anil Lonappan, Dr. Bijukumar, Dr. G.S. Binoy, V.P. Dinesh Kumar, Mr. Rohith, Mrs. Mirdula, Mrs. Binu Paul and Dr. Jaimon Yohannan were very co-operative and helped me a lot. I express my gratitude to all of them.

Dr. Joe Jacob, Department of Physics, Newman College, Thodupuzha, has been a great source of motivation and encouragement throughout my research work. With immense sense of gratitude, I remember his valuable suggestions and selfless assistance.

I sincerely thank all the teaching and non-teaching faculty of Model Engineering College, Thrikkakkara, especially Prof. Jyothi John, Principal, Dr. V.P. Devassia and Dr. Mini. M.G, Prof. Jacob Thomas for their encouragement and support.

I am greatly indebted to my mentors Dr. K. G. Nair, former HOD of DOE, Dr. A Unnikrishnan, Senior Scientist, NPOL, Dr. Murthy, retired scientist from NPOL, Dr. Srinivas and Dr. G.V Anand. I thank all of them.

I also take this opportunity to thank all the M Tech and MSc students of DOE, CUSAT and to my students in Model Engineering College who contributed and helped me in completing my thesis.

I thank the library and administrative staff of the Department for their cooperation and support.

It is beyond words to express my gratitude to my family members especially to my wife for her dedication and sacrifice in connection with preparation of my thesis. I am sure; I could not have completed this great task without her support. I also thank my affectionate friend Mr. T.K. Sreekumar for his encouragement and timely help.

Mani. T.K

Contents

List of Figures

List of tables

Abbreviations

2D	--	Two Dimensional
ADC	--	Analogue to Digital Converter
ARG	--	Acoustic Rain Gauges
AWS	--	Automatic weather stations
B&K	--	Brüel & Kjaer
CCN	--	Cloud Condensation Nuclei
DSD	--	Drop Size Distribution
EMI	--	Electromagnetic interference
GD	--	Gamma Distribution
GEV	--	Generalised Extreme Value
GIS	--	Geographical information system
I	--	Rain Intensity
ISO	--	International Organisation for Standardisation
IUT	--	Indoor User Terminal
JD	--	Joss-Drizzle
JT	--	Joss-Thunderstorm
JWD	--	Joss-Waldvogel Distrometer
KE	--	Kinetic Energy
KLI	--	Kinetic Laboratories Incorporated
LP	--	Laws-Parsons
LPF	--	Low Pass Filter
MP	--	Marshall and Palmer
MPD	--	Marshall - Palmer Distribution
MPM	--	Microwave Propagation Model

NADP	--	National Atmospheric Deposition Program
OAP	--	Optical Arrya Probe
OEU	--	Outdoor Electronics Unit
OSP	--	Optical Spectro-Pluviometer
PDI	--	Phase Doppler Interferometric
PGA	--	Programmable Gain Amplifier
PMS	--	Particle Measuring System
PNG	--	Papua New Guinea
POSS	--	Precipitation Occurrence Sensor System
R	--	Rain Rate
SU	--	Sensor Unit
TBR	--	Tipping Bucket Rain gauge
TCEV	--	Two Component Extreme Value
TRMM	--	Tropical Rainfall Measuring Mission
USLE	--	Universal Soil Loss Equation
WMO	--	World Meteorological Organization
Z	--	RADAR reflectivity

Chapter 1

Introduction

Global climate greatly depends on the precipitation. Clouds are responsible for different types of precipitation. In this chapter a brief introduction to rain, climate, clouds and precipitation are given. Precipitation reaches the ground as liquid or as solid form and is classified into many types depending on the size of the precipitate, its physical form, etc. A brief description of the general rain classification and their features are also presented in this chapter. Since this thesis deals with the measurement of liquid precipitation, studies have been confined to rain parameters only. Various rain parameters like rainfall rate, the size and shape of raindrops, velocity and orientation of precipitation particles, etc. are of fundamental importance in the field of telecommunications and for the studies related to soil erosion. Distinct shape and size of raindrops and its distribution in rain, which are of much importance to these studies, are also elaborated in this chapter, alongwith the basic methods used to measure rain parameters. This chapter also deals with clouds and formation of rain, type of precipitations and the effects of rain.

The measurement of global precipitation is of great importance in climate modelling since the release of latent heat associated with tropical convection is one of the principal driving mechanisms of atmospheric circulation. The knowledge of the large-scale precipitation field has important potential applications in the generation of

initial conditions for numerical weather prediction models. Knowledge of the relationship between rainfall intensity and kinetic energy, and its variations with time and space is important for erosion prediction. The vegetation on earth greatly depends on the total amount of rainfall as well as the drop size distribution (DSD) in the rain.

All of the above applications require global, large-scale, area-averaged rainfall estimates that are available through remote sensing satellites. While methods using visible, infrared and microwave radiometer data have been shown to yield useful estimates of precipitation, validation of these products for the open ocean has been hampered by the limited amount of surface rainfall measurements available for accurate assessment, especially for the tropical oceans.

Surface rain fall measurements, often called the ground truth are carried out by rain gauges working on various principles like weighing type, tipping bucket, capacitive type and so on. The acoustic technique is yet another promising method of rain parameter measurement that has many advantages. The basic principle of acoustic method is that the droplets falling in water produce underwater sound with distinct features, using which the rainfall parameters can be computed. The acoustic technique can be used for developing a cost effective and accurate device for automatic measurement of rainfall rate and kinetic energy of rain, especially suitable for telemetry applications. This technique can also be utilized to develop a low cost Disdrometer that finds application in rainfall analysis as well as in calibration of nozzles and sprinklers.

1.1 Clouds and Precipitation

Clouds are a crucial component of the hydrological and radiative balances that sustain life on Earth. One of the challenging aspects of this cloud–climate problem is

the fundamental importance of the processes occurring on extremely small scales in determining the macroscopic properties of clouds, including their lifetime, extent, precipitation efficiency, and radiative properties. Thus, if one is able to understand the role of clouds in human affairs and the global environment, it is possible to increase our understanding of the processes occurring on seemingly unrelated scales, such as cloud droplet activation, ice nucleation, and the subsequent temporal and spatial evolution of cloud particle size distributions. A major goal of cloud physics is to understand the formation and evolution of cloud droplet size distribution. Droplet size distributions are fundamental to the studies of cloud radiative properties and precipitation efficiency, problems of broad interest.

There are various processes that control the physical phenomenon of micro-particles, cloud drops, raindrops and ice crystals. These include nucleation (formation of new cloud drops) on Cloud Condensation Nuclei (CCN) or ice nuclei, condensation/evaporation of water, gravitational settling (i.e. falling), and collision – coalescence. The mean size of the cloud droplet is in the range of 10-20 μm. These cloud droplets will not have sufficient volume to fall as raindrops. Condensation occurs when the water vapour wraps itself around the tiny particles. Each particle surrounded by water becomes a tiny droplet between 0.001 and 0.05 mm in diameter. However, these droplets are too light to fall. For these tiny droplets to fall, one droplet has to collide with another droplet, the bigger droplet will fuse into the smaller droplets making a larger drop. This new bigger droplet will collide with smaller droplets and become even bigger; this is called coalescence. As soon as the droplet reaches the size of 0.5 mm or bigger in diameter, it is considered as a raindrop. Drops larger than 5.8 to 6 mm will usually split into two separate drops [Doviak and Zrnic 1993; Sauvegnot 1992; Bringi and Chandrasekar 2001]. General information on rain formation can be found in open literatures, Pruppacher and Klett (1978).

The release of latent heat by condensation of water vapour is a major component of Earth's energy budget and is one of the major driving components of the global atmospheric circulation.

1.2 Rain and Climate

Rainfall characteristics affect the amount of runoff and greatly affect the severity of erosion possible in various parts of the country, and our dependency on irrigation for crop growth. Specific important characteristics of rainfall are:

Size and Shape: Rainfall occurs when the moisture in the atmosphere condenses into drops. Raindrops occur about in any shape upto approximately 6 mm mean diameter after which they tend to break up. However, they do tend, if turbulence does not interfere, toward an aerodynamically stable shape (tear-drop) because this affords the least surface resistance to motion.

Intensity and Duration: These are usually inversely related, i.e., high intensity rainstorms are likely to be of short duration and low intensity rainstorms can have a long duration.

Intensity and Area: One can expect a less intense rainfall over a large area than over a small area.

Intensity and Drop Size: High intensity rainstorms have a larger drop size than low intensity storms.

Drop size and Terminal Velocity: The terminal velocity of raindrops increases with the dropsize. The terminal velocity of the biggest drop can attain a speed of upto 9 m/sec. Rainstorms with large drop sizes have high erosion potential.

Rainfall Distribution and Supply: These are difficult to predict for a given season, but average values based on long-term records tell us much about the kind of water management necessary for an area.

1.2.1 Amount of rainfall and intensity

The most common historical rainfall data available are daily total quantity at selected locations. Such data have usually been obtained from a standard rain gauge that gives the depth of rainfall accumulated between observations. Data that are more useful are the one obtained from a recording type instrument that gives a record of accumulation as a function of time. Hence, intensities can be determined from recording gauges. The rainfall over a region is obtained from point data by an arithmetic or area-weighted average of the amount of rainfall. The general formula to calculate area-weighted averages is:

$$\bar{P} = \frac{A_1 P_1 + A_2 P_2 + \cdots\cdots + A_n P_n}{A_T} \qquad (1.1)$$

where the cross-product of each "n" sub-area and its corresponding amount of rainfall are summed and then divided by the total area. The two accepted methods for applying this formula are the Thiessen polygon method and the Isohyetal method. Each use different techniques to delineate the sub-areas for which individual precipitation measurements are presumed to be applicable.

Isohyetal Method: Rainfall readings from a set of gauges are plotted on a map of the region. Lines connecting all points of equal precipitation are then connected to create an isohyetal map which are analogous to contour lines on a topographic map. Obviously, this works best when there are numerous rain gauges. The area between each isohyetal line is then measured using a planimeter if done manually or computer software if done with software package like Geographical Information System (GIS). This is the more accurate of the two methods and is laborious, if done manually because the isohyetal lines must be redrawn and re-measured for every storm event.

Thiessen Method: This technique has the advantage of being quick to apply for multiple storms because it uses fixed sub-areas. It is based on the hypothesis that, for

every point in the area, the best estimate of rainfall is the measurement physically closest to that point. This concept is implemented by drawing perpendicular bisectors to straight lines connecting the two rain gauges. This yields, when the watershed boundary is included, a set of closed areas known as Thiessen polygons. Figure 1.1 gives an illustration of this with the four rain gauges A, B, C and D.

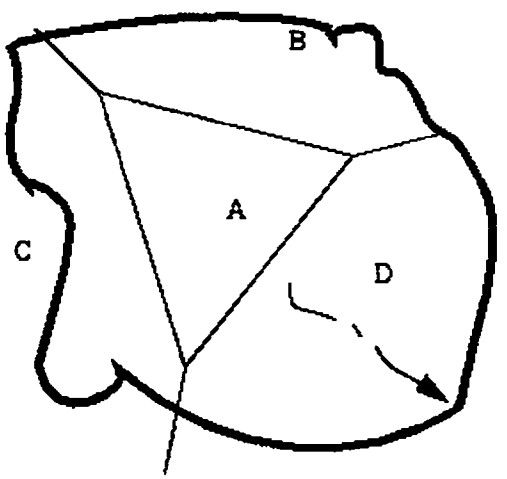

Fig. 1.1: Thiessen polygons with 4 rain gauges

1.2.2 Raindrop size

The minimum size of raindrops falling on the ground depends on the vertical wind speeds in clouds. In clouds with updrafts of less than 50 cm s^{-1}, drops of 0.2 mm, terminal velocity of which is 70 cm s^{-1} or more will fall out. In air of 90% humidity, such a drop can fall 150 m before total evaporation and thus never reach the ground. A drop of 1 mm can fall 40 km and thus reaches the ground.

The nature and shape of raindrops have been studied in detail by many researchers. Well-known results reported in open literature describe the models on the

shape of the raindrops. These models either suggest that raindrops are similar to oblate spheroids and that they are defined by their axial ratio or they define a function describing the surface of a body of revolution in polar coordinates. In the events of homogenous stratiform rain, the drop shapes and the drop distributions are predictable and this could be done according to the models available in the literature. In storm events, the raindrops assume various irregular shapes. In spite of all the irregularities in the shapes, the ratio of the drops maximum vertical to its maximum horizontal dimensions is always easily determined.

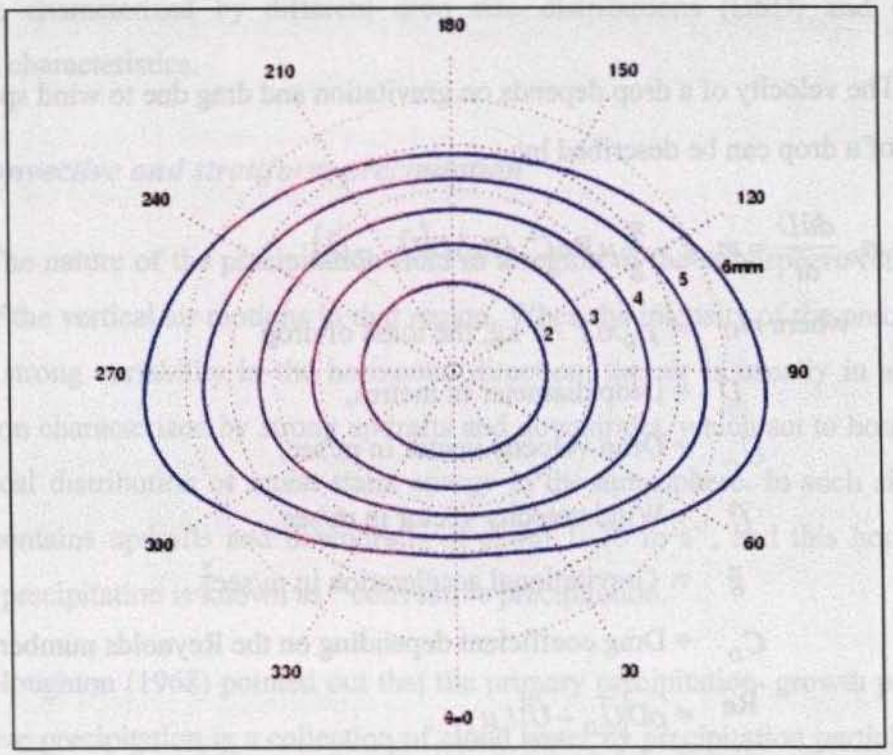

Fig. 1.2: Drop shapes and distribution

Only drops of diameters of less than 0.3 mm are nearly perfect spheres at terminal velocity. Therefore for larger drops one cannot unambiguously describe the shape by one dimension. This problem is solved by the definition of an equivalent

diameter, which describes the diameter of a sphere with the same volume as the deformed drop. Falling drops of equivalent diameters of 0.3 to 1 mm resemble oblate spheroids. Drops larger than 1 mm resemble oblate spheroids with flat bases (Fig. 1.2).

Wind tunnel experiments conducted by Pruppacher and Beard (1970) indicate that

$$a/b = 1.03 - 0.062\,D \tag{1.2}$$

where a/b is the ratio of the minor to the major axes and D (in mm) is the equivalent diameter of drops $\geq$ 1 mm.

The velocity of a drop depends on gravitation and drag due to wind speed. The motion of a drop can be described by:

$$m_D \frac{d\vec{u}D}{dt} = m_D\vec{g} - \frac{\pi}{8}\mu \,\mathrm{Re}\, C_D(\mathrm{Re}) D\left(\vec{U}_D - \vec{U}\right) \tag{1.3}$$

where m_D = $\rho_D \pi D^3 / 6$ kg, the mass of drop

D = Drop diameter in metres,

$\vec{U}_D$ = Drop velocity vector in m/sec,

$\vec{U}$ = Wind velocity vector in m/sec,

$\vec{g}$ = Gravitational acceleration in m/sec^2,

C_D = Drag coefficient depending on the Reynolds number Re

Re = $\rho D\left|\vec{U}_D - \vec{U}\right| / \mu$,

ρD = Density (kg m^{-1}) of water,

ρ = Density (kg m^{-1}) of air, and

μ = The dynamic viscosity (kg m^{-1} s^{-1}) of air.

1.3 Rain Classification

Rain is characterised by raindrop spectra. In meteorology raindrop spectra (also called "raindrop distributions") are often expressed in number of drops per unit volume of air per (equivalent) drop diameter. It is called ``raindrop number concentration spectrum", denoted by *n(D)* and its unit is m^{-3} mm^{-1}.

Different types of rainfalls have different heating profiles within the atmosphere and this calls for the classification of rainfall. Different classifications of rains are characterized by different drop size distributions (DSD) and different temporal characteristics.

1.3.1 Convective and stratiform precipitation

The nature of the precipitation field in a region of the atmosphere reflects the nature of the vertical air motions in that region. When the intensity of the precipitation exhibits strong variability in the horizontal direction, the air is usually in a state of convection characterized by strong updrafts and downdrafts, which act to homogenize the vertical distribution of moist static energy in the atmosphere. In such situations, the air contains updrafts and downdrafts of about 1–10 m s^{-1}, and this horizontally variable precipitation is known as ``convective precipitation.''

Houghton (1968) pointed out that the primary precipitation- growth process in convective precipitation is a collection of cloud water by precipitation particles in the strong updraft cores. Convective up and downdrafts are usually within a range of 1–6 km [Yuter and Houze 1995a]. Typically, several updraft–downdraft pairs occur in the vicinity and produce a horizontally variable precipitation pattern over an area approximately 10 to 100 km in horizontal dimension. Such a pattern of precipitation is called a ``convective region''.

When the intensity of the precipitation over an area approximately 10–100 km in horizontal dimension exhibits less variability and the radar reflectivity field appears to be in layers, the precipitation is typically referred to as "stratiform". The upward air motions sustaining stratiform precipitation are weaker (1–10 cm s^{-1}) but more widespread than the locally strong updrafts and downdrafts present in regions of convective precipitation. Thus, the fall speeds of the precipitating ice particles (1–2 m s^{-1}) [Locatelli and Hobbs, 1974] far exceed the magnitude of the vertical air motion. Houghton (1968) pointed out that under these conditions, the primary precipitation-growth process is vapour deposition on ice particles, which is a slow process, and particles must fall from the near cloud top to attain the maximum possible growth by vapour diffusion. Stratiform precipitation areas are thus distinct from convective areas by virtue of the particles always settling downward and growing slowly by deposition of vapour, in contrast to the convective updraft cores, in which large concentrations of droplets condense rapidly and are readily available for collection by larger precipitation particles.

When a convective updraft weakens, ice particles grown by collection of cloud droplets and carried upto the top of the cell during the active phase of the convective updraft slowly fall out through the weaker upward motion, while continuing to grow by vapour diffusion. The convective precipitation core thus turns into a region of stratiform precipitation. As the parcels of air in the convective updrafts rise out of the boundary layer and reach the upper atmosphere, they broaden and flatten because of the decreasing pressure and of reaching their level of neutral buoyancy [Lilly 1988; Yuter and Houze 1995c]. As progressively more weakened, spreading convective elements congregate in the upper troposphere, and they get amalgamated to form a larger horizontal area, which are identified as the stratiform regions on the RADAR.

1.3.2 Types of precipitation

As per the meteorological terms, precipitation is classified into three, viz., the liquid, the freezing and the frozen precipitation. These precipitation classifications are:

i) Rain: Liquid precipitation having drops of diameter greater than or equal to 0.5 mm. Raindrops that reach the earth's surface are seldom larger than 6 mm, as collisions between the raindrops tend to break them apart into many smaller drops.

ii) Drizzle: According to the Glossary of Meteorology [American Meteorological Society, 1959], a drizzle is a very small, numerous, and uniformly dispersed, water drops that may appear to float while following air currents. Unlike fog droplets, drizzle falls to the ground. It usually falls from the low stratus clouds and is frequently accompanied by low visibility and fog. In weather observations, the drizzle is classified as:

(a) "very light", comprised of scattered drops that do not completely wet an exposed surface, regardless of duration

(b) "light," the rate of fall being from a trace to 0.25 mm per hour

(c) "moderate," the rate of fall being 0.25-0.50 mm per hour

(d) "heavy" the rate of fall being more than 0.5 mm per hour.

When the precipitation equals or exceeds 1mm per hour, at the entire or part of the precipitation is usually rain; however, true drizzle falling as heavily as 1.25 mm per hour has also been observed. By convention, drizzle drops are 0.5mm or less in diameter.

iii) Virga: The precipitation that falls from a cloud but evaporates before reaching the ground is known as Virga.

Freezing rain and freezing drizzle are coming under the freezing class and the frozen precipitations are:

i) Snow: Much of the precipitation reaching the ground begins as snow. During summer, freezing level is usually high and snowflakes falling from a cloud melt before reaching the ground. During winter when freezing level is much lower, the snowflakes have a better chance of survival. Snowflakes can fall upto 300 metres before it melts completely. When snowflakes fall through very cold air with low moisture content, they do not readily stick together and hence powdery flakes of 'dry' snow accumulates on the ground.

ii) Fall streaks: This refers to the falling ice crystals that evaporate before reaching the ground.

iii) Flurries: These are light snow showers that fall intermittently for short duration; often from developing cumulus clouds.

iv) Snow Squall: This refers to more intense snow showers, comparable to summer rain showers and are usually formed from cumuliform clouds.

v) Blizzard: These refers to a weather with low temperature and more than wind speed 30 knots bearing large amounts of fine, dry, powdery snow. Blowing of snow is known as Blizzard.

vi) Sleet: Snowflake or very cold raindrop passing through warmer air undergoes partial melting. When it again goes through subfreezing surface layer of air, this partially melted snowflake or cold raindrop turns back into a tiny transparent ice pellet, called, sleet.

The table 1.1 summarises different types of precipitations:

Table 1.1: Types of precipitations

Type	Approximate size	State of water	Description
Mist	0.005 mm to 0.05 mm	Liquid	Droplets are large enough to be felt on the face when air velocity is 1 m/sec. Associated with Stratus clouds.
Drizzle	< 0.5mm	Liquid	Small uniform drops that fall from stratus clouds, generally for several hours.
Rain	0.5 to 5 mm	Liquid	Rain is generally produced by nimbostratus or cumulonimbus clouds. When rain is heavy, the drop size can be highly variable from one place to another.
Sleet	0.5 to 5 mm	Solid	Small, spherical to lumpy ice particles that form when raindrops freeze while falling through a layer of subfreezing air. Because the ice particles are small, any damage is generally minor. Sleet can make travel hazardous.
Glaze	Layers 1 mm to 2cm thick	Solid	Produced when super cooled rain drops freeze on contact with solid objects. Glaze can form a thick coating of ice having sufficient weight to seriously damage trees and power lines.
Rime	Variable accumulations	Solid	Deposits usually consisting of ice feathers that point into the wind. These fine frost like accumulations form when super cooled cloud or fog droplets encounter objects and freeze on contact.
Snow	1 mm to 2 cm	Solid	The crystalline nature of the snow allows assuming many shapes, including six sided crystals, plates and needles. Produced in super cooled clouds where water vapour is deposited as ice crystals that remain frozen during their descent.
Hail	5 mm to 10cm or larger	Solid	Precipitation in the form of hard rounded pellets or irregular lumps of ice. Produced in large convective, cumulonimbus clouds, where frozen ice particles and super cooled water co-exist.
Graupel	2 mm to 5 mm	Solid	Some times called "soft hail", Graupel forms when rime collects on snow crystals to produce irregular masses of "soft" ice. Because these particles are softer than hailstones, they normally flatter out upon impact.

1.4 Effect of Rain

Rain causes several physical changes on the earth. Rain generates rivers, lakes and is responsible for calamities like flood, landslides, etc. Soil erosion is one of the most important effects that change the geography of places on earth. Insufficient rain can cause damages to life on the earth.

1.4.1 Soil erosion

When drops impinge on the ground surface, the kinetic energy of the drops is transferred to the soil particles and thus it dislodges itself from the present position. Water erosion dislodges soil particles from the soil aggregates within the surface soil layer due to the impact of rainfall drops (Fig. 1.3) or due to the dynamic forces of overland flow. Erosion can also occur along stream and riverbanks.

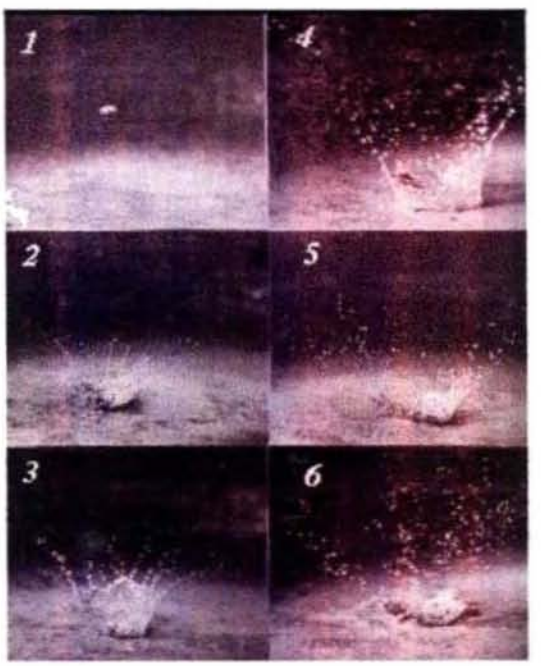

Fig. 1.3: Photographic sequences illustrating the impact of raindrop splash. Note the presence of soil particles (frame 6), which have been kinetically detached from the soil surface by the splash.

Soil erosion has three main forms:

Sheet erosion: The uniform removal of soil particles from the surface without causing channelisation.

Rill erosion: The removal of soil through the cutting of a large number of small rivulets and tiny channels. These channels are not permanent and change location with each storm event. However, under certain conditions, some rills may develop into larger channels causing the third form of water erosion, which is the gully erosion.

Gully erosion: The removal of soil through cutting relatively large channels or gullies by the force of concentrated flow.

Erosion due to water run off and sediment transport are complex processes involving interactions among climate, soil properties, topography, surface cover, and human activities [Renard, 1992]. Of these, climate represents the active force of erosion, while soil, topography, and surface cover represent passive factors. Human activities cause changes in the passive factors, thereby altering a catchment's response to climate. The break-up of surface soil aggregates, together with the dislodgment and dispersion of soil particles, may seal the surface soil and result in decreased infiltration rates and increased runoff, which augments overland flow. Soil properties such as granulation, texture, structure, water holding capacity, and permeability are factors that determine the amount of runoff, as well as the soil erodibility and the ability of overland flow to transport detached sediments. Rain kinetic energy beyond a threshold intensity is highly correlated with the sediment transportation [A. I. J. M. Van Dijk et. Al 2003].

1.4.2 The Universal Soil Loss Equation (USLE)

One of the most widely used soil erosion models is Wischmeier and Smith's

(1978) Universal Soil loss Equation (USLE). In its original version, the model takes the form:

$$A = R \times K \times L \times S \times C \times P \tag{1.4}$$

where A = the sediment yield for the period in question,

R = the rainfall-runoff erosivity index,

K = the soil-erodibility factor,

L = the length-of-slope factor,

S = the degree-of-slope factor,

C = the crop-management factor and

P = the conservation-practice factor.

R characterizes the level of attacking (active) forces, while the remaining terms characterize the level of resisting (passive) forces. These factors have been determined from experimental studies that compared erosion rates from different erosion-monitoring plots. Central to the USLE is the concept of a *unit plot*. A universal unit plot is utilized to determine the soil-erodibility factor K. Additional plots are used to determine other parameters. Except for the factor being assessed, such plots must represent the field for which parameters are being determined, and must be identical to its counterpart in the universal plot. For example, determining the *slope-steepness factor* for a field that has 5% slope requires two experimental plots. The first plot should have the actual field slope of 5%, while the second plot should be identical in length, tillage, soil, and land cover to the first plot, with a 9% slope (the USLE standard). Similarly, in order to estimate the slope-length factor L for a slope of 5% and a length of 100 m, two identical plots must be used. Both plots must have the 5% slope. The first plot (the field plot) must be 100 m long, while the unit plot must be 22.13 meters long as per the USLE standard. Determining the factors K, C, and P is experimentally intensive. It requires constant monitoring and in some cases rainfall simulation experiments. The standard approach of obtaining experimental values of the USLE factors involves fixing five of the six factors by means of standardised plots

and monitoring rainfall, runoff and erosion. Once the data are available, the USLE equation can be solved for the unknown factor. However, plot studies cannot measure sediment delivery from large watersheds, where A is determined primarily by the capacity of waterway to transport sediment.

1.4.3 The rainfall-runoff erosivity index

Rainfall ersovity index R is a statistical measure calculated from a summation of rainfall energy in every storm over a fixed period (correlated with raindrop size) multiplied by its maximum 30-minute intensity. Empirically, R was found to have the highest correlation with soil erosion from experimental plots. For each intensity period, a rainfall energy e_m per unit intensity is computed [Foster, 1981] from:

$$e_m = 0.119 + 0.0873 \log(I) \quad \text{for } I \leq 76 \text{ mm/h}$$

$$e_m = 0.283 \qquad \text{for } I > 76 \text{ mm/h} \tag{1.5}$$

where e_m = the kinetic energy of the m th intensity period for a unit rainfall,
I = the rainfall intensity period energy (mm/h).

The amount of soil loss during a single rainfall event correlates more strongly with the maximum intensity of the storm than with total rainfall. By providing rainfall intensity data, a better understanding of the rainfall-erosion relationship for each of the sampling locations can be ascertained. Therefore, in order to achieve this, it is preferable to have an intensity record at many number of observatory sites.

1.5 Summary

A brief introduction of different types of precipitations and the importance of precipitations are presented in this chapter. Effects of rain like soil erosion are also discussed.

Chapter 2

Rain Parameters and Measurement Methods

The importance of measurement and quantification of rainfall was discussed in the previous chapter. This chapter discusses the various rainfall parameters, and the techniques and devices used to measure these parameters. One of the main rain parameters is the drop size distribution (DSD). By knowing the DSD, other parameters like kinetic energy of rainfall can be estimated. Hence a detailed discussion of the DSD measurement and features of DSD are attempted here. Construction of various popular rain gauges and their performance comparisons are also presented in this chapter.

2.1 Introduction

Rainfall was the earliest recorded meteorological measurement dating back to the fourth century BC in India. In 1442, Korea had a network of bronze vases (rain gauges), 14 cm in diameter whose measurements were reported to the royal court. The Japanese used one type of rain gauge to determine the annual rice tax that each region should pay. These early measurements were made for agricultural purposes. By 1639,

there was also an interest in the effect of rainfall on the outflow of lakes in Italy. The first rain gauge in Europe was developed by Richard Townley in Burnley, Lancashire, in 1677 [Mark New et. Al,(2001)]. The first manually read rain gauges were constructed in that century, almost two centuries before the modern gauges were appeared. They were designed to reduce splash out and evaporation between measurements.

Gauges were made of copper and brass, though earlier versions had sheet metal bases. The type B rain gauge, which came into service in the early 1970s, is constructed of ABS plastics. This Canadian standard rain gauge is the smallest gauge used throughout the world. It has an orifice of diameter 11.3 cm (100 cm^2 area). European countries use 12.7 cm gauges and the USA uses 20.3 cm gauges. It has a resolution of 0.1 mm and its accuracy is better than 1% when compared with a pit gauge, the international standard. Precipitation measurements are made twice a day at climatological stations and four times a day at synoptic reporting stations such as airports.

2.2 Drop Size Distribution

Drop Size Distribution (DSD) gives one of the most complete descriptions of rain. DSD is a function that expresses the number of drops per unit size interval (usually diameter) and per unit volume of space. The DSD defines most of the parameters intervening in a broad spectrum of applications, such as the attenuation of microwave by rain, the retrieval of rainfall properties utilizing RADAR remote sensing techniques, and the understanding of the microphysical mechanisms responsible for precipitation formation.

2.2.1 Methods of measurement

Raindrop-size measurements extend as far back as Lowe (1892), [Blanchard, 1953], who described observations of splash patterns on slates. However, the first detailed report on splash pattern was published by Wiesner (1895) [Neuberger et al, 1942]. This method consists of exposing sheets of filter paper, dusted with a water-soluble dye, to the rain for a brief interval about a few seconds. After striking the paper, the drops cause spots that are rendered permanent by the dye. The diameter of the spot is then assumed to depend only on the diameter of the drop. In actual practice, the diameter of the spot is also a function of the effective thickness of the paper and drop fall-velocity. The humidity in the paper also affects the relationship between the diameters. An empirical relationship between the drop diameter and the spot diameter is then used to obtain the raindrop size. This method was widely used in calibration of sprinkler nozzles [Hall, 1970] and is very attractive because the tedious job of measuring and counting the drop stains can now be accomplished by the use of electronic scanners and image analysers using digital image processing techniques [Attle et al, 1980]. Besides the complexity, this method has a notable drawback that large drops splatter when striking the paper and the precise determination of their size is practically difficult.

Another early method for measuring raindrop sizes was the flour method, originally presented by Bentley (1904) and modified by Laws and Parsons (1943). The procedure consists of allowing the raindrop to fall into a layer 2-3 cm deep of fine, un compacted flour; the smooth flour surface is held in a shallow container about 10 cm in diameter, which is generally exposed to the rain for a few seconds. The raindrops remain in the flour until the formed dough-pellet produced by the drop is dry and hard. These dough-pellets are then separated by a set of standard sieves into

groups of several sizes. However, the limits of drop-size cannot be found from the dimensions of the sieve-openings because of the flattening of the drop when becoming a pellet. Due to this effect, the mass of the average pellet is used to characterize the size separation; this average is found by dividing the mass of each group by its corresponding number of pellets. To convert the mass of the average pellet into the mass of the average drop, several pellets are previously generated from drops of known sizes in order to obtain the ratio of the mass of the drop to the mass of the pellet. Unfortunately, this ratio does vary with the diameter of the drop, and it cannot be determined for smaller sizes, because the production of smaller drops is practically difficult. The immersion method [Fuchs and Petrjanoff, 1937; May, 1945; McCool, 1982] and the oil method [Eigel and Moore, 1983] are the other two types of methods that are used in determining DSD of sprinklers. A more interesting survey of European investigations of raindrop size and corresponding instrumentation, prior to 1942, is reported by Neuberger (1942).

The sampling of drops in an illuminated volume, at a given time, was introduced later [Jones, 1959]. This method is known as the raindrop-camera method, and it consists of two short-exposure cameras synchronized for simultaneously photographing a volume in space from two different, perpendicular angles (east-west and north-south axis), allowing a three-dimensional view of the shape of the raindrops. Subsequently, the raindrop images from the two cameras are measured after magnification in two projectors placed side by side. The correction of the measured image sizes to the true drop sizes depends on the angular differences between the film planes and the axes of the drops. It demands considerable computations that are not worthwhile when compared with the small amount of precision gained [Jones, 1959]. As a result, the raindrop-camera method is restricted mainly to investigations of the physical shape of the individual raindrops in natural rains.

More automatic recording devices were developed later, introducing sophistication in the data analysis of DSDs. The most widely used instrument of this kind is the *Distrometer* developed by Joss and Waldvogel (1967), which consist of an electromechanical sensor that transforms the momentum of the raindrops, falling on an area of 50 cm^2, into electrical pulses. With a very few modifications [Sheppard, 1990a], the Joss-Waldvogel Distrometer (JWD) is now the standard instrument for measuring the DSD.

Optical devices were developed more recently [Knollenberg, 1970; Donnadieu, 1980; Illingworth and Stevens, 1987; Illingworth *et al.*, 1990]. For example, the Particle Measuring System (PMS) spectrometer [Knollenberg, 1976; Joe and List, 1987], which sizes the particles passing through a laser beam by the shadow created on a linear array of photodiodes. This method introduced the possibility of measuring precipitation particles far from the ground, for example by installing the PMS on an aircraft. In addition, the capability of measuring simultaneously the diameter and the velocity of the drops were also explored by using optical devices. One of them is the 'Optical Spectro-Pluviometer' (OSP), whose measurements are based on the optical occultation of a parallel beam of infrared light by raindrops during their fall [Hauser *et al.*, 1984].

Finally, the necessity of sampling DSDs over a larger volume was solved by using RADAR measurements of the Doppler velocity spectrum, generated by scatterers in a volume above the sensor [Rogers, 1967]. With this measurement, the type of precipitation and its intensity are identified from the spectral mode (the velocity corresponding to the mode of the spectrum), and the spectral power (the signal amplitude at the mode of the spectrum), respectively. Vertical and horizontal winds, however, also produce a Doppler signal, which must be carefully analysed

when retrieving the DSD. The Precipitation Occurrence Sensor System (POSS) falls under this category of methods; it is an X-band, bistatic RADAR that has been successfully used for the observation of precipitation occurrence, type, and intensity in an automated observing network [Sheppard, 1990b].

2.2.2 Drop data analysis

The first analytical description of the DSD was proposed by Marshall and Palmer (1948), and is now the most widely accepted one. They derived the inverse exponential dependence between the DSDs and the drop diameters:

$$N(D) = N_0 e^{\Lambda D} \tag{2.1}$$

where $N(D)$ is the number of drops having diameters (in mm) between D and $D+dD$ in unit volume of space, and $N_0 = 8 \times 10^3$ m^{-3} mm^{-1} is the value of N for $D = 0$ mm (the intercept parameter that intercepts at $D = 0$). The distribution depends entirely on the parameter Λ (the slope of the distribution) which is determined by the rainfall rate R and is given by the equation, $\Lambda = 4.1R^{-0.21}$ mm^{-1}, with R the rainfall rate in mm/h.

Unfortunately, the MP model is not sufficiently general to describe all the DSD cases; it applies situations where sufficient averaging in time is performed [Joss and Gori, 1978]. In particular, N_0 and Λ have been found to vary considerably within each rainfall event [Waldvogel, 1974)] and from one rainfall to another [Joss and Waldvogel, 1969]. Gamma distribution have also been used to obtain an analytical expression for the DSD [Ulbrich, 1983], *i. e.*,

$$N(D) = N_0 D^{\mu} e^{\Lambda D} \tag{2.2}$$

where μ (the distribution shape parameter) = α *-1*. α is a coefficient

experimentally determined that can have a range of values from 0.8 to 1.28. A physical meaningful parameter known as the median volume diameter D_{50} can be defined such that all drops with diameter $\leq D_{50}$ contribute to one-half the total liquid water content. Ulbrich (1983) has shown that $\Lambda D_{50} \approx 3.67+\mu$. D_{50} is be related to Rain rates by the relationship $D_{50} = \alpha R^{\beta}$ *where* β*is* another coefficient with a range of values 0.123 to 0.293.

Figure 2.1 shown below illustrates different drop distribution characteristics reported in earlier works.

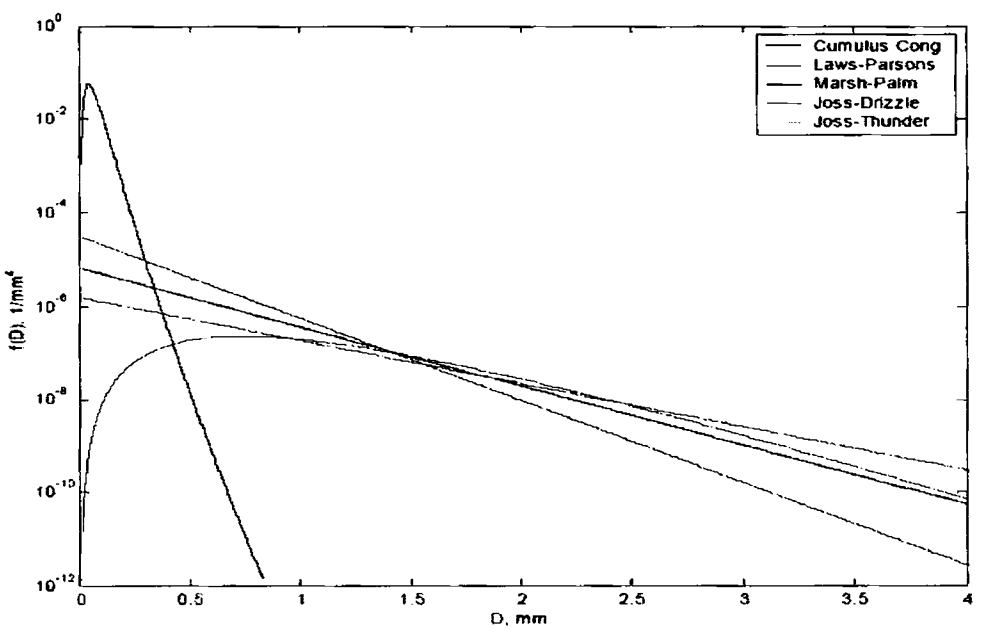

Fig. 2.1: Normalised drop-size distributions versus D for R=5mm/h, P=P_0: LP (Red), MP (Blue), JD (Green) and JT (cyan). The figure also depicts the distribution of a cumulus congestus (black)

It is often assumed that the exponential distribution is most applicable to stratiform precipitation and with longer period while the gamma distribution is more representative of shorter time periods and for convective rainfalls. Importantly, the

exponential distribution has two governing parameters (N_0 and Λ); and the gamma distribution has three parameters (N_0, Λ, and μ). Successful application requires two and three radar measurements, respectively. An example of measured DSD fitted to the Gamma distribution is shown in Fig. 2.2 [Guifu Zhang, J. et. al, 2001].

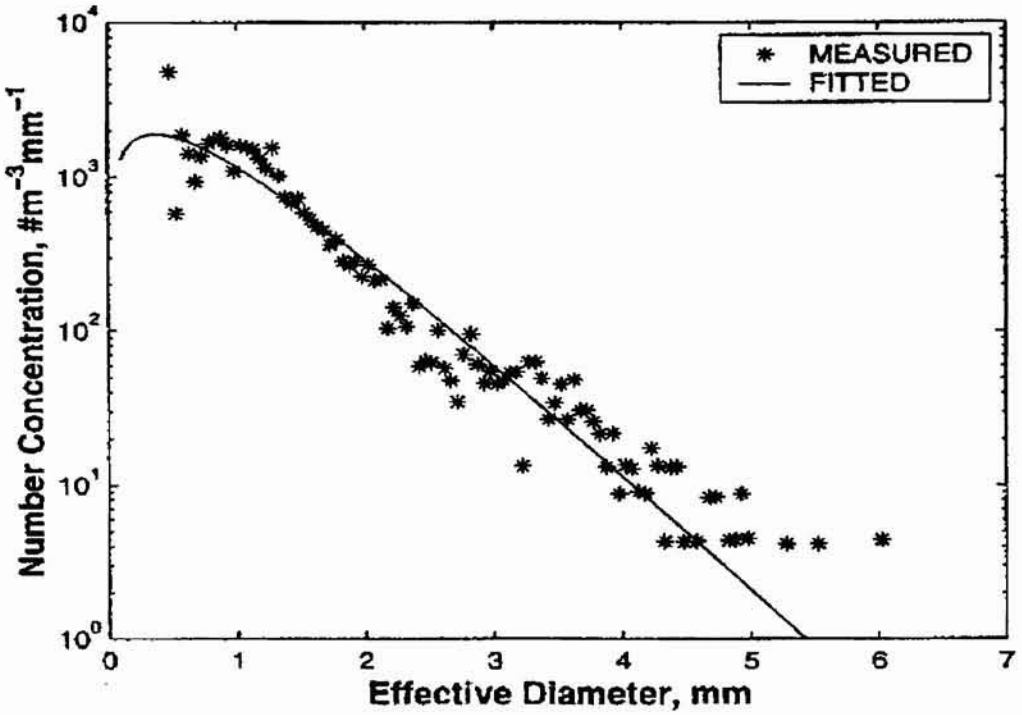

Fig. 2.2: Example of rain DSD and it's fitted Gamma distributions.
(Guifu Zhang, J. et. Al., 2001)

The widely observed distribution functions are the LP [Wolf (2001), Marshall and Palmer (1948)] (MP), Joss-Drizzle (JD) and Joss-Thunderstorm (JT) [Joss et al. (1978)]. For standard pressure P_0, the parameters of the normalized functions are shown in Table 2.1, where $Norm(R, P_0)$ is fitted by second-order polynomials in $X=ln(R)$, the natural logarithm of R, the rainfall rate.

Table 2.1: Parameters of Equations (5) and (8) for normalised distributions at standard pressure P_0: LP according to de Wolf (2001), Marshall and Palmer (MP), Joss-Drizzle (JD) and Joss-Thunderstorm (JT) from Joss et al. (1968).

Distribution Function	***N0(R)*; 1/mm^4**	***Norm(R,P0)*; *X*=ln(*R*), *R* in mm**	**Λ(*R*); 1/mm**	**μ**
LP	$1.98 \times 10^{-5} R^{-0.384}.Norm$	$1.047-0.0436X+0.00734X^2$	$5.38R^{-0.186}$	2.93
MP	$0.80 \times 10^{-5}.Norm$	$0.842-0.00915X+0.0072X^2$	$4.1R^{-0.21}$	0
JD	$3.00 \times 10^{-5}.Norm$	$1.1194-0.0367X+0.0079X^2$	$5.7R^{-0.21}$	0
JT	$0.14 \times 10^{-5}.Norm$	$1.0945+0.0052X+0.0124X^2$	$3.0R^{-0.21}$	0

As other alternatives, the 'lognormal distribution' [Feingold and Levin, 1986] and 'Weibull distribution' [Jiang et *al.*, 1997] have been suggested. Nevertheless, comparisons between DSD actually observed and any analytical distribution shows that only a partial fit can be achieved at best [Sauvageot and Lacaux, 1995; Cerro *et al.*, 1997].

In general, all the empirical distribution that fits to the observed DSDs can be expressed as a distribution function of D and an integral variable Ψ [Sempere-Torres *et al.*, 1994], *i.e*

$$N(D,\Psi) = \Psi^{\alpha} g\left(\frac{D}{\Psi^{\beta}}\right) \tag{2.3}$$

with α and β being constants for a given Ψ, and g being a general distribution function. For example, if Ψ is the rainfall rate R, then $N(D,R) = R^{\alpha} g(D / R^{\beta})$, with $\alpha + 4.67\ \beta = 1$. However, the integral variable Ψ can be any of the following bulk variables:

Total concentration of drops (in m^{-3}), $N_T = \int_0^\infty N(D)dD$ (2.4)

Specific attenuation (in m^{-1}), $k = \int_0^\infty \sigma_{ext}(D)N(D)dD$ (2.5)

where σ_{ext} is the extinction cross section of a raindrop. The precipitation liquid water content (in g m^{-3}) is expressed by

$$L = \frac{\pi}{6}\rho_L \int_0^\infty D^3 N(D)dD \tag{2.6}$$

where ρ_L is the density of water.

Rainfall rate R is

$$R = \frac{\pi}{6}\rho_L \int_0^\infty D^3 v(D)_{(T)} N(D)dD \quad \text{mm h}^{-1} \tag{2.7}$$

where $v(D)_T$ is the terminal velocity for drops of size D

2.2.3 Observations

Raindrops have a size-dependent shape that cannot be characterized by a single dimension. When a raindrop falls freely in stagnant air, it tends to flatten at the bottom and spread laterally while remaining round at the top surface. It is conventional to describe raindrop size in terms of the equivalent spherical diameter (D_{eq}) defined as the diameter of a sphere of the same volume as the deformed drop. In general, drops falling at terminal velocity are nearly perfect spheres if $D_{eq} \leq 0.28$ mm. For equivalent diameters between 0.28 and 1.0 mm, the drop shapes are slightly

deformed and resemble oblate spheres. Drops with D_{eq} near 1.0 mm or larger resemble oblate spheroids with flat bases. Throughout this work, 'D' (diameter) is used to denote the equivalent spherical diameter. Drops larger than about 10 mm in diameter are hydro dynamically unstable and break up; however, the largest drops recorded have diameters as large as 8 mm [Pruppacher and Klett, 1997].

Early observations of DSDs for light to moderate stratiform rain, characteristic of mid-latitude continental precipitation, were done by Laws and Parsons (1943) as well as by Marshall *et al.* (1947); the former used the flour method, while the latter adopted the filter-paper method [Marshall and Palmer (1948)] (hereafter MP) and the observations are summarized below, indicating that, for the medium to larger drop sizes, an approximate inverse-exponential shape in the DSD, with slope depending on the rain rate.

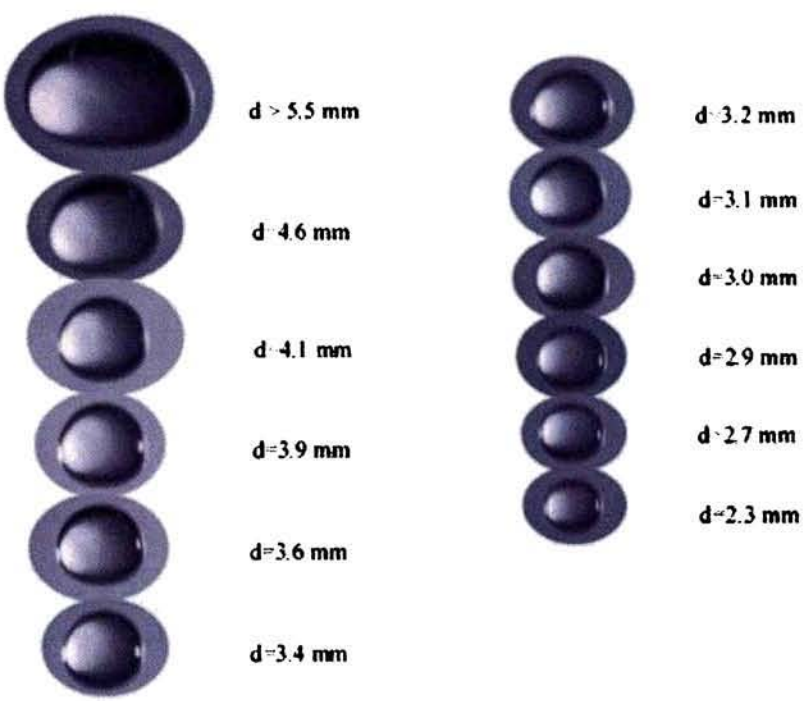

Fig. 2.3: Drop photographs showing the shapes with respected to mean diameter

The observations of MP Distribution have been confirmed with many experiments using modern sensors. Nevertheless, DSDs with shapes very different from inverse exponential have been found from a large number of raindrop measurements made in Hawaii, using the filter paper method [Blanchard, 1953; Blanchard and Spencer, 1957; Fujiwara, 1967]. These observations are characteristics of warm rain processes, and can be categorized as orographic in which rains are formed from clouds on the windward side of a mountain, or non-orographic maritime rain. Orographic precipitation shows bi-modal or widely skewed DSDs. The drop concentration at the far end of the spectrum increases with rain intensity, although the opposite is observed at diameters smaller than 0.5 mm. In general, these DSDs are narrow, with plenty of small drops whereas the largest diameters rarely exceed 2 mm [Fujiwara, 1967]. The non-orographic distributions, on the other hand, do not show the inverse relationship of intensity versus raindrop concentration at the lower end of the spectrum, and the curves exhibit a more uniform distribution of drops beyond 0.7 mm [Blanchard, 1953].

Measurements over tropical Brazil [Zawadzki and Antonio, 1988], using the JWD sensor, characterized tropical continental rain under equilibrium conditions, when the coalescence and break-up process balance each other, such as the cases with cloud base and freezing level sufficiently high. For DSDs in weak rain rates of less than 6 mm h^{-1}, the shape follows approximately the inverse exponential expression given by Marshall and Palmer (1948). More intense rain rates, usually accompanied by updrafts, indicate that DSDs for different rain intensities appear to be multiples of a generic distribution, this latter distribution being characterized by a deficit of large and small drops and excess of medium sized drops.

2.2.4 Theoretical aspects

The shape of the DSD is determined by the microphysical processes that are responsible for the rain formation. The first mechanism responsible for the development of rain is the presence of large aerosol particles acting as nuclei for the droplets near cloud base (nucleation). Then, large droplets will grow further by condensation and coalescence by the capture of smaller droplets by a drop of 0.02 mm diameter or larger. Nevertheless, the growth is limited by the drop break-up resulting either from the collision between two raindrops reformed as collisional break-up, which produces only a temporary coalescence, or from the hydrodynamic instability of larger single drops which is a spontaneous break-up.

More growth is also possible when a drop re-circulates from the edge of the downdrafts into updrafts with large numbers of cloud droplets. When the updraft weakens, the larger drops fall through a region which is almost free of droplets, thus minimizing the collisional break-up. The strength of the updraft itself determines the shape of the DSD, truncating the DSD spectrum at some minimum size. However, this effect is largely masked by the smaller drops produced during break-up and evaporation. The smaller drops are then collected by larger drops or disappear by evaporation.

The collisional break-up of drops was first described by Brazier-Smith *et al.* (1972) and, with more detail, by Low and List (1982). Young (1975) found more realistic conditions for the collisional break-up parameterisation than for the spontaneous break-up proposed by Komabayasi *et al.* (1964).

Another interesting case occurs at the beginning of a shower. Here, the DSD at ground level is expected to be biased towards extreme sizes, the larger-size bias is due

to the faster fall speeds of larger drops and the smaller-size bias owing to an initially high evaporation rate.

The drop growth by coalescence was first described as a continuous process [Bowen, 1950; in Rogers and Yau, 1991], according to which all large drops of the same size grow at the same continuous rate. A more realistic approach is to consider this growth as a stochastic process [Telford, 1955], which considers the fact that a small fraction of the larger drops will experience, by chance, greater than average frequency of collection events. The core of the stochastic approach is the quasi-stochastic growth equation [Gillespie, 1975; Hu and Srivastava, 1995; among others]:

$$\frac{\partial n(m,t)}{\partial t} = \frac{1}{2}\int_0^m n(m',t)n(m-m',t)K(m',m-m')dm' - n(m,t)\int_0^\infty n(m',t)K(m',m)dm' \qquad (2.8)$$

where $n(m,t)$ is the number of drops at time t with mass between m and $m+dm$, $K(m,m')$ describes the probability that a drop of mass m will collect a droplet of mass m'. The first term on the right-hand side of Eq. (2.8) represents the increase of drop concentration by coalescence, and the second term on the right-hand side corresponds to the decrease of droplet concentration due to collisions. In recent literature on the subject, Eq. (2.8) is also referred as the stochastic coalescence equation or kinetic equation or coagulation equation or stochastic collection equation.

Zawadzki *et al.* (1994) extended the model of Valdez and Young (1985) to allow raindrops sedimentation. They showed that for low rain rate conditions, the distribution was in good agreement with Hawaiian orographic rain observations, suggesting that break-up of drops is not important at these rain rates. Zawadzki *et al.* found that the Marshall-Palmer distribution does not hold for warm rain DSDs at low rain rates, but it is applicable under melting snow conditions.

2.2.5 Summary of DSD

All the methods used for measuring the DSD are far from perfect. The absorbent-paper and flour methods, for example, are not reliable for smaller drops due to the practical difficulty in generating very small drops of known diameters. Moreover, the relationships between the drop size and the dough or spot size cannot be determined precisely as larger drops sprinkle when striking the sampling surface. DSD measurement using Electro-acoustic sensors and optical devices still have very small sample volumes whereas Doppler estimations of DSD are affected by updrafts, downdrafts, and horizontal winds.

These operational problems are normally ignored, when dealing with theoretical studies of DSDs. In fact, the most common procedure is that observations are specifically designed to test a specific theoretical conclusion, rather than a theoretical approach being used to explain the observations. This approach can guide towards unrealistic methods of analysis and/or artificial theoretical results. This problem is detected, for example, in the misunderstanding generated by coincidental agreement between artificial modes observed in DSDs [Sheppard, 1990a; Mc. Farquhar and List, 1993] and the modes obtained by particular parameterisations of collisional break-up [List *et al.*, 1987]. This is also witnessed in the search for statistical distributions that nicely fit the observed DSD, but that are physically meaningless [Jiang *et al.*, 1997].

2.3 Rain Gauges for Measurement of Rain Intensity

The in-situ rainfall observations are made by rain gauges. The quantification of the rainfall rate is carried out by measuring the rainfall over a fixed duration. Rain gauges are widely classified into manual gauges and automatic rain gauges. Automatic rain gauge systems are required to collect rainfall data at remote locations that is not

2.2.5 Summary of DSD

All the methods used for measuring the DSD are far from perfect. The absorbent-paper and flour methods, for example, are not reliable for smaller drops due to the practical difficulty in generating very small drops of known diameters. Moreover, the relationships between the drop size and the dough or spot size cannot be determined precisely as larger drops sprinkle when striking the sampling surface. DSD measurement using Electro-acoustic sensors and optical devices still have very small sample volumes whereas Doppler estimations of DSD are affected by updrafts, downdrafts, and horizontal winds.

These operational problems are normally ignored, when dealing with theoretical studies of DSDs. In fact, the most common procedure is that observations are specifically designed to test a specific theoretical conclusion, rather than a theoretical approach being used to explain the observations. This approach can guide towards unrealistic methods of analysis and/or artificial theoretical results. This problem is detected, for example, in the misunderstanding generated by coincidental agreement between artificial modes observed in DSDs [Sheppard, 1990a; Mc. Farquhar and List, 1993] and the modes obtained by particular parameterisations of collisional break-up [List *et al.*, 1987]. This is also witnessed in the search for statistical distributions that nicely fit the observed DSD, but that are physically meaningless [Jiang *et al.*, 1997].

2.3 Rain Gauges for Measurement of Rain Intensity

The in-situ rainfall observations are made by rain gauges. The quantification of the rainfall rate is carried out by measuring the rainfall over a fixed duration. Rain gauges are widely classified into manual gauges and automatic rain gauges. Automatic rain gauge systems are required to collect rainfall data at remote locations that is not

easily accessible and prevents regular visits. The rain gauges fall in two categories, namely disdrometers and collection type gauges. Collection type gauges inherently measure rainfall rates. Collection type gauges are classified into weighing, capacitance, and tipping bucket depends upon the principle of operation. Disdrometers are gauges that detect individual raindrops. Most of the disdrometers are working on the principle of optical scintillation and underwater acoustical inversion. All of these measurement techniques perform well. However, each method has it's own limitations.

2.3.1 Tipping bucket rain gauge

A tipping bucket rain gauge (TBR) is a collection type rain gauge. Tipping bucket rain gauges measure rainfall by catching the rainwater using a collection funnel and allowing rainwater to drain into a bucket. The bucket tips and then drains after a known amount of rainwater has been collected. Each tip triggers a magnetic reed switch that sends a signal to a recording device. Figure 2.4 shows the sketch of a tipping bucket rain gauge. These instruments are widely used in automatic measurement systems used in land. This type of rain gauge is unsuitable for deployment at sea.

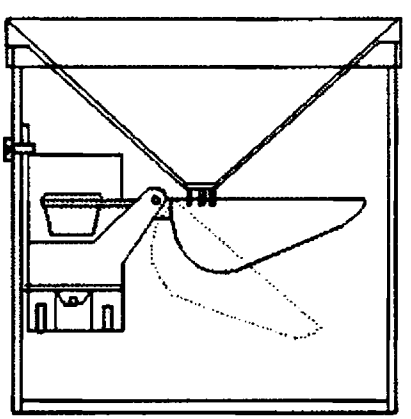

Fig. 2.4: Tipping bucket rain gauge (single bucket type)

TBR slightly underestimate the rainfall because of the fact that some amount of water is lost during every "tips". Wind also affects the readings as it reduces the catchments collection. However, it is possible to apply standard wind corrections [Legates et al 1993]. Weather measure Model 6010 is a popular TBR. This gauge is widely used to measure precipitation, especially in cold weather. This is an electrically heated tipping-bucket precipitation gauge. This gauge has a thermostatically controlled electric heater in the collection funnel that melts frozen precipitation, resulting in an actual water-content measurement. Rain measurements do not require the heater system. The measurement device is a teeter-totter mechanism that tips with each one-hundredth of an inch of precipitation collected. A bucket tipping causes a momentary switch closure that is counted by the data logger, resulting in a totalling of precipitation for the data-output period of 15 minutes.

The gauges are installed with windscreens, which prevents (stills) the airflow over the top of the gauge. A bare rain gauge (i.e., without a wind screen) is expected to underestimate precipitation as high as 25%. The tipping-bucket gauge selection was made after comparisons with weighing buckets in several locations. TBR is especially suitable for measurement for semiarid climate.

The Typical Tipping bucket specifications are as follows:

Range: unlimited

Sensitivity: 1 tip/0.01 inch

Accuracy: 0.5% at 0.5 inch/hour

Resolution: 0.01 inch

Errors in TBR: Blockages in the water guiding tube into the bucket introduces errors in measurement. Partial blockages lead to misleading estimates of rain rates and to inaccurate descriptions of the lengths of wet and dry periods. Complete blockages lead to underestimation of total rainfall. Another problem common to all gauges using collecting funnels is that of 'wetting'. This refers to water, remaining on the funnel surface without passing into the collecting chamber, which subsequently evaporates. Losses due to wetting are typically around 0.05 mm per rainfall event [Niemczynowicz, 1986]. Losses due to evaporation may be of the order of 0.004 mm/h [Fankhauser, 1998]. Delay in measurement is another drawback of these types of gauges. This problem is noticeable when rainfall rate is too low which takes more time to tip the bucket. During this period of time, portion of the collected rainwater may evaporate, which will cause underestimation of rainfall.

TBRs are of in two types: the single bucket type and the twin bucket type. The basic TBR consists of a pair of adjacent buckets. Figure 2.5 shows the schematic of a twin bucket rain gauge. When a bucket is filled with water, its centre of gravity is moved such that it overbalances. This results in the second bucket moving into position while the first bucket is emptied. The tipping process may take as much as half a second [Marsalek, 1981] during which rain continues to fall. The result is an under-estimation of the rain rate [Marsalek, 1981; Adami and Da Deppo, 1985, Niemczynowicz, 1986] that can be addressed by the so-called dynamic calibration.

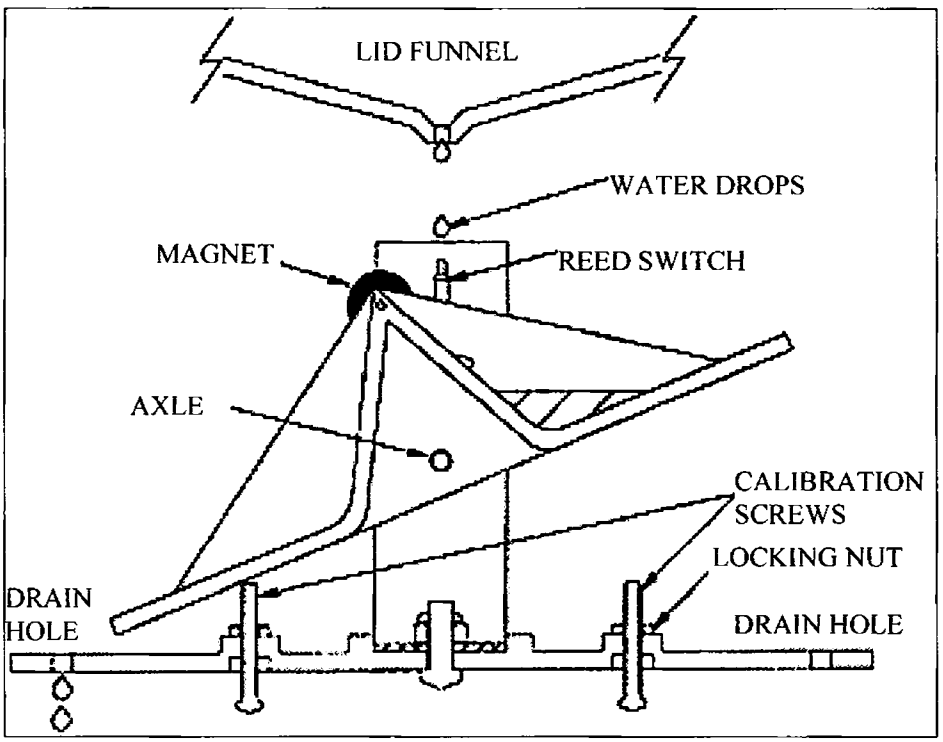

Fig. 2.5: Schematic of twin bucket tipping bucket rain gauge

Although the under-recording of light rainfall is usually nominal, the under-estimating of extreme rain rates can be considerable [La Barbera *et al*, 2002]. There can be non-linear relation between apparent and real rain rates that depends both on the age of the equipment [Adami and Da Deppo, 1985] and the gauge type [Niemczynowicz, 1986], so that each individual gauge requires its own calibration.

Wind introduces about 5 to 10 % error in the measurement of rainfall [Doviak et al, 1993]. However, it is possible to apply standard wind corrections. [Legates et al. 1993].

Besides the drawbacks applicable to all the collection type rain gauges, the TBR has another disadvantage: the water sprinkles out when the bucket is about to trip that causes errors and the delay in measuring solid precipitation. Figure 2.6 shows the error curves for a typical TBR.

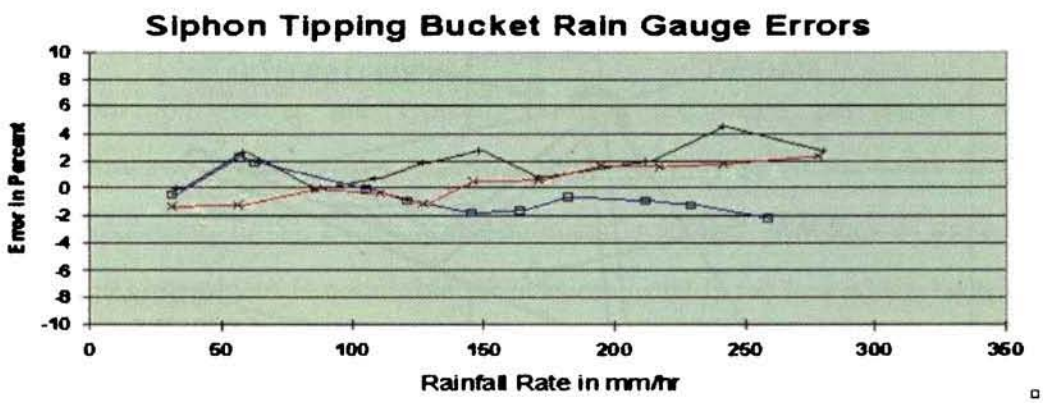

Fig. 2.6: Siphon Tipping bucket rain gauge errors

2.3.2 Weighing type rain gauges

Weighing type rain gauges weighs the precipitation using strain gauges. When loaded, the strain gauge changes its electric resistance, and this change is read by the electronic circuitry that evaluates the changes. This can measure both liquid and solid precipitation, captured in a vessel, which is continuously weighed. The increments in weight will then indicate the amount of precipitation. In the vessel, a thin oil film covers the surface of the liquid, which prevents evaporation of captured precipitation. The vessel also contains an anti-freeze solution. When the threshold weight is exceeded, the liquid is automatically pumped out of the weighing vessel and passed into a second recovery vessel, while the anti-freeze solution flows from the other side of the recovery vessel into the weighing vessel. Water evaporates from the recovery vessel naturally. This processes is supported by the design of the gauge.

The inlet opening through which precipitation is collected normally, is set at a level of one meter above the ground. The other opening is sunk in a hole in the ground, and the inlet opening was flushed with the ground surface. Around it, at the surface level, a grill with sharp edges is installed, allowing access to the gauge while preventing the bouncing of raindrops falling on the surrounding soil back into the gauge. This in turn reduces the error due to bouncing drops entering into the collection funnel.

An electronic weighing cell measures the weight of precipitation gathered in the collecting container. Beneath the defining ring of the measuring surface, the precipitation gets directly into the collecting container. Thus liquid or solid precipitation can immediately be measured, because there is no time delay as with tipping buckets.

For high accuracy of measurement, the device can have the facility of automatic self-calibration by means of a calibration weight. The processor-controlled evaluation unit supplies a temperature-compensated and linearised output signal, which is available either directly as a pulse output or in the integrated data logger. The measuring system consists of a maintenance free electronic load-cell, amplifier and an analogue to digital converter (ADC). The sensing element (load cell or strain gauge) must be hermetically sealed against dust, atmospheric pressure, etc. Processor control with software filter algorithm is applied for accurate measurement by compensating against the error due to temperature variation and wind effects.

Automatic siphoning is to be employed for measuring high rainfall rates by draining off water.

The accuracy of the measurements depends on two things, the sensor strain gauge and the ADC. Thermal compensation is normally needed to compensate for the errors in strain gauge output due to extreme temperature.

The accuracy of rainfall measurement depends on the precision of the water accumulation measurement that depends on the rate at which rainwater drains from the catchments basin into the measurement chamber and the sampling interval. The weighing type rain gauge often overestimates the rainfall rate. [Jeffrey A Nysteun 1999]. The DSD does not affect the reading and also did not provide any information regarding the DSD or related parameters. Because of the need for a stable platform, the weighing type gauge is not suitable for measurement over ocean by installing it on a buoy or ship deployment. Since reading directly depends on the gravity to make the rainfall measurement, platform acceleration if mounted on a buoy or ship causes error in reading

2.3.3 Capacitor type rain gauges

Capacitive type rain gauges are widely used in ocean moored weather stations. The instruments have a 100 cm^2 (11.3 cm diameter) catchment cylinder mounted on top of a fill tube. Rainwater is captured by the upper cylinder and funneled into a cylindrical measuring tube below via the fill tube. A schematic of the rain gauge is provided in Fig. 2.7. The measuring tube has a maximum capacity of 500 ml, equivalent to 50 mm of rain between siphon events. The volume of water in the tube is determined by capacitance. A stainless steel capacitive probe covered with Mylar is located at the center of the measuring tube. The capacitance is measured between the steel probe and the water, with the Mylar acting as the dielectric between these two *plates* of the capacitor.

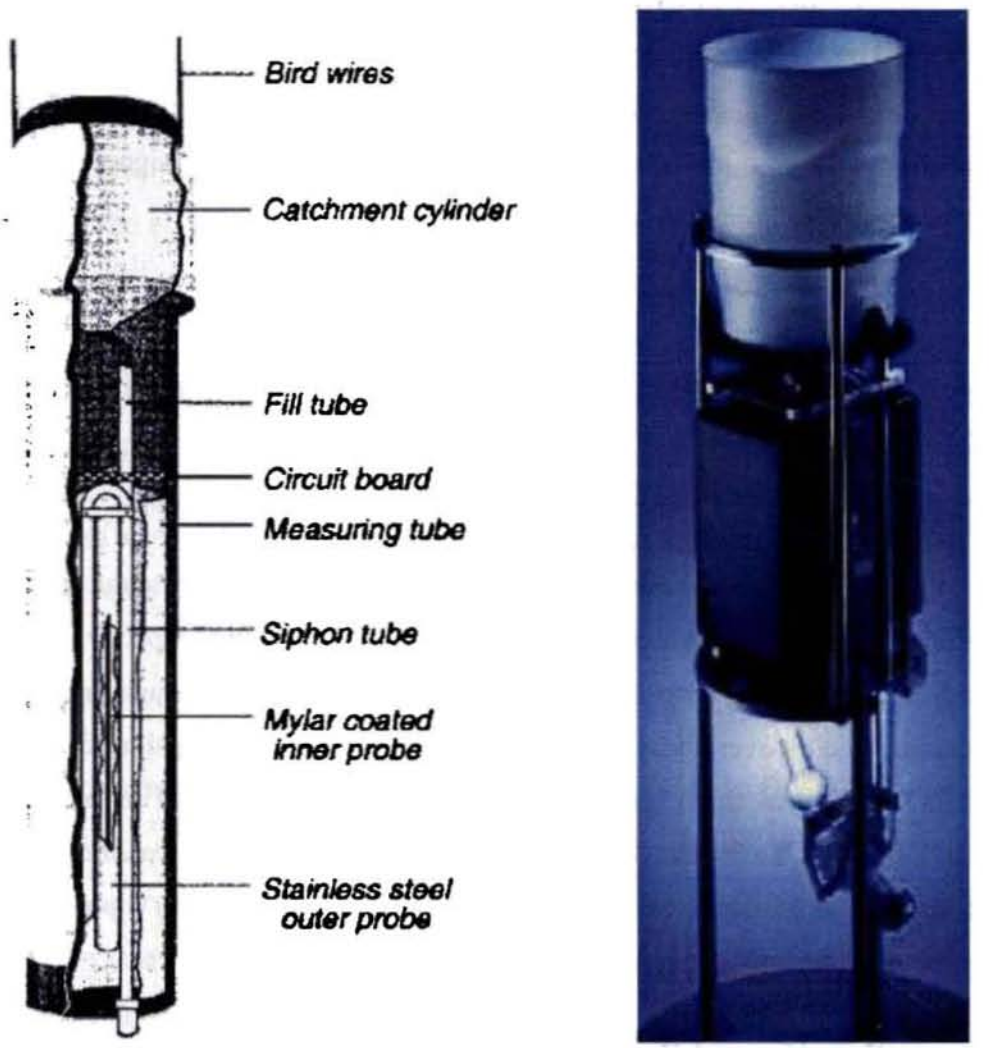

Fig. 2.7: Schematic of R. M. Young self-siphoning rain gauge model 50202/50203

An outer stainless steel probe surrounding the inner Mylar coated probe closes the circuit. The water surrounding this probe forms the outer plates of a co-axial type capacitor and the probe acts as the inner plate of the capacitor. As the water height in the collection chamber rises, the capacitance increases. The capacitance is measured and converted into water height in the collection chamber. The rainfall rate is

calculated as the averaged difference in rainwater accumulation over a given time interval. The capacitance variation can be measured by using a capacitance to frequency converter (C/F) circuit. The output frequency from the C/F circuit is counted over one minute interval and is output as a digital signal (counts). The conversion from counts to volume is given by the equation,

$$V = \frac{a}{N} + b \tag{2.9}$$

where V is the volume in ml the measuring tube, N is the number of counts, and a (in ml-counts) and b (in ml) are calibration coefficients to be determined through a least squares regression of V on N^{-1}.

Conversion from volume to accumulations require removing the siphon events. A siphon event occurs when the gauge reaches its maximum capacity of 500 ml, at which time water is expelled from the measuring tube through a siphon tube. Siphoning occurs over about a 30-seconds period and is identified as sharp decreases in volume. In real time, one or two data points are identified as a siphon event (equivalent to 1 to 2 minutes of data) and are ignored when calculating the daily statistics. In post deployment processing, data associated with siphon events are flagged, typically removing 3 min worth of data centered on the event.

2.3.3.1 Sources of errors of capacitor type gauges

One serious problem with this type of instrument is that the sensing probe subjected to electrical noise will affect the accuracy of measurement. This noise effect is more pronounced during light rain due the rate of dripping from the catchment basin to the collection chamber [Nystuen et al 1996]. As rain rates are inferred from changes in the water volume of the gauge, noise in the volume measurements can result in small positive or negative rain rates. The noise is partially removed by filtering the volume data with a 16-point Hanning filter to produce smoothed 10-minute accumulations [Serra et al. 2001].

Wind also causes the instrument to malfunction due to the wind-generated vibration of the chamber and the movement of water in the chamber. One way to reduce the noise effect is to increases the averaging time between measurements. The accuracy of measurement is affected by the errors introduced in measurement. It was observed that the error is proportional to the volume of the measuring tube [Yolande et al. 1990]. Temperature variations also introduce errors in measurement. Under catch due to wind is expected to be the largest source of error for rain gauge measurements. Correction methodologies for wind-induced catchment errors are available in the literature [Koschmieder 1934].

$$p(w) = -0.0141w^3 + 0.4409w^2 + 0.9927w + 0.1010 \qquad (2.10)$$

where p represents the percent under-catchment at the given wind speed w.

2.3.4 Drop counting rain gauges

In drop counting rain gauges, the precipitation is collected by a funnel and formed into drops at the nozzle of the funnel stem below. The drop size is so designed as to exactly determine the rainfall rate per drop and is specified by the manufacturer (say a drop = 0.005 mm rainfall). The total rainfall over a period is determined by counting the number of drops passing through an optical counter (a light chopper) underneath the nozzle within that time. The sketch of a typical rain gauge is as shown in Fig 2.8. There is an upper limit of rainfall rate that can be measured with this type of rain gauge. The measurement of rainfall by the drop-counting rain gauges assume a constant drop size. Some times, these types of rain gauges are also equipped with a 0.1 mm tipping bucket directly under the nozzle and thus provide two sets of rainfall data to enable internal consistency checking of the measurements.

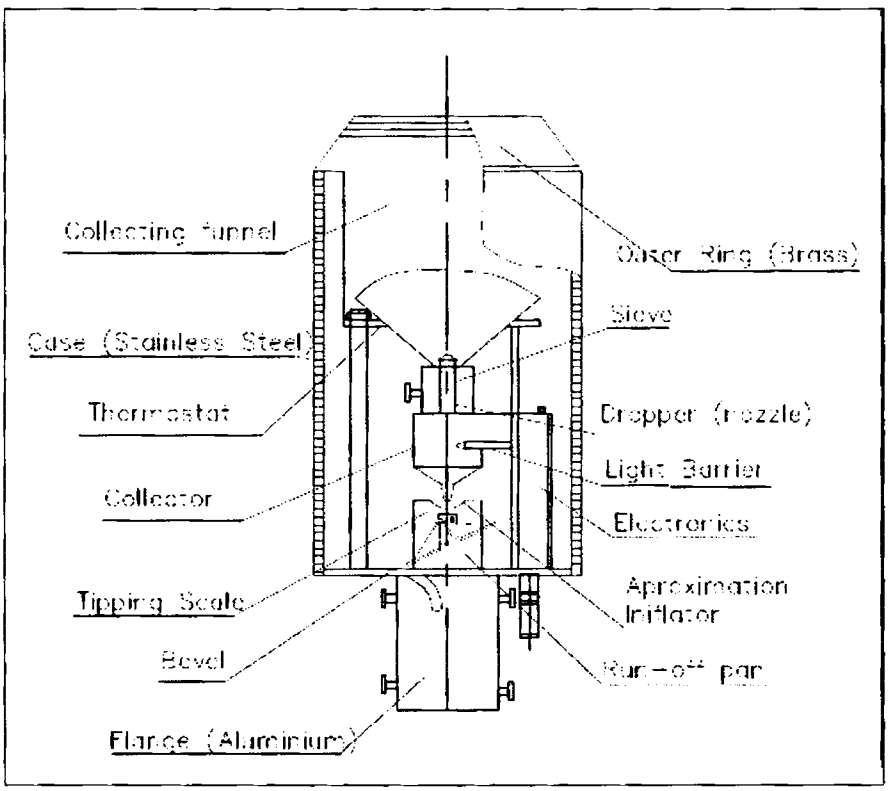

Fig. 2.8: Drop counting rain gauge

The relationship between the drop volume size v and the rainfall rate R is:-

$$v(mm^3/drop) = \frac{R(mmh^{-1}) \times A(mm^2)}{f(drops/h)} \tag{2.11}$$

where f is the frequency (number of water drops per hour) measured by a drop counter during the calibration, and A the area of the gauge orifice. v is usually taken to be a constant by virtue of the rain-gauge design. From physical consideration, however, it is related to the rain gauge's drop-formation mechanism, and the formation of drops is a result of interaction between the static pressure of the rain water accumulated inside the funnel and the surface tension of the water drop formed at the nozzle. It follows

that if the static pressure is not constant, the drop size may vary instead of remaining constant. From Eq. (2.11), as the errors in f and A are relatively small, the error in the drop size is directly proportional to the error in rainfall rate.

Experimental evidence shows that there is variation in drop size in accordance with the rainfall rate [P.W. Chan et al., 2004]. If the rainfall rate is increased, there is a tendency for the water to stay longer in the collecting funnel. It takes time for the water to drain away, and the situation worsens with higher rainfall rates as more water is accumulated. This results in the build-up of a larger static water pressure inside the funnel, which favors the formation of larger water drops. This observation is consistent with the general trend of drop size increasing with the rainfall rate.

According to the regulation of the World Meteorological Organization [WMO, 1996], the achievable operational accuracy of rainfall measurement shall be ± 5%. For a drop-counting rain gauge, it is a common practice to assume a nominal constant drop size for operational rainfall measurement. However, as the measurement results show, the actual drop size does vary with the rainfall rate. The difference between the actual drop size and the constant drop size assumed is equal to the error in rainfall measurement. This means that the actual drop size shall not differ from the constant drop size assumed by more than 5%, the WMO accuracy requirement for rainfall measurement. One possible approach is to identify a constant drop size that differs from the actual drop size by no more than 5% within the largest possible range of rainfall rates.

Nevertheless, in subtropical places like Kerala, it is common for the rainfall rate to exceed the maximum range of the rain gauge. The use of a constant drop size therefore limits to some extent the application of the drop-counting rain gauge. An alternative approach is to use a variable drop size that changes with the rainfall rate in accordance with the laboratory calibration results.

2.3.5 Disdrometer

The disdrometer is a reliable instrument, its measurements are highly reproducible, and no time drift has been observed so far. It measures the drop size, drop shape, drop distribution and velocity of the raindrops. Two types of optical disdrometers (single slot disdrometer and 2-D disdrometer) are in use.

2.3.5.1 Single slot Disdrometer

The Single slot Disdrometer comprises a set of converging lenses and an infrared diode placed at the focus, transmitting a parallel light beam. At the output, a rectangular mask or slot, limits the beam, which is then focused by a similar optical system and is received by a photodiode that delivers an electric signal varying in proportion to the received energy (Fig. 2.9). When a drop passes through the beam the received power decreases. After removal of the DC offset, inversion, amplification and square root extraction, the signal becomes a positive pulse with an amplitude and a duration that depends on the effective diameter of the drop's cross-section and on its fall velocity.

The measurement principle relies on the assumption that the likelihood of having several raindrops simultaneously in the beam at a given time is very small and only affects little, if at all, the measurement accuracy. The instrument comprises two parts, a sensor, shown in Fig. 2.9a and a processor carrying out data collection. Every T_i seconds (this parameter can be set by means of the acquisition PC's software), a two-dimensional array or histogram is available with 16 x 16 classes, the elements $N_{i,j}$ of which give the number of raindrops counted by the device, having a diameter in the range $D_i \pm \Delta D_i/2$ and a fall velocity in the range $v_j \pm \Delta v/2$.

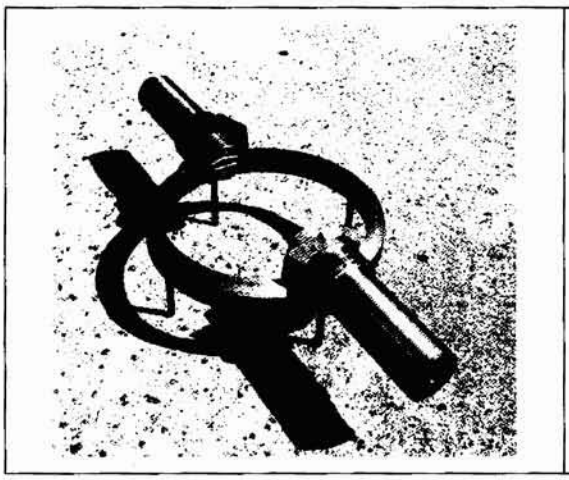

Fig. 2.9a: Single slot disdrometer sensor

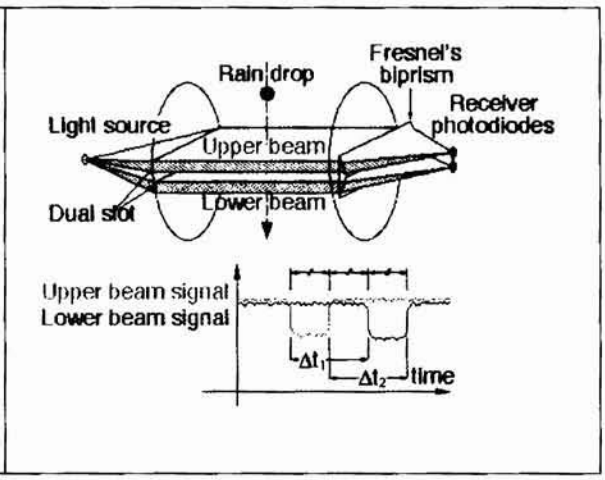

Fig. 2.9b: Principle of operation of dual beam sensor

The various analogue and digital processing applied to the photodiode output signals introduce a fixed instrumental error on the raindrop diameters. The disdrometer should therefore be carefully calibrated.

A study carried out on a one-month period (Olympus Experiment) showed a very good correlation between the results it provided and those of a tipping bucket rain gauge, but with an under estimation of rain rate (as determined from the 16x16 arrays mentioned above) of up to 10 % to 30 %.

Dual beam Disdrometer (Fig 2.9b) is a modification of the single slot Disdrometer. Figure 2.10 shows a typical disdrometer output graph indicating the drop sizes with respect to time. The number of drops in every class of drop sizes is indicated by intensity variations in the graph.

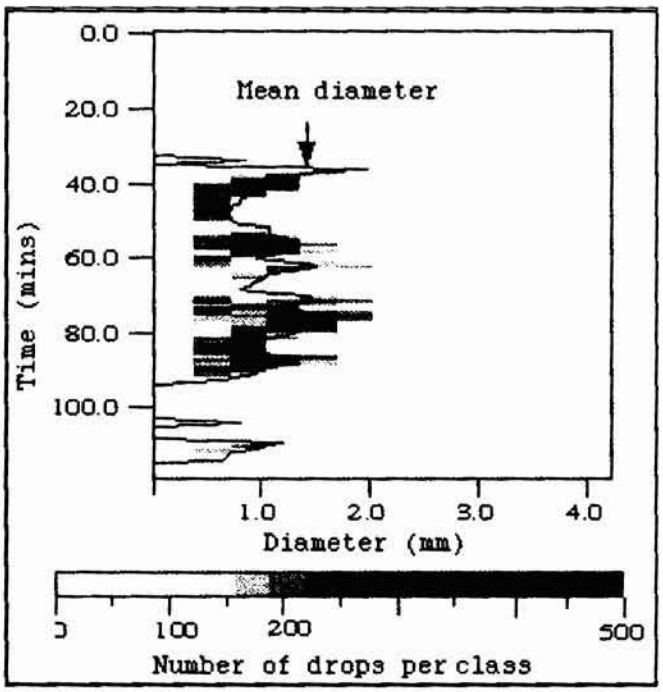

Fig. 2.10: Typical disdrometer output graph

2.3.5.2 2D Video Disdrometer

The 2-D video disdrometer is an optical device that measures the drop size, drop shape, and drop fall speed. Of each raindrop, snowflake or hailstones reaching the measuring area, the front view, the side view and the velocity are measured and recorded. The resolution of the digitizing grid is in the order of 0.25 mm. For a reliable classification of precipitation events, distributions of size and velocity of particles as well as of oblateness of drops are generated in real time. The instrument operates fully automatically.

Joss-Waldvogel Disdrometer is the best example of a classical Disdrometer. The 2D Disdromter consists of three major system components: (a) the Sensor Unit (SU) housing two video systems for measuring the front and the side view of the hydrometeors, (b) the Outdoor Electronics Unit (OEU) that controls the video cameras, acquires the raw data and performs pre-processing and data compression and

(c) the Indoor User Terminal (IUT) that stores the data and provides a graphic display. A cooling unit is needed to keep the electronics inside at a controlled temperature in hot humid environments. The sensor unit has two light sources that generate orthogonal light sheets. The light sources are projected through narrow slits onto two line-scan digital cameras. The disdrometer has a nominal measuring area of 100 cm^2. More information regarding the description and operation of the 2-D video disdrometer can be found in a manuscript by Schonhuber et al. (1994). Figure 2.11 presents a schematic drawing while Fig.2.12 illustrates the measurement principle.

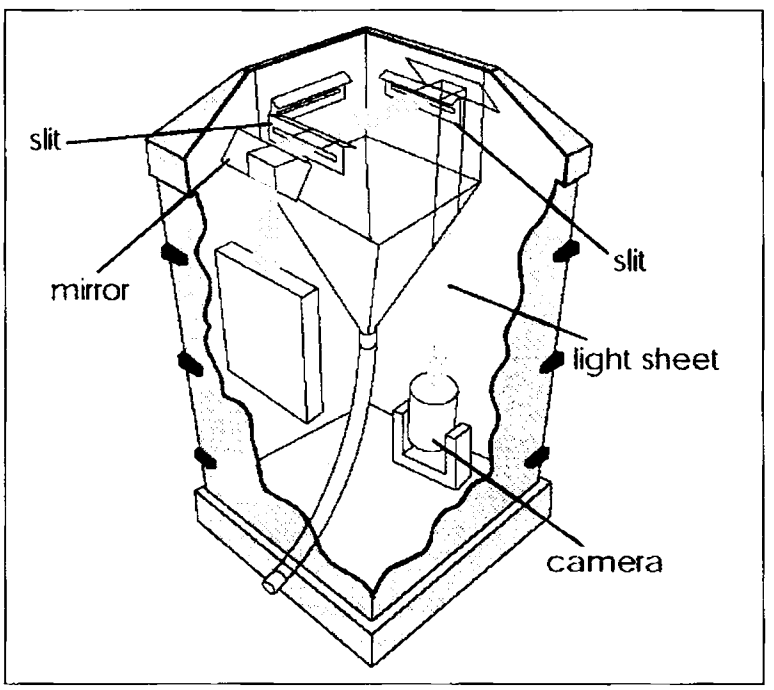

Fig. 2.11: Schematic arrangement of Video Disdrometer

Two line scan cameras are directed towards the openings of the illumination devices. The optical system is designed in such a way that (seen through the camera lens) the slit of the illumination device appears as an evenly illuminated background

of extreme brightness. To the camera, any particle falling through the beam of light will appear as a dark silhouette against this bright background. Note that in the actual instrument each of the two optical paths contains two mirrors that are used to bend the beam (not shown in the drawing for simplicity). The virtual measuring area is located few centimetres beneath the rims of the collecting funnel, thus avoiding the unwanted effect of splashing from these rims into the virtual measuring area. The mechanical structure consists of two parts. The inner part carrying all optical components is mounted on four rubber shock absorbers only. This guarantees that the adjustment of the optical parts is not impaired by any mechanical influences like heavy wind, opening of the housing and others. The outer part carries the inner one and shields it against water. Calibration and maintenance procedures are easy to perform and quickly done.

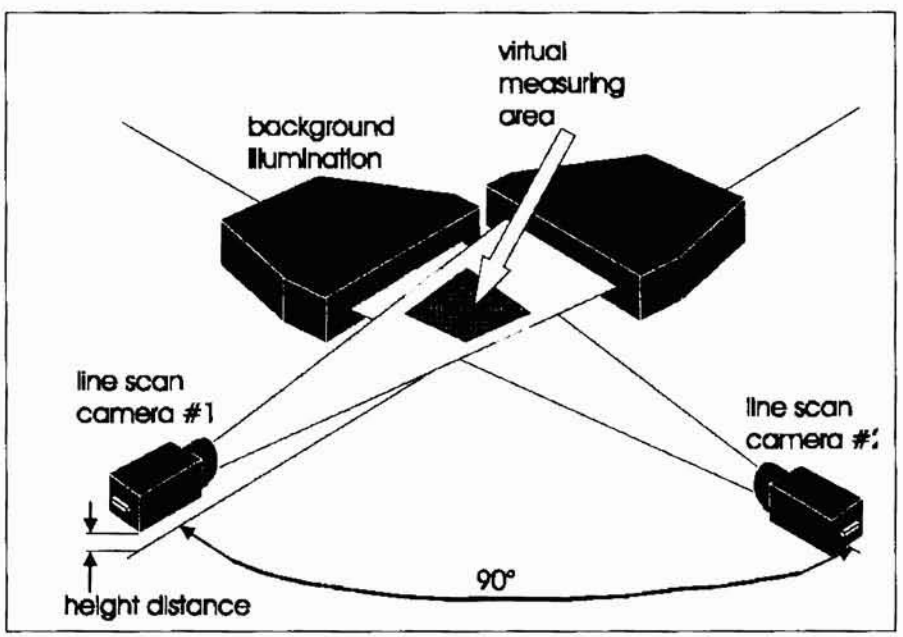

Fig. 2.12: Principle of measurement of 2D Video Disdrometer

To check the calibration, a number of precision spheres of various diameters have to be dropped into the receiver. Fall velocities of the calibration spheres differed from those of raindrops with the same size, thus for the bigger drops pretending a slightly better (i.e. smaller) spread around the mean oblatenesses. Results are given on the IUT. Normally there is no need for readjustments.

Fig. 2.13 presents a scatter diagram comparing rain rates by a tipping bucket rain gauge versus those of a 2D-Video-Distrometer.

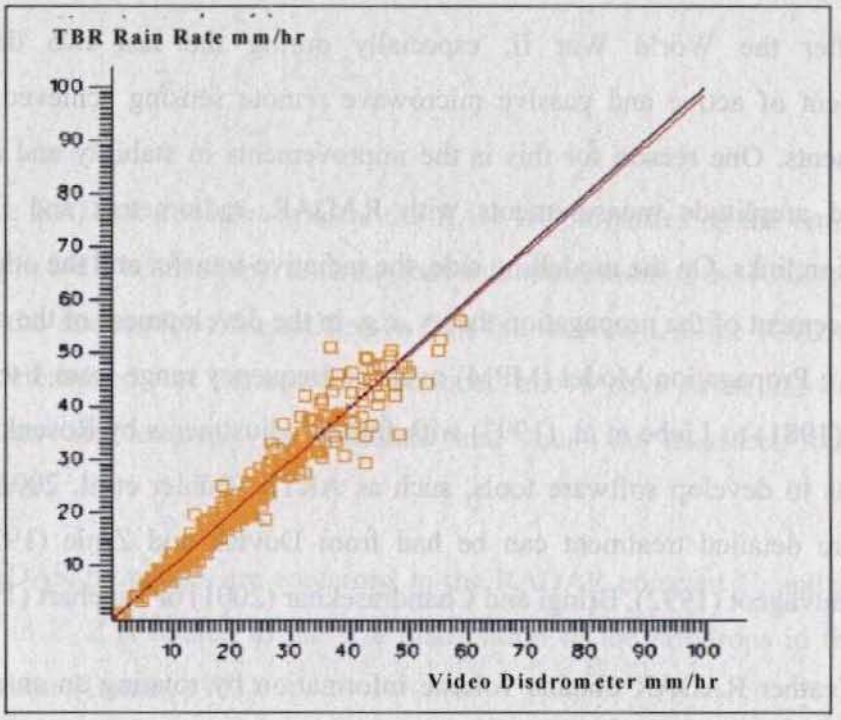

Fig. 2.13: Scatter diagram-comparing rain rates by tipping bucket vs. 2D-Video-Distrometer (Papua New Guinea (PNG), in Colorado, USA) (A rain amount of 41.1 mm was recorded for this particular (tropical) rain event, the mean difference for the individual tips is less than 1 % with a correlation coefficient of 0.97 [M. Schönhuber et al. 1994]

2.3.5.3 Errors in video disdrometer

Common errors found are as shown below:

1. Errors due to obscureness of optical path (Insects, dirt, raindrop on mirror or faceplate, raindrop(s) hanging from awning.
2. Software hangout due to too high rain rate or too big drop sizes (hailstones)
3. Calibration errors. (Small errors in drop size results in large errors).
4. Need for alignment of lens and other mechanical assembly.

2.3.6 RADAR rain gauges

After the World War II, especially during the last two decades, the development of active and passive microwave remote sensing achieved significant advancements. One reason for this is the improvements in stability and accuracy of phase and amplitude measurements with RADAR, radiometers and line-of-sight transmission links. On the modelling side, the radiative-transfer and the other reason is the advancement of the propagation theory, e.g. in the development of the atmospheric Microwave Propagation Model (MPM) over the frequency range from 1 to 1000 GHz by Liebe (1981) to Liebe et al. (1993) with further adjustments by Rosenkranz (1998) and efforts to develop software tools, such as ARTS [Bühler et al. 2002] presented here. More detailed treatment can be had from Doviak and Zrnic (1993), Collier (1996), Sauvageot (1992), Bringi and Chandrasekhar (2001) or Rinehart (1997).

Weather RADAR obtains volume information by rotating an antenna with a variable vertical angle according to a predefined scanning strategy. The RADAR antenna emits a short pulse of electromagnetic radiation in a known direction and a small fraction of this energy is reflected by targets (meteorological and non-meteorological) back to the RADAR antenna. The back-scattered mean power $\overline{P_r}$ received by the RADAR is proportional to the reflectivity factor Z (*radar reflectivity*

expressed as $mm^6 m^{-3}$), provided the scattering particles are considerably smaller than the wavelength by orders of magnitude and are of spherical shape, and to the factor $|K|^2 = \left|\frac{m^2-1}{m^2+2}\right|^2$ which is a function of complex refractivity index m and thus dielectric constant of the target. The received power is also proportional to the radar constant C and inversely proportional to the square of the target distance (r^2) and the square of the one-way atmospheric attenuation (L_{Atm}).

The simplified form of the RADAR equation is then e.g. [Joss and Waldvogel, 1990]:

$$\overline{P_r} = \frac{C}{L_{Atm}^2}\frac{|K|^2 Z}{r^2}, \tag{2.12}$$

The RADAR constant reflects the RADAR properties as the emitted power, pulse length, 3-dB beam shape, antenna gain and attenuation of the RADAR hardware including the attenuation of amplifiers within the receiver. As the RADAR constant must be determined, the parameters mentioned above have to be known. Some of these values are assumed as constants and thus are measured once by the manufacturer.

All RADAR properties are contained in the RADAR constant C, and all raindrop properties in Z. Z is related to the size distribution of the raindrops in the RADAR sample volume [Battan, 1973].

$$Z = \int_0^\infty D^6 N_V(D) dD \tag{2.13}$$

where $N_V(D)dD$ (the subscript V standing for volume) represents the mean number of raindrops with equivalent spherical diameters between D and $D+dD$ (mm) present per unit volume of air. Since the variations in RADAR reflectivity may span several

orders of magnitude, it is often convenient to use a logarithmic scale. The logarithmic RADAR reflectivity is defined as and is expressed in units of dBZ [Battan, 1973].

2. 3.6.1 RADAR reflectivity- rain rate relationships

The RADAR measurements of the spatial and temporal distribution of the mean received power $\overline{P_r}$ is related to Z by the relations

$$Z = \frac{r^2 \overline{P_r} L_{Atm}^2}{|K|^2 C} \tag{2.14}$$

Since rain rate is related to the DSD, Eq. (2.7) with Eq. (2.14) demonstrates that it is the raindrop size distribution (and to a lesser extent also the drop velocity relationship) is related to Z [Smith and Krajewski, 1993; Steiner *et al.*, 2004]. There exists overwhelming empirical evidence [Battan, 1973] that such relationships generally follow power laws of the form $Z = aR^b$ where a and b are coefficients that may vary depends on the location, season etc., but are independent of R itself. Figure 2.14 compares these relationships.

Taking geometric mean of 'a' and arithmetic mean of 'b' of all the reported relationship of Z-R, yields a mean power law relation equation,

$$Z = 238R^{1.5} \tag{2.15}$$

and is very close to the relationship with the Marshall-Palmer (MP) Z–R relationship,

$$Z = 200R^{1.6} \text{ [Marshall and Palmer, 1948; Marshall } et\ al.\text{, 1955].} \tag{2.16}$$

Since Z and R are related to DSD (refer Eq.2.7 and 2.13) it should be possible to express a and b as functions of the parameters of DSD.

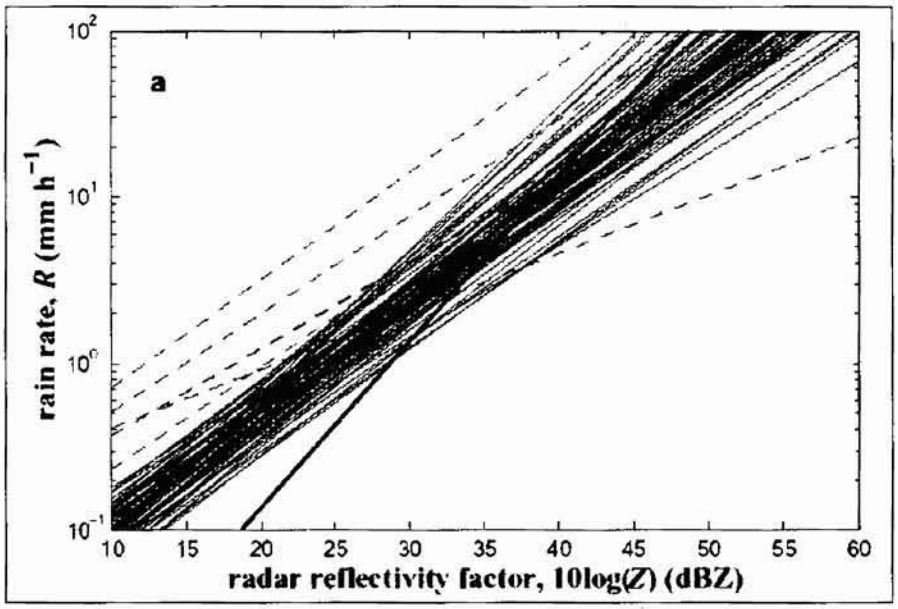

Fig. 2.14: Different power law Z–R relationships quoted by Battan (1973), including five deviating relationships (dashed lines), four of which have prefactors a significantly smaller than 100 and 1 of which has an exponent b as high as 2.87. The bold line indicates the linear relationship [List, 1987].

2.3.6.2 Multi-source method of identification of precipitation type

Single polarization RADAR has only a modest capability of determination of the precipitation type. Linear polarisation RADARs can generally transmit pulses that are alternately polarised horizontally and vertically, and can measure the two cross polar returns Z_h (horizontal polarised), Z_v (vertical polarised). If a cross-polar receiver channel is installed, then the cross polar return Z_{HV} is also available. In addition, if the RADAR is Dopplerised, then the phase of the return signal with horizontal and vertical polarisation, Φ_h and Φ_v, can be estimated. The four parameters thus obtained are: the differential reflectivity, Z_{DR}; the specific differential phase shift, K_{DP}; the linear depolarisation ratio, L_{DR}; and the co-polar correlation, $\rho^{2,hv}$.

Research studies of the past decade indicate that polarimetric weather

RADARs provides good opportunities for improvement in rainfall measurements. These studies have shown that polarimetric rainfall estimation algorithm based on specific differential phase *KDP* outperforms the conventional *R(Z)* method in the presence of hail contamination, partial RADAR beam blockage, attenuation in rain, and RADAR miscalibration [Zrnic and Ryzhkov, 1999]. Measurements of differential phase are especially beneficial at shorter wavelengths (at C or X band) for which attenuation is a major problem in heavy precipitation [May et al. 1999, Carey et al. 2000; Testud et al. 2000; Matrosov et al. 1999, 2001]. The $R(K_{DP})$ estimator, however, is somewhat prone to DSD variations, although to a lesser degree than the conventional algorithm *R(Z)*.

Four algorithms widely used for RADAR rainfall estimation are as shown in the Table 2.3.

Table 2.2: *Various Z-R relationships*

$R(Z) = 1.7 \times 10^{-2} Z^{0.714}$	Standard for WSR-88D	(1)
$R(K_{DP}) = 42.8 \lvert K_{DP} \rvert^{0.802} sign(K_{DP})$		(2)
$R(K_{DP}, Z_{DR}) = 53.7 \lvert K_{DP} \rvert^{0.910} Z_{DR}^{-.421} sign(K_{DP})$	if $Z_{DR} > 0.5$ dB	(3a)
$R(K_{DP}, Z_{DR}) = 70.0 \lvert K_{DP} \rvert^{0.878} 10^{-0.131 Z_{DR}} sign(K_{DP})$	if $Z_{DR} < 0.5$ dB	(3b)
$R(Z, Z_{DR}) = 6.42 \times 10^{-3} Z^{0.824} Z_{DR}^{-0.654}$	if $Z_{DR} > 0.5$ dB	(4a)
$R(Z, Z_{DR}) = 1.39 \times 10^{-2} Z^{0.813} Z_{DR}^{-0.266 Z_{DR}}$	if $Z_{DR} < 0.5$ dB	(4b)

K_{DP} is in deg km^{-1}, Z_{DR} is in dB. Algorithms (3a) and (4a) are not robust at low Z_{DR}, therefore, 3b) and (4b) are more stable with respect to Z_{DR} measurement errors if Z_{DR} is close to zero. The relations (2) - (4) were derived for the Cimarron RADAR [Alexander R and Dusan Z, 1998] wavelength of 10.97 cm using the 3-year statistics of DSDs measured with the 2D-video-disdrometer and assumption of equilibrium

raindrop shape given by Beard and Chuang (1987).

It is obvious from Table 2.3 that the $R(K_{DP}, Z_{DR})$ algorithm is the best for both local and aerial estimates. This was expected from the simulations based on the DSD statistics in central Oklahoma [Schuur et al. 2001]. K_{DP} based relations are especially well suited for aerial rainfall estimation. The use of the best of Polarimetric algorithms, $R(K_{DP}, Z_{DR})$, results in more than two times reduction in the standard deviation of the areal accumulation estimate compared to the standard $R(Z)$ method.

Rain rate estimation from RADAR measurements is based on empirical models that describes the RADAR reflectivity – rain rate $(Z\text{-}R)$ relationship, $R(Z, Z_{DR})$ and $R(K_{DP})$. The empirical relations cannot give accurate results of estimation for various types of rain and drop size distribution (DSD). Accurate rain rate estimation requires detailed knowledge of rain DSD. In the past, rain DSD was commonly assumed to be an exponential distribution. Some observations, however, indicate that natural rain DSD contains fewer of both very large and very small drops than exponential distribution.

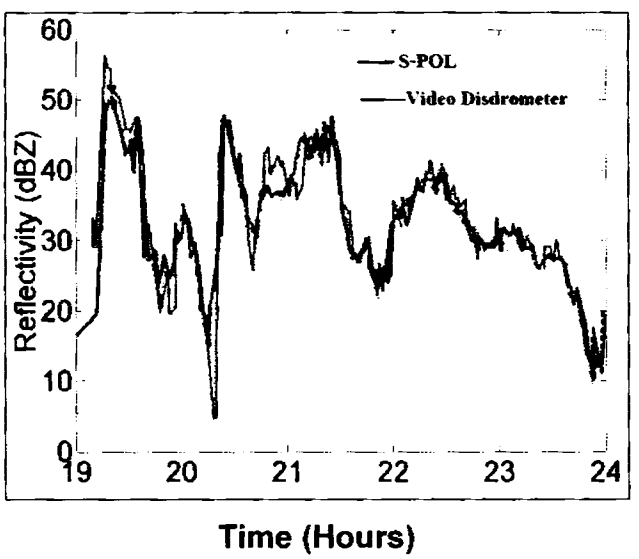

Fig. 2.15: Reflectivity (dBZ) measured by S-Pol and the video disdrometer reading

Figures 2.15 and 2.16 shows the RADAR reflectivity and its relationship with the DSD measured by using 2 d Disdrometer.

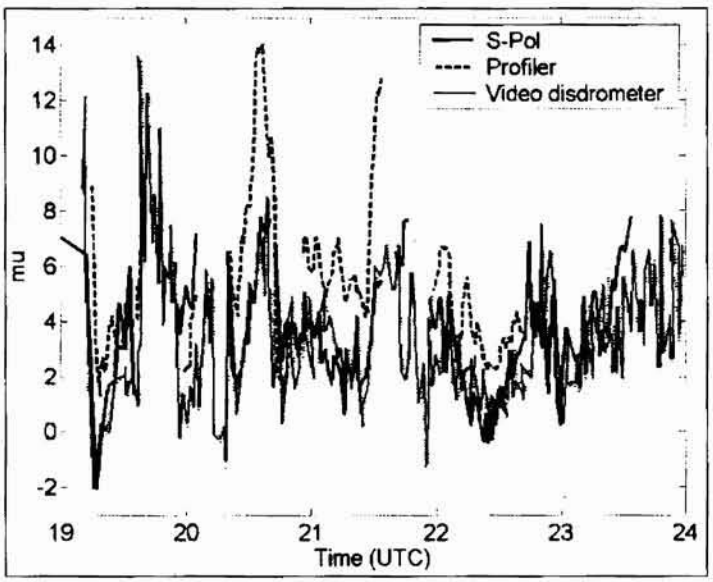

Fig. 2.16: Rain rates computed from the retrieved gamma DSDs from S-Pol (solid), the profiler (dashed) and the video disdrometer (dotted).

2.3.6.3 Errors in RADAR rain estimates

Quantitative precipitation estimates by RADAR have a number of inherent errors. The quantification of the errors in RADAR is difficult because there are several independent error sources. Relative importance of these sources varies greatly with weather conditions, distance to the RADAR, scan strategy, temporal and spatial resolution, etc. This makes it impossible to give precise percentage accuracy of RADAR precipitation measurement.

The RADAR measurement errors may be classified into instrumental (or non-meteorological) errors and errors caused by changes in the meteorological conditions (meteorological errors). Non-meteorological errors are caused by beam propagation,

clutter, RADAR hardware and overall data processing. Shape of the RADAR beam, its side lobes, antenna gain, RADAR transmitter and receiver characteristics etc. must be carefully calibrated. Comparisons of RADARs in different countries around the Baltic Sea showed a disagreement up to 7 dB during the early stage of the BALTEX experiment [Koistinen et al., 1999, Michelson et al.., 2000].

The physical quantity that should be averaged is the rain intensity but the primarily measured quantity is the reflectivity, which is nonlinearly related to the rain intensity. Thus averaging in reflectivity introduces a bias. This bias increases with the in-homogeneity of the reflectivity field and with the size of a recorded range gate, i.e. it increases especially with distance from the RADAR. The largest values are reached when the bright band is partially included in the scattering volume and in convective storms, when horizontal gradients are strong. Zawadzki et al. (1999) used highly resolved data from vertically pointing X-band RADAR to calculate the reflectivity values of a RADAR with a resolution of 1 dB from a distance of 60 km. The standard deviation was between 1.43 dB and 4.34 dB, indicating that the coarse spatial resolution of RADAR is in certain situations a significant source of uncertainties.

Other errors that can be present in the RADAR precipitation estimation include reflections received from various non-meteorological targets that include insects, birds, aircrafts, solar radiation etc. Shape of the droplets, type of precipitation, and multiple echoes are other common sources of errors. Table 2.2 summarizes the various meteorological factors affecting the accuracy of RADAR based weather measurement.

Table 2.3: The effects of meteorological factors on values of equivalent rainfall rate deduced from radar measurements and conditions under which they are significant [adapted from Collier, 1996]

Factor	Magnitude of the effect and situations where it is significant	Methods for compensations
Variations in the raindrop-size distributions	Drops larger than average in intense convective storms; reflectivity increased by 1-2 dB	Use of relation $Z=400R^{1.3}$ or similar rain gauge adjustment
	Drops smaller than average in warm-frontal rain; reflectivity decreased by 3-4 dB	Use of relation $Z=100R^{1.4}$ or similar rain gauge adjustment
	Any other deviation from average drop-size distribution is usually too small to be detected or is masked by other effects	
Enhancement of signal by presence of hail	Predominant factor in intense convective storms (Max $Z \geq 53$ dBZ); may increase reflectivity in storm cores by 10 dB or more above that of the rain alone	Limiting R (or Z) to a maximum value ("hail cap"); usually *Rmax* ≈100 mm/h (from 75 to 150 mm according to the climate type (Fulton et al., 1998); some compensation by downdraft effect
	Probably 4-5 dB enhancement in moderate convective storms (45 dBZ ≤ max $Z \leq 53$ dBZ) which are non-frontal	Automatically compensated for by downdraft effect
Diminution of reflectivity by downdrafts associated with heavy rain in convective cells	Predominant factor in moderately convective storms, which are associated with cold fronts or stationary fronts. Reflectivity in storm cores diminishes by 4-5 dB.	Use of relation $Z=230R^{1.2}$. Some compensation by updraft (overestimating) effect
	Similar effect in intense convective storms and in non-frontal moderate convective storms	Automatically compensated for by hail effect or updraft effect
Low-level growth of raindrops in fog or stratus clouds	Occurs when fog or low stratus is present. Increase in rainfall rate unlikely to be more than 25 % in light rain or 15 % in heavy rain (except orographic enhancement)	Recognition of possible underestimation by radar when fog is present; rain gauge adjustment; correction procedures using knowledge of reflectivity profile
Orographic seeder-feeder enhancement (intense low-level growth of raindrops in fog or stratus clouds in the mountains)	Significant factor in heavy rainfall when accompanied with high wind; occurs usually in widespread (stratiform) rain; underestimation can reach 1-5 dB according to the height of the beam above the ground and the intensity of the enhancement;	Recognition of possible underestimation by radar when fog and high wind in the mountains are observed; local (possibly altitude-dependent) rain gauge adjustment; correction procedures using knowledge of reflectivity profile or using climatology of the enhancement (dependency on the wind vector and humidity);
Low-level evaporation of drops in relatively dry air	Unlikely to be a significant factor except ahead of warm fronts	Recognition of possible overestimation when relative humidity is low; rain gauge adjustment

2.3.7 Impact type disdrometer

Impact type disdrometer is another instrument used to measure DSD. The disdrometer consists of a sensor, analog electronics, and a front-end processor. A schematic arrangement of such an instrument is as shown in Fig. 2.17. It consists of a piezo electric sensor that converts the momentum of the falling raindrop into an electrical pulse, the amplitude of which is monotonically related to the drop size.

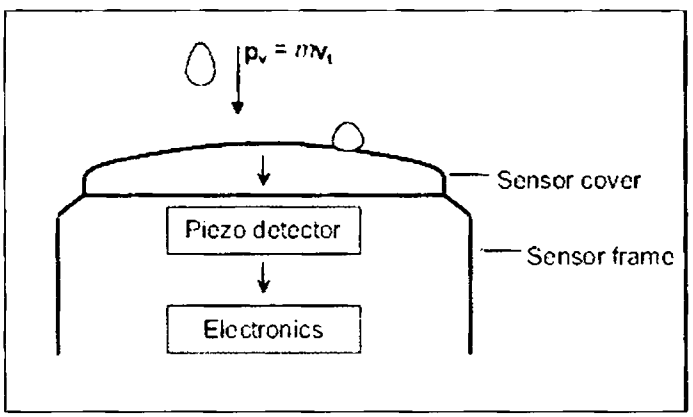

Fig. 2.17: A schematic drawing of the piezoelectric precipitation sensor

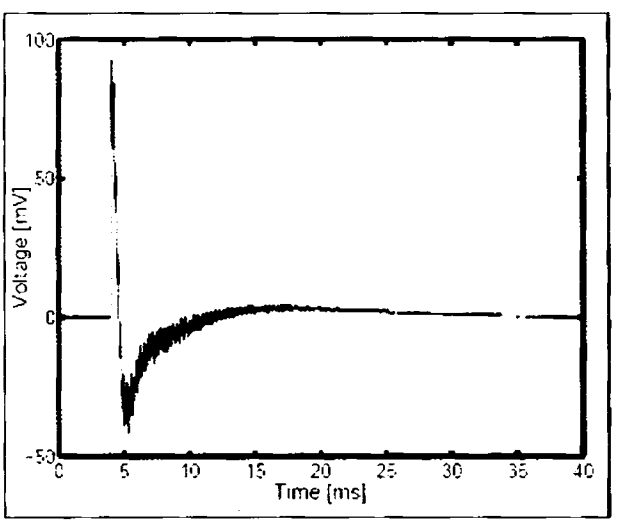

Fig. 2.18: Typical output signal generated by a raindrop.

Figure 2.18 shows a typical output signal generated by a single raindrop. Since the signals resulting from the impacts are proportional to the volume of the drops, the signal of each drop can be directly converted to accumulated precipitation.

The analog electronics amplify, rectify, and logarithmically compress the signal and prepares the signal for digitization at fixed voltage levels. The front-end processor continuously digitizes the conditioned analog output at a high rate, while examining the data for drops. The peak value of each drop is computed and this value is used to increment the counts in to a raindrop size histogram. Once a minute, the front-end processor reports the date, time, and histogram counts. The data is recorded to an internal data logger during unattended operation. The processor sorts the digital output into a number of channels of drop diameter ranging from about 1 to 7 mm. The amount of liquid precipitation measured can be less than the actual amount reaching the ground by up to 30 per cent or even more.

2.4 Comparing Performance of Rain Gauges

The correct measurement of liquid precipitation and other meteorological and hydrological variables, as well as the correct interpretation of historical data will be of foremost importance in the future for the prediction of changes in weather patterns affecting the whole climate of the Earth. In this respect, rain gauges provide the only direct measurements of rainfall intensity at the ground and are usually referred to as the ground truth in rainfall monitoring.

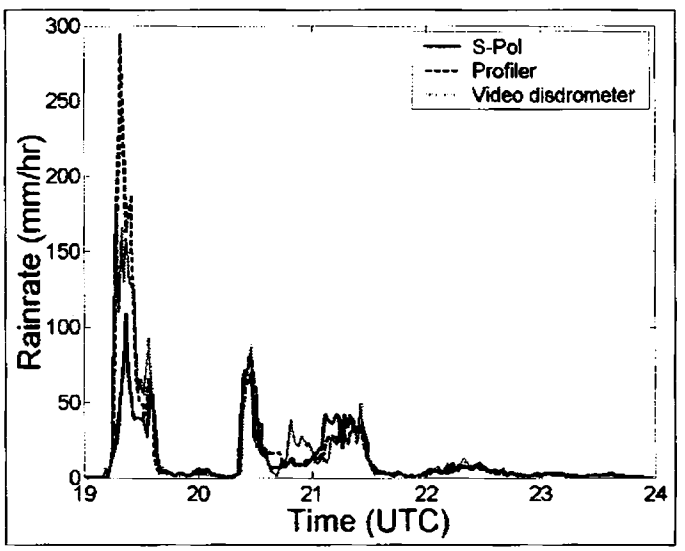

Fig. 2.19: Time history plots of Λ estimated by SPOL RADAR, the profiler and the video disdrometer.

A significant problem with comparing satellite and rain gauge data is that the satellite and surface instruments measure fundamentally different quantities. The microwave instrument, for example, measures the volume-integrated microwave emission within the instrument's instantaneous field of view, from which a surface precipitation rate can be inferred. Because the instrument responds to hydrometeors at different altitudes, there is an implicit averaging time related to the time required for drops to fall the surface (10 minutes). A major limitation of low-Earth orbiting satellites, however, is that they typically view a given location only about once per day. If the desired result is, say, the monthly-mean precipitation rate over a region, the poor temporal sampling means that sampling errors will necessarily be a large component of the total estimation error. Rain gauges, on the other hand, make essentially point measurements in space, usually with relatively high temporal resolution. While gauges can have good temporal sampling, poor spatial sampling can lead to significant errors in estimates of area-averaged precipitation rates. Comparing

the two types of measurement schemes can be challenging. For example, it is frequently the case that TRMM observes precipitation in the area surrounding a rain gauge while it is not raining at the gauge itself.

Newly developed techniques for extensive rainfall observations based on remote sensing (essentially weather RADAR, airborne radiometers and satellites) provide a space-time description of rainfall fields, but still require the use of rainfall measurements from rain gauges for calibration and validation purposes. Improvement of the reliability of Rain Intensity (RI) measurements as obtained by traditional TBRs and other types of gauges (optical, weighting, floating/siphoning, etc.) is therefore required for use in climatologic and hydrological studies. Standardisation of high quality rainfall measurements is also required to provide a basis for the exchange and valuation of rainfall data sets among different countries, especially in case trans-boundary problems such as severe-weather/flood forecasting, river management and water quality control are operationally involved.

Liquid precipitation measurements are affected by different sources of both systematic and random errors, due to wind, wetting and evaporation induced losses [Sevruk, 1989], which makes the measurement of light to moderate rainfall scarcely reliable without adequate correction. Snow measurements are even more difficult as snow is more sensitive than rainfall to weather related errors. The traditional TBR is also known to underestimate the higher rain rates because of the rainwater amount that is lost during the tipping movement of the bucket [Marsalek, 1981]. Though this inherent shortcoming can be easily remedied by means of dynamic calibration [Calder and Kidd, 1978; Niemczynowicz, 1986], the usual operational practice in meteorological services and instrument manufacturing companies relies on single-point calibration, based on the assumption that dynamic calibration has negligible influence on the total recorded rainfall depth. This results in systematic

underestimation of intense rainfall rates that can be quantified. The error increases as a function of the rain intensity and heavily affects the derived statistics, with non-negligible consequences on the numerical estimates of parameters involved in the common statistical tools that are used for the characterization of extreme events (GEV and TCEV distributions, depth-duration-frequency curves, etc.). Rain gauges in general are thought to underestimate rain due to wind effects at the mouth of the gauge [Koschmieder 1934; WMO 1962; Yang *et al.* 1998]. Under catch errors during windy conditions can be large, the errors are not completely understood, and studies have not addressed the particular problems of rain gauges on ocean buoys [Serra *et al.* 2001].

2.5 The Bias Induced by Systematic Mechanical Errors on Rainfall Statistics

Since mechanical errors mainly affect the higher intensities (i.e. rain amounts that are measured in very short intervals in time) the recovering of historical series is only possible when very fine resolution data are available. Unfortunately most of the historic information is either obtained from the interpretation of rain charts or at best stored in terms of cumulated values over time intervals of 30 to 60 minutes. Small-scale details of the rain process are definitively lost for most sites where suitably calibrated gauges are progressively installed. Any correction of past data sets must be therefore applied on disaggregated series at least down to 5 minutes in time, where the rain intensity is higher and the errors are significant. Such an exercise only permits statistical correction of the aggregated data and requires accurate studies of the temporal structure of the rain process at fine scales, and of specific processes – such as the intermittence that might play a relevant role at such scales [Molini *et al.*, 2001].

Accordingly, techniques to correct historical records of short duration rainfall observations after proper desegregation of the original figures have been developed

and, on the basis of the corrections resulting from application of the proposed techniques, the influence of the errors has been investigated with reference to one of the most popular tools used for the statistical characterisation of rainfall extremes, i.e. the depth-duration-frequency curves. These have been derived under the hypothesis of a Gumbel (EV1) distribution for rainfall extremes, and the results reported here refers to the meteorological station of the Historical Observatory of Chiavari (Italy) where rainfall data have been continuously recorded since 1883 on a daily basis and since 1960 on a hourly basis.

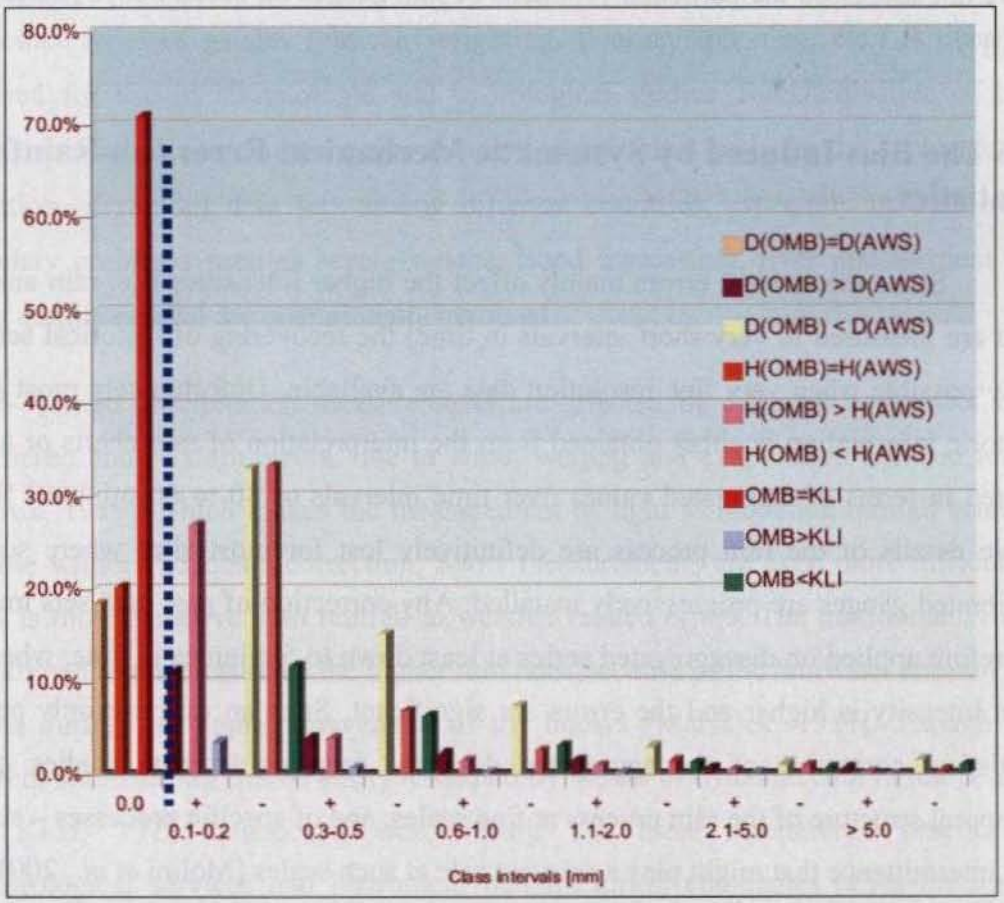

Fig. 2.20: Distribution of differences between different gauge types into given intervals

The results of the experimental study conducted at meteorological station in Liesek in Slovakia during the period 1999-2001 has been a good opportunity for comparison of the differences of daily precipitation sums, measured by Standard Rain Gauge (KLI), Pluviograph (OMB) and TBR (Fig. 2.20). There are graphically depicted mean differences of daily sums from all stations (OMB – KLI and OMB – AWS) and differences of hourly sums (OMB – AWS), divided with respect to amount of precipitation. It is seen that the agreement of precipitation sums OMB and KLI in the days with precipitation occurs makes 70% from all evaluated cases.

The agreement of daily sums OMB and AWS is about 20 % of cases. The KLI sums are higher than OMB sums in 20% and lower in 5 % of days with precipitation. The daily sums measured by AWS are higher than sums measured by KLI (60%), lower (20 %). Whereby, around 65% of difference values OMB – AWS are in interval ± 0.2 mm and the difference higher than ±1 mm is in 9 % of days with precipitation.

2.6 Standards and Certification Procedures for Rain Gauge Instruments

In the European Commission Working Document on Research and Standardisation (COM98/31), standards being one of the tools to foster homogeneous quality are recognised to be in a strategic position to promote the competitiveness and interoperability of products and services. Standards thus provide a bridge between the technical domain and the regulatory and economic framework. The development of new standards and their implementation however depend on considerable amount of preliminary research. The opportunity to combine scientific and technological developments with investigations on pre-normative issues, provide a measure of the suitability of any newly developed instrument and calibration methodology to act as the basic technical references for a new European standard gauge.

This would complement the interests of CEN/TC 318 *Hydrometry*, aimed at the standardisation of methods and instrumentation relating to techniques for hydrometric determination including precipitation. In CEN TC 318 an EN (European Standard that carries with it the obligation to be implemented at national level by being given the status of a national standard and by withdrawal of any conflicting national standards) on a standard reference rain gauge pit has been already prepared within the efforts of WG5 towards a Reference rain gauge station.

The economic impact of standardisation in this field is evident, recalling that the total turnover of the water industry in Europe is estimated to be EU 58,000 million of which the hydrometric element is estimated to be EU 190 million. Most national members have a selection of their own national standards within the scope of TC 318. For many years, the World Meteorological Organisation (WMO) has been publishing its own Technical Recommendations on some aspects of the work, and the International Organisation for Standardisation (ISO) has published, and continues to publish, a large number of International Standards and Technical Reports. Following the Terms of Reference of the WMO Commission for Instruments and Methods of Observations an expert meeting on rainfall intensity measurements was held and the organization of a related laboratory inter-comparison is now suggested, together with the introduction of precipitation correction procedures and development of further correction procedures based on simulations. On this basis the need for some further steps towards homogenisation of standard quality of instruments as well as towards the establishment of criteria to assess data quality is more than evident.

The development of a qualification module for rain intensity measurement instruments allowing quality assurance and metrological confirmation of rain gauges

according to the European Standard ISO/EN30012-1 is just a first step ahead in this direction, although much work is still required in terms of the accuracy and range requirements, the proper configuration of the calibration equipment, the expected performances and the definition of a standard method of testing. Controlled laboratory conditions should be ensured and a common procedure established that could be easily repeated in any equipped laboratory.

2.7 Summary

One of the very important rain parameter is the DSD. There exist several automatic measurement methods to measure rainfall rate. Measurement methods based on DSD is an important technique since it provides more insight into the phenomenon and DSD information has been very useful in studies like soil erosion. RADAR based measurement is widely used as it can cover vast area. Since this method can provide only an area averaged results, and some times fails to give a correct ground truth, other forms of land-based measurement techniques are often needed. Rain gauges like TBR, video disdrometer etc. are in use for meteorological as well as for scientific research. Low cost instruments more often gives erroneous readings while accurate systems like optical devices are very costly. A rain gauge that can provide accurate reading and lower in cost is always welcome to fill in the gap between the low cost less accurate instruments and the high cost precise measurement systems.

Chapter 3

Review of the Past Work

Raindrop falling on water produce impact and as a consequence of events that are happening underwater, acoustic noise is produced. This rain generated acoustic noise has some distinct features and by extracting these features, the rain parameters can be measured. A variety of experiments were conducted to study the rain generated noise and the results of these investigations are available in open literature. Classical results of those studies over the last two decades are promising and the development systems for measuring rainfall based on the acoustic methods are also reported in literature. This chapter presents a review of the research work carried out on the mechanism of rain generated acoustic noise, its analysis and the techniques developed to quantify the rainfall.

3.1 Introduction

Precipitation at sea is one of the important resource of freshwater in ocean surface, and thus their density. However, it is very difficult to measure rainfall over the ocean because of the arduous process involved in spatial and temporal scales and the formidable need for long-term measurements. Even though satellite remote sensing is suitable for global monitoring, there is still a need for in situ measurements using sensors to resolve and to provide validation of the satellite data. One of the most

promising methods is the manipulation of the acoustic noise produced by the raindrops. The use of sub surface hydrophone removes the problem of operating at the rough ocean surface and provides a mechanism for obtaining average rainfall over an area.

Rain is one of the principal natural sources of underwater sound. The idea that underwater sound can be used as a signal to detect and quantify rainfall has been developed through laboratory studies on individual drop splashes. [Pumphery et al 1989; Medwin et al, 1990; Medwin et al 1992; Medwin and Nytsuen 1992]. Field studies were also carried out by various researchers [Nysteun 1996; Nysteun et al 1995; Nysteun and Selsor, 1997]. Because of the fact that different raindrop sizes produce distinctive sound underwater, the sound field can be decomposed to measure the drop size distribution in the rain [Nystuen 1996].

The sound produced by the splashes radiates both into the air and into the water. Since the sounds in air were of musical in nature, the phenomenon attracted many researchers. Reports on general observation of the sounds produced by splashes by a number of researchers were published. The early investigators studied the air-borne sound produced by splashes of water droplets and spheres falling in water.

In his classical work, M. Minnaert [Minnaert M., 1933] explained the generation of underwater sounds by bubbles, and suggested that the sounds of running water are associated with these resonant bubbles. His major contribution was the determination of the resonant frequency of the bubble

$$f_r = \frac{1}{2\pi a}\sqrt{\frac{3\gamma P_0}{\rho_0}} \tag{3.1}$$

where a is the bubble radius, P_0, the local pressure, ρ_0 the water density and $\gamma = 1.4$, the ratio of specific heats.

3.2 Mechanism of Acoustic Wave Production

The principal sources of rain-generated sound in water are due to the: (1) drop impact, (2) natural vibration of the dop, (3) volume pulsation of air filled cavities formed in the water. Other sources of underwater sound are the secondary flashes of water droplets. oscillations of air bubbles and of cavities open to atmosphere. Most of these possible sources can be grouped into three general phases: the flow establishment phase, the body vibration phase and the cavity and bubble phase.

Richardson (1955) observed both the airborne and waterborne sounds from splashes of spheres entering into the water and correlated the sound with motion pictures of the cavity formed on entry. He concluded that most of the sound was produced by the bubbles behind the spheres. A rapidly damped high frequency underwater sound of low amplitude was detected immediately after the instant of impact.

The impact of raindrops usually forms cavity behind the drops and may entrain air bubbles of various sizes. If the cavity is open to the atmosphere, it may act as a Helmholts resonator [Thomas B. Greenslade, 1996]. The cavity can be excited by the rapid changes in cavity volume and the surface constriction. In the air, the cavity would appear to be a simple source of sound. When air is trapped in the water as bubbles, sound may be propagated through the water. Bubbles radiate sound mainly by volume pulsations of air filled cavities at a frequency given by Minnaert's equation (Eq. 3.1).

When bubbles rise to the free surface and break, sound will be produced. Because of the action of the surface tension, the pressure inside the bubble is higher than the pressure just outside the bubble. Thus when the bubble breaks, a pressure wave is radiated both into air and to the water.

Findings of G.J Franz (1959), show that the frequency spectrum and the amplitude of the sound radiated into water by the water droplets may depend on many primary important variables like the size and shape of the droplets, the velocity of impact, density and acoustic properties of water. Other variables, which would also be expected to influence the sound produced, are the surface tension of water, its viscosity, density, compressibility as well as pressure and viscosity of air above the water. He also observed that the underwater sound pressure P resulting from the impact of water droplets varies in amplitude and duration in a systematic manner with changes in impact velocity and droplet size.

Scientists have studied the nature of sound effects when a drop of water strikes the water surface for more than a century. Photographs of the impacting drops were taken as early as AD1890's [Worthington, 1897]. Later theories behind the process were put forward by Mallock (1919) and Bragg (1920). These theories later proved to be incorrect. However, Bragg's work prompted Minneart to study the sound radiated by an oscillating bubble that was released into a tank of water. He also derived the formula for resonance frequency of a gas bubble in liquid (Eq.3.1)

Franz in 1959 made the first thorough investigation of sounds produced by the drop impacts. Since then, this has been a classical work and standard reference in this field. Franz used high-speed movie techniques to show how water behaved during the impact process. Simultaneously he recorded the sound produced during the impact process. The initial impact sound was a sharp pulse, while the bubble sound was a

decaying sinusoid. Franz observed that bubbles were not produced by every drop and the occurrence was more or less random. Franz found that the sound pressure radiated due to drop impact increases systematically with the drop size and impact velocity.

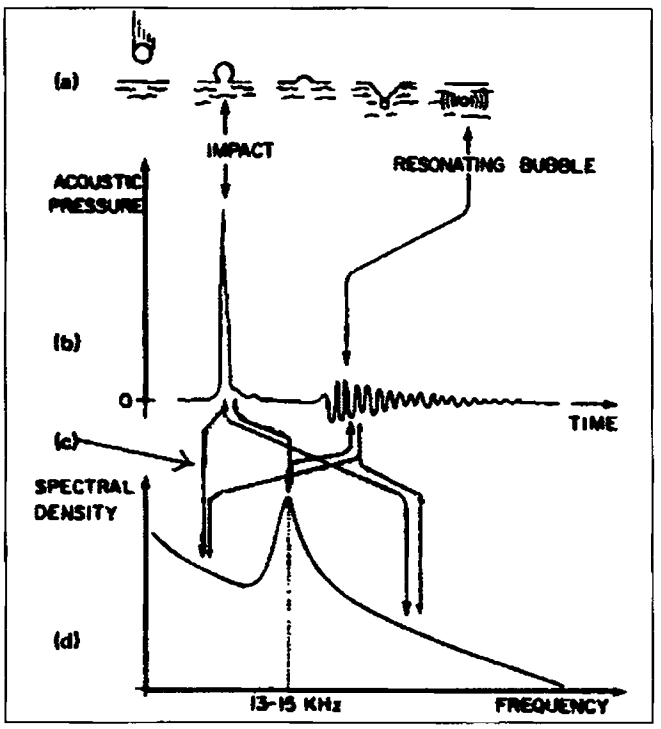

Fig. 3.1: Schematic of underwater sound produced by rainfall: (a) raindrop fall, (b) acoustic signal in time domain, (c) relationship between time and frequency plots, (d) the noise spectrum [laville et. al. 1991]

Franz did experiments on simultaneous droplets falling in water (spray) and attempted to predict the acoustic power spectrum of rain generated underwater sound.

3.3 The Acoustics of Rain Generated Noises Underwater

One of the first attempts to describe the underwater noise spectra produced by rainfall was published by Hiendsman et al. (1955). He observed that during the

heaviest rainfall the sound pressure spectrum level was nearly constant at 77dB re 1μ *Pa* [Hiendsman et al. (1955)]. The sound produced from the impact of rain on water surface has been observed and Nystuen suggested a quantitative measurement of the rainfall estimation [Nystuen, 1996].

Scrimger (1987) reported that there is spectral peak around 15 kHz with a steep slope towards the lower side. Similar results were also reported by Nystuen [Nystuen, 1986]. He used a numerical model for the drop splash flow field. He also discussed the description of initial impact pulse and explained the peak that he observed in the spectrum in terms of the initial impact sound alone, ignoring the bubble. However, a contradictory observation by Laville et al (1991) reports that the spectral peak around 13-15 kHz is due to bubble resonance.

Raindrops range in sizes from 0.2 mm to about 6 mm in equivalent diameter. A raindrop falling from a height more than 20 meters attains terminal velocity. Pumphery et al (1989) discovered a bubble entrapment mechanism for small raindrops striking at smooth water surface at normal incidence. Longuet- Higgins (1990) modelled this mechanism and later simulated numerically [Oguz et al, 1990]. It has been reported that the bubble entrapment mechanism is different for large drops (2.2 to 4.6 mm diameter) [Snyder, 1990; Medwin et al., 1992]. It has been also reported [Medwin et al., (1992), Jacobus (1991)] that there is a drop size range (1.1 to 2.2 mm diameter) where no bubble entrapment has been observed [Elmore et al. 2001]. Pumphery et al (1989) conducted an experimental study and tried to establish the condition for bubble production. Although bubble sound is predominant, the impact sound produced by drop impact on water surface is important. Nystuen et al studied the impact pressure field at the drop impact site by numerical simulation and reported that the acoustic component due to impact is of short duration with a wide band of the order of 100 kHz [Nystuen et al (1992)].

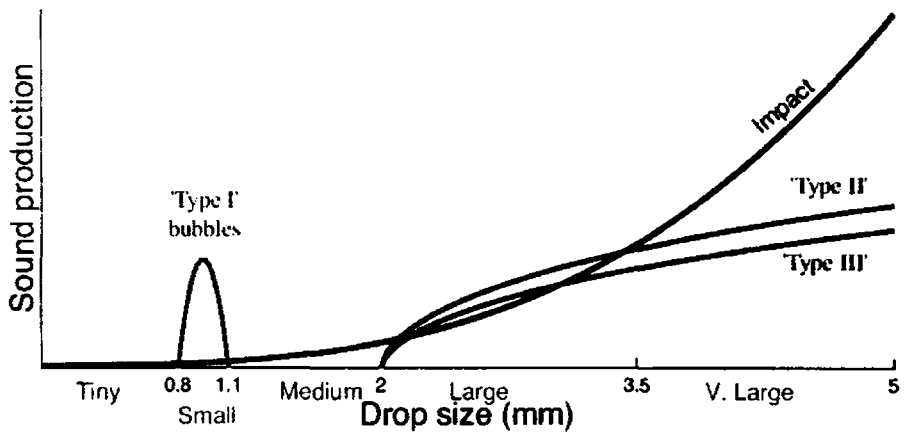

Fig. 3.2: Schematic showing relative importance of various sound-generation mechanisms as a function of drop size.

Table 3.1 summarises the various observations related to the physics of the drop splash associated with various drop sizes

Table 3.1: Raindrop sizes and corresponding spectrum of underwater noise [Nystuen 2001]

Drop size	Diameter	Sound source	Freq. range	Splash Character
Tiny	<0.8mm	Silent		Gentle
Small	0.8-1.2 mm	Loud bubble	13-25 kHz	Gentle, bubble for every flash
Medium	1.2 –2.0 mm	Weak impact	1 - 30 kHz	Gentle, No bubbles
Large	2.0-3.5 mm	Impact Loud bubbles	1-35 kHz 2-35 kHz	Turbulent Irregular bubble entrainment
Very large	>3.5 mm	Loud impact Loud bubbles	1-50 kHz 1-50 kHz	Turbulent Irregular bubble entrainment penetrating jet

3.4 The Acoustic Inversion

The sound intensity I_0 at the water surface is related to the drop size distribution in the rain by

$$I_0(f) = \int A(D,f)V_T(D)N(D)dD \tag{3.2}$$

where f is the frequency, $A(D,f)$ is the transfer function describing the radiated sound as a function of frequency for a given drop size D, $V_T(D)$ is the terminal velocity of the drop, and $N(D)$ is the DSD of rain.

For practical measurement, the equation becomes discrete and can be written as

$$\mathbf{I_0}\,(f) = \mathbf{A}(D,f).\mathbf{DRD}(D) \tag{3.3}$$

where **DRD** is the drop rate density, $\mathbf{DRD} = V_T.N(D)$. If the inversion matrix **A** is known, then using the singular value decomposition, Eq. (3.3) can be inverted to make a measurement of drop size distribution in the rain as shown below.

$$\mathbf{A} = \mathbf{U}\Lambda\mathbf{V}^T \tag{3.4}$$

$$\mathbf{DRD} = \mathbf{V}[\Lambda^{-1}(\mathbf{U}^{-1}\mathbf{I_0})] \tag{3.5}$$

Using laboratory results as a guide, the data obtained from field measurements can be decomposed to obtain mean spectral signature of each drop size. It has been reported that drop sizes less than 0.8 mm (tiny droplets) are undetected because these drops does not produces measurable acoustic signal strength. The upper size for small raindrop is set to be 1.2 mm based on laboratory studies [Pumphery et al. 1989; Medwin et al. 1992]. The mean spectral signal for small raindrops was determined by isolating rainfall conditions in which when only small and tiny droplets are present and then dividing the observed sound intensity by the number of small rain drops present to obtain a spectral density per drop. Similarly signatures for all drop categories can be obtained as shown in Fig. 3.3.

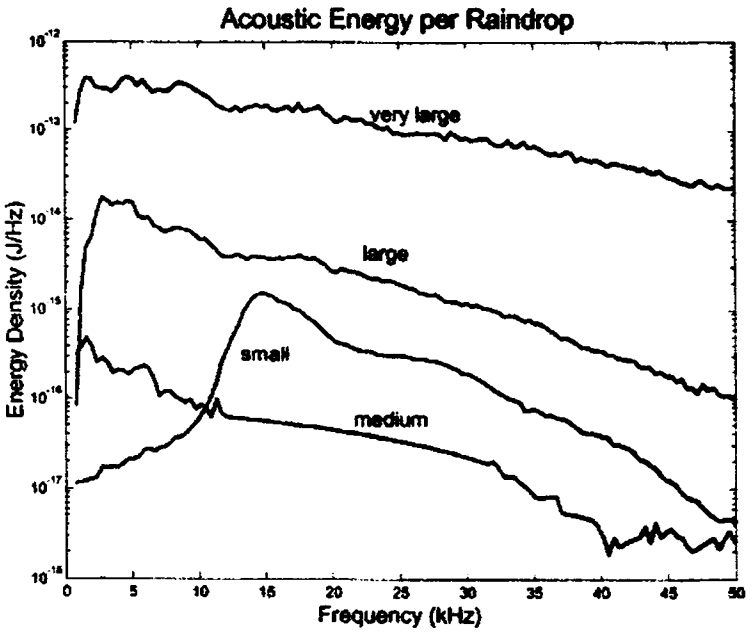

Fig. 3.3: The acoustic signature of individual drop size categories

Eq. (3.5) is the formulation for the inversion of the sound pressure field. Given a sound spectrum, the DSD can be calculated from it. However there are problems that may lead to inaccuracy. A detailed analysis can be found the paper authored by Nystuen (2001).

An alternative acoustic estimate of rainfall is to develop an empirical relationship between the sound level within a particular frequency band and rainfall rate, as measured by one of the standard rain gauges. The relationships as proposed by Nystuen et al. (1993) are

$$\log_{10} R = (SPL_{25} - 51.5)/17 \qquad \text{and} \qquad (3.6)$$

$$\log_{10} R = (SPL_{410} - 50)/17, \qquad (3.7)$$

respectively, where SPL_x is the sound pressure level in the frequency band 2-5 kHz and 4-10 kHz in dB relative to $1\mu Pa^2\ Hz^{-1}$. Rain intensity estimate based on the above relationship tends to overestimate rainfall when rain contains relatively many larger

drop sizes [Nystuen et al., 1993]. Two drawbacks of using these relationship are: (1) difficulty in detecting smaller drops especially when very large size drops are present, and (2) the error due to over estimation. These errors can be minimised by adopting conditional inversion techniques [Nystuen 2001].

3.4.1 Acoustic classification of rainfall

Classification of rainfall type is an important issue. The ability to classify the rainfall type ultimately depends on the DSD. Examination of the underwater sound spectra during rainfall suggests that at least four classifications of rainfall are likely using underwater sound.

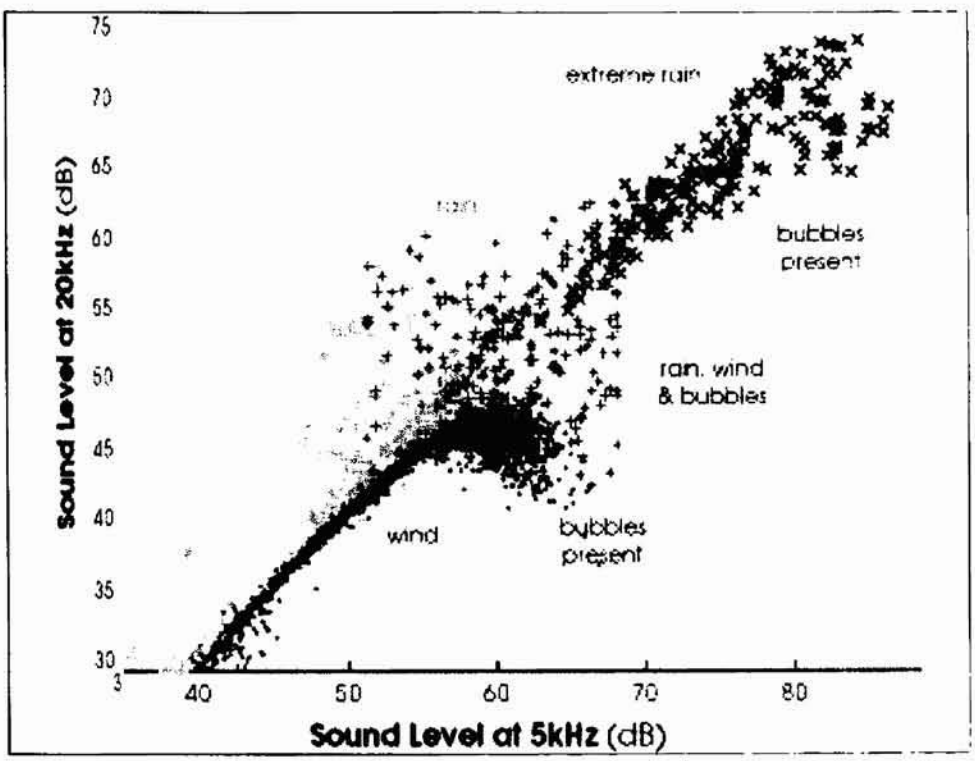

Fig. 3.4: Acoustic weather classification uses features of the underwater sound spectrum to identify the sound source: wind (green), drizzle (light blue), rain (medium blue), extreme rain (dark blue) and to detect ambient bubbles. (Jeffrey A. Nystuen)

Most often, It is only needed to detect if the rain is convective or stratiform type. Black et al. (1997) proposed a discrimenent method based on the shape of the acoustic spectrum. Figure 3.4 shows that different rainfall types do have distinguishable characteristics, which can be detected.

It is also possible to classify rainfall events by measuring the DSD. Given the DSD, any moment of the drop size can be calculated by using the equation,

$$M_x = \int D^x N(D) dD, \tag{3.8}$$

where x is the order of the moment. The DSD expressions (for example Eq. 2.2 (Ulbrich, 1983)) can be fitted into any set of data to get the rainfall classified. N_0 and D_0 are the most promising parameters in classifying the rainfall. N_0 is likely to be the best measure to use to distinguish between the moderate convection and stratiform rainfall types [Nystuen, 2001].

One important aspect of acoustic analysis of rainfall is the high temporal resolution. The sampling area for acoustics measurement depends on the depth of hydrophone placed underwater and is very high than that for other in situ rain gauges. Hence, large sample size of rain can be obtained within a short span of time.

3.4.2 Noise in acoustic measurement

There may be many sources of underwater sound, which appears as noise while trying to measure rainfall using the Acoustic Rain Gauges (ARG). One of the key features of ARGs is their capability of recording sound levels over a wide range of frequencies, which can be used to distinguish between various possible sources of sound (Nystuen and Selsor, 1997). One of the major sources of noise in underwater is the wind. Wind induced waves can break up, forming white caps whose acoustic

spectrum is wide band. Figure 3.5 shows the acoustic spectra of underwater acoustic noise due to wind only and that due to rain.

When measuring the ambient sound in an open sea, acoustic signals from several sources may be present, such as rain, wind and associated breaking waves, shipping and biologics. First, a classification scheme is used to determine which sound sources are present. The presence of shipping or biological noise is flagged as contaminated, and for the remaining data, algorithms are used to invert the ambient sound to give rain rate and wind speed.

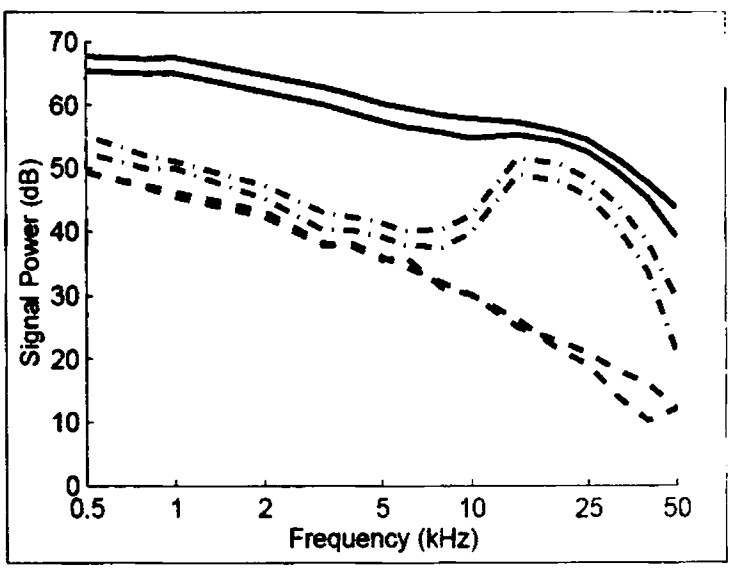

Fig. 3.5: Acoustic spectra generated by different environmental sources: wind only (dashed), drizzle (dash-dot), and heavy rain (solid). [Signal power is in dB re $1\mu Pa^2Hz^{-1}$]

In the absence of rain or nearby shipping, the underwater acoustic spectrum between 1 and 10 kHz is linear as shown in Fig. 3.6, with the intensity at all frequencies increasing with wind speed. A wind speed algorithm has been developed by [Vagle S et al. 1990] that uses the intensity at 8 kHz, as this frequency is immune from sounds of distant shipping and light rain.

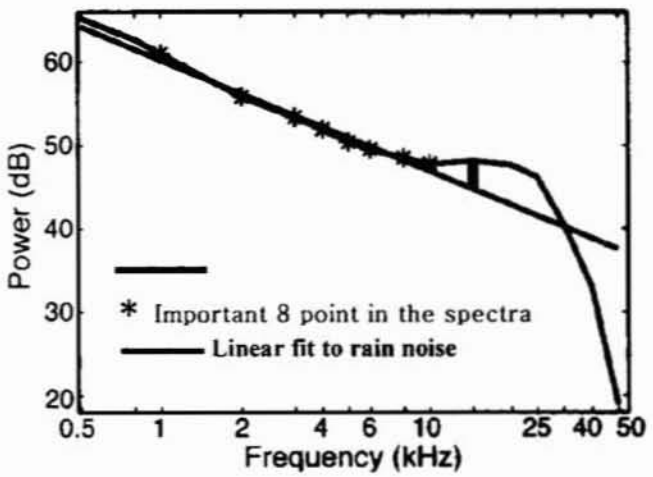

Fig. 3.6. Illustration of underwater spectra associated with rain. The blue line shows all frequencies recorded; the green line is a linear fit to the 8 values in the range 1-10 kHz (highlighted by the red asterisks). The grey bar indicates the enhancement at 14.5 kHz due to the 'drizzle peak'.

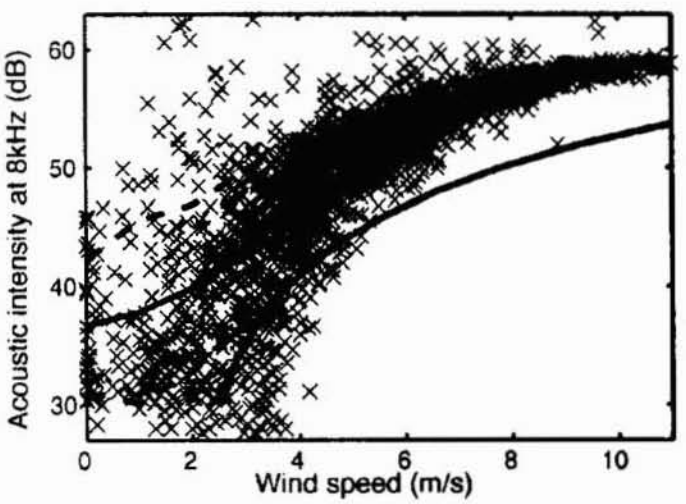

Fig. 3.7: Scatter plot of acoustic intensity at 8 kHz as a function of wind speed. Blue crosses indicate individual 10-min averages, with the solid red line showing the mean relationship, and the dashed lines indicating the spread (±1 std. dev). The solid black curve gives relationship noted previously for the deep N. Atlantic [Vagle S et al].

The acoustic signal level observed at 8 kHz shows (Fig. 3.7) a close correlation with the wind values from the meteorological buoy, having very little spread in the acoustic values at high wind speeds. However, the mean relationship is about 7dB higher than that expected.

3.5 Weather Classification Algorithm

Before estimating the rain parameters, it is necessary to identify the source of the acoustic signal. This is possible because of the characteristic spectra associated with each sound source. Wind for example produces breaking waves and spray on the ocean surface, hence giving rise to a broad band effect, with a typical spectral decay of -19 dB/decade [Vagle et al. 1990]. Drizzle produces the same spectra under 10 kHz, but gives rise to a peak at around 14 kHz. This is due to the small diameter (0.8-1.1 mm) raindrops present in light rain, which produce sound in this frequency by the ringing of small bubbles generated by the raindrops. Medium sized raindrops (diameter 1.1- 2.2 mm) are too big to generate small bubbles and so make no significant contribution to the spectrum. Heavy rain however comprises small, medium and large bubbles, and hence generates sound by ringing and by the noise associated with large raindrop impact. Heavy rain therefore augments the sound intensity at all frequencies in the range 4-21 kHz, producing a plateau in the spectrum. Because of this spectral characterisation, it is possible to separate the contributions due to wind and/or rain from other sources, and hence classify the acoustic signal as shown in Table 3.2.

Table 3.2: Weather classification table [Nystuen 1996]

Classification	Description
1	Wind only, low sea states
2	Wind only, high sea states (bubble clouds present)
3	Wind with drizzle
4	Heavy rain
5	Contamination

Having classified the sound source, the ARG then applies algorithms to infer wind speed and rain rate. Wind speed measurements use the algorithm developed by Vagle et al. (1990) to determine wind speed estimates from the sound intensity at 8 kHz. This algorithm is limited to wind speeds of greater than 2.1m s^{-1}, since below this wind speed there are no breaking waves or wavelets, and hence no sound is generated. This wind estimate is made for all wind conditions, that is, classifications 1 to 3 [Nystuen 1996]. In the case of drizzle, a rain rate of 1 mm/hr is assigned, since no inversion is possible due to the effects of wind. For heavy rain, two possible rain rate algorithms can be applied. The first is a simple empirical relationship to the acoustic intensity at 5 kHz. The second uses the intensity at every frequency bins in the 16-channel range to infer DSD, describing the proportion of drop sizes present, and calculates a rainfall rate from this. The inversion coefficients used by the *Metocean* system were tuned for a brackish pond near Miami [Nystuen, 1996], where rainfall estimates were found to show deviations from expected values, leading to the suggestion that the coefficients for this inversion are regionally specific.

3.6 A typical Acoustic Rain Gauge

A practical ARG produced by *Metocean Ltd of Nova Scotia*, comprises of a sensor that incorporates a sub-surface hydrophone, deployed at a depth of 20 m, providing a sampling area of approximately 1200 m^2. (If absorption and refraction are neglected, the acoustic intensity is independent of depth). The hydrophone samples the underwater sound spectrum in 16 bands spanning 500 Hz to 50 kHz, and carries out on-board processing to classify the sound source and then calculates the rain rate as well as wind speed.

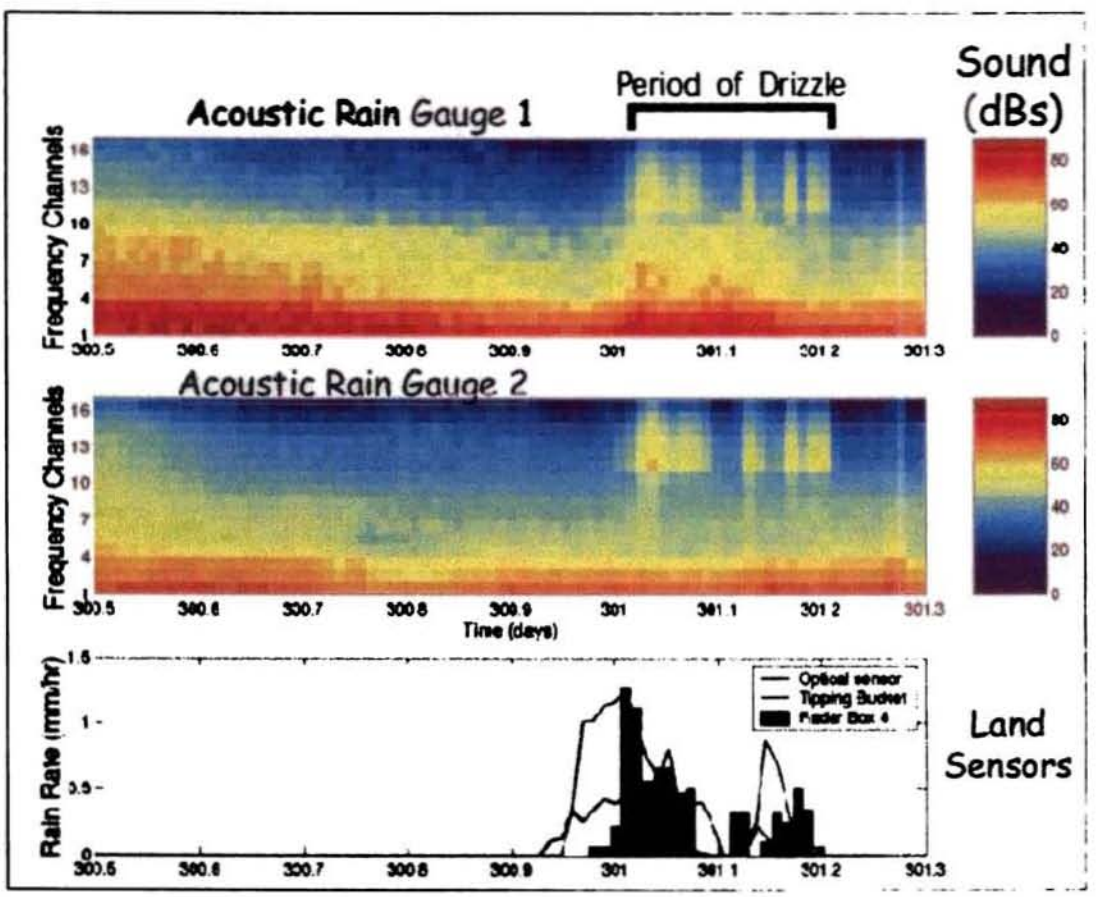

Fig. 3.8: Drizzle signatures in acoustic spectra

The system also incorporates a surface-mounted package to measure air pressure and air/sea-surface temperature. The hydrophone is suspended from a surface float by a [illegible] with a terminal weight suspended below the hydrophone to maintain depth.

Figure 3.8 shows the characteristic acoustic signature of drizzle. Drizzle is composed of tiny raindrops (diameter 0.8mm) that produce sub surface bubbles as they hit the sea surface. The bubbles oscillate, producing a loud ringing sound with a peak at 14.5 kHz (channel 10). Figure also shows the corresponding land sensor reading that was used to validate the presence of drizzle for the same time period.

The number of channels used for ARG depends upon the inversion algorithms used. Although the technology for detecting and measuring underwater noise spectra are well known, the algorithms for acoustic classifications are being modified for improving the measurement accuracy.

3.6.1 Measurement of rainfall using acoustic rain gauge

Results of many experiments with ARGs have already been published and established the effectiveness in employing the same for rainfall measurement. Figure 3.9 shows a comparison between different sensors used to measure rainfall event. This experiment was performed at Southampton Oceanography Centre, Empress Dock, Southampton.

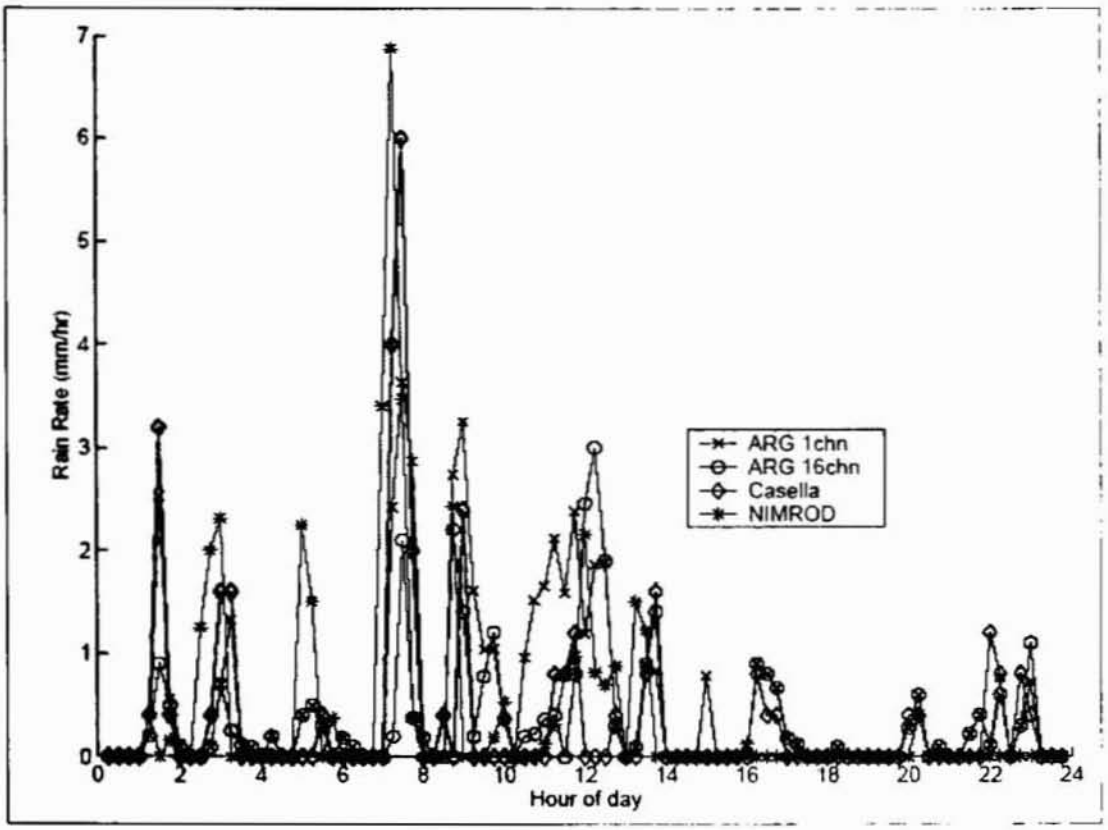

Fig. 3.9: Inferred rainfall rates for ARG, *Casella* and *NIMROD* systems
(Courtesy: *Southampton Oceanography Centre, Empress Dock, Southampton*)

Accuracy of the measurement is greatly affected by the presence of wind and other noises present in the acoustic spectrum. Monahan and O' uircheartaigh (1986) have shown that wave breaking does occur well below the perceived wind speed threshold of 5 m s^{-1}; however, the amount of bubble formation for low wind speeds is minimal. The sound generated by these bubbles covers the range from 3.5 kHz to 30 kHz, with a simple spectral shape s shown in Fig. 3.10 over almost the entire range. The spectral slope is typically about -17 dB/decade. The noise level can be wind is given by:

$$NL \approx 92 + 16 \log_{10}(u_{10}) - 17 \log_{10}(f),\ u_{10} > 2\ m\ s^{-1} \qquad (3.9)$$

where u_{10} is the wind speed (in m s^{-1}) at 10 m above the surface, and frequency, f is in [illegible] dependence on wind speed below 2 m s^{-1}, due to the [illegible]. At high wind speeds (> 10 m s^{-1}), a layer of bubbles [illegible] signals above 10 kHz; thus, Eq. (3.9) is no longer valid for high frequencies and in high wind speed conditions.

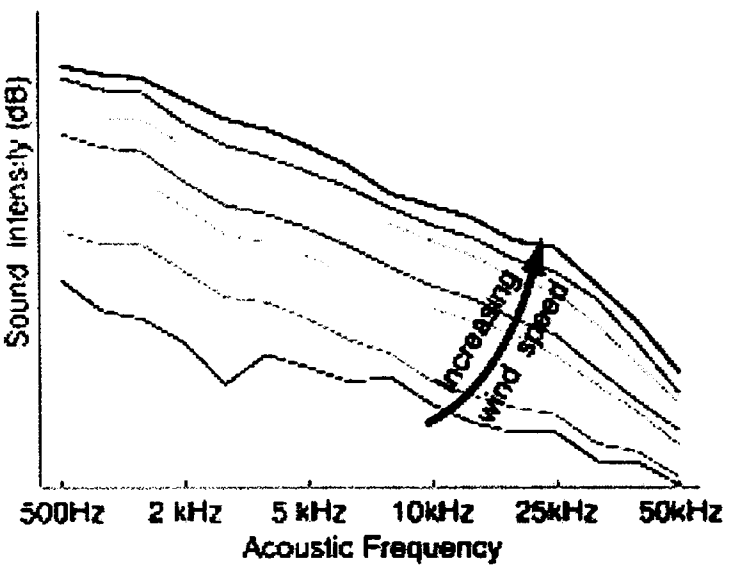

[illegible] Sound level generated by wind increases with wind speed and decreases with frequency

3.6.2 Problems encountered in measurement

One major problem encountered in this type of measurement technique is that not all the drops produce bubble underwater. One of the major drawbacks of this measurement technique is that bubble is not always produced and the bubble [illegible] on many other variables like surface tension, salinity and drop diameter. Hence, necessary corrections are to be applied for eliminating the error contributed by the silent drops. Another serious difficulty is the effect due to

secondary drops. Falling drops and bursting drops can produce jets called the Worthington, or Rayleigh Jet. Jet production is influenced by [illegible] such as the surface tension. The production of jet is illustrated [illegible] in Fig. 3.11 The jet after formation will break up, generating [illegible]

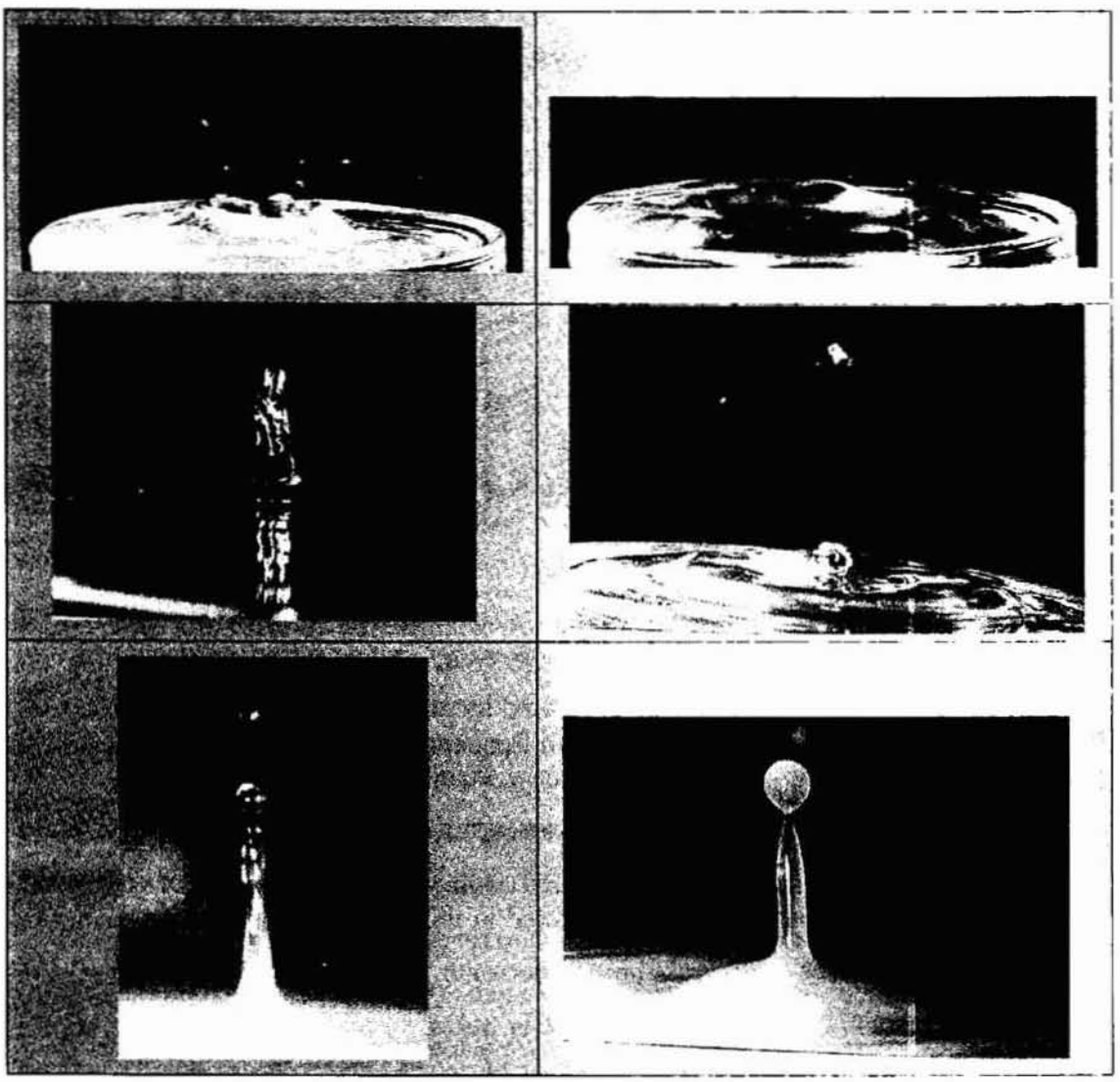

Fig. 3.11: The jet produces secondary droplets. The radius size of the first droplet produced is about one tenth of the drop that produced the jet [D. E. Spiel, 1995].

A drop impacting on water surface can thus generate secondary droplets, which will fall on to the water surface and creating secondary bubble. Secondary [illegible] jet formation and this process is repeating in nature as evident from the series of photographs shown in Fig. 3.11. Since the jet formation is [illegible] the bubble signal will not be unique for same size of drops at different situations that depends upon surface tension, temperature, etc.

Another important aspect is that the bandwidth required for processing the signal. Since the bubble noise lies in the frequency range of 14 kHz to 25 kHz, the [illegible] the signal is high. The entire bandwidth of the signal [illegible] (16channel ARG) and processing is done for every [illegible] cross-correlation is performed to classify the rainfall. This process is very complex. Because of the intensive processing requirement, conventional ARGs are not capable of continuously processing the rain noise. Instead, the processing is done intermittently, say every 1.5 minutes interval.

3.7 Summary

[illegible] of the distinct features of the underwater noise spectra (in the range of [illegible] due to rain it is possible to extract rain parameters from the acoustic noise. A suitable hydrophone immersed in water can be used to capture the signal and special processing techniques (acoustic inversion technique) can be employed to estimate rain. This method is extremely useful in detecting rainfall over the ocean where [illegible] of measurement is successfully employed. Accuracy of such measurements is affected by noises like, biological noise, wind noise, etc. Even though

such systems can be employed in classifying the weather. It is also more perfect. Researches are continuing in this direction and perfecting the rain measurement algorithm to measure rain accurately. ARGs are being used in various experimental stations.

Chapter 4

Methodology

A discussion of the experimental set-up to capture and analyse the drop generated underwater sound is discussed in this chapter. A sensor assembly in conjunction with a drop generating mechanism has been used to investigate the rain-generated noise under controlled conditions in a laboratory. The signals captured were analysed and found to agree with the results published in open literature. Thus the effectiveness in using this experimental set-up for further studies was ensured. Field experiments were then carried out to capture and analyse the rain generated acoustic signal. One important observation that was made during these experiments is the identification of the presence of a low frequency component in the acoustic noise whose amplitude depends on the drop size.

An experimental set-up to study the acoustic nature of the drop-generated signal underwater has been designed. This set-up consists of a suitable underwater transducer, drop generating mechanism, which can generate drops of different measured dimensions, hardware for the data acquisition and processing systems. The sensor assembly was found suitable for capturing and analysing the rainfall. Upon analysing the signals captured, it was noticed that there is a low frequency component in the acoustic spectrum that was not reported in the open literature. The results

reported in open literature discusses the high frequency signals in the range of 10 kHz to 25 kHz, while certain reports describes the occurrence of low frequency noise due to the rain impact, [Nicolaas BOM (1969)]. He had conducted studies in the frequency range 300 to 9600 Hz. Further studies on the low frequency component of the acoustic signal revealed that it is possible to extract drop parameters and rainfall parameters from these low frequency spectra.

4.1 Development of a Rain Sensor for Capturing Acoustic Noise

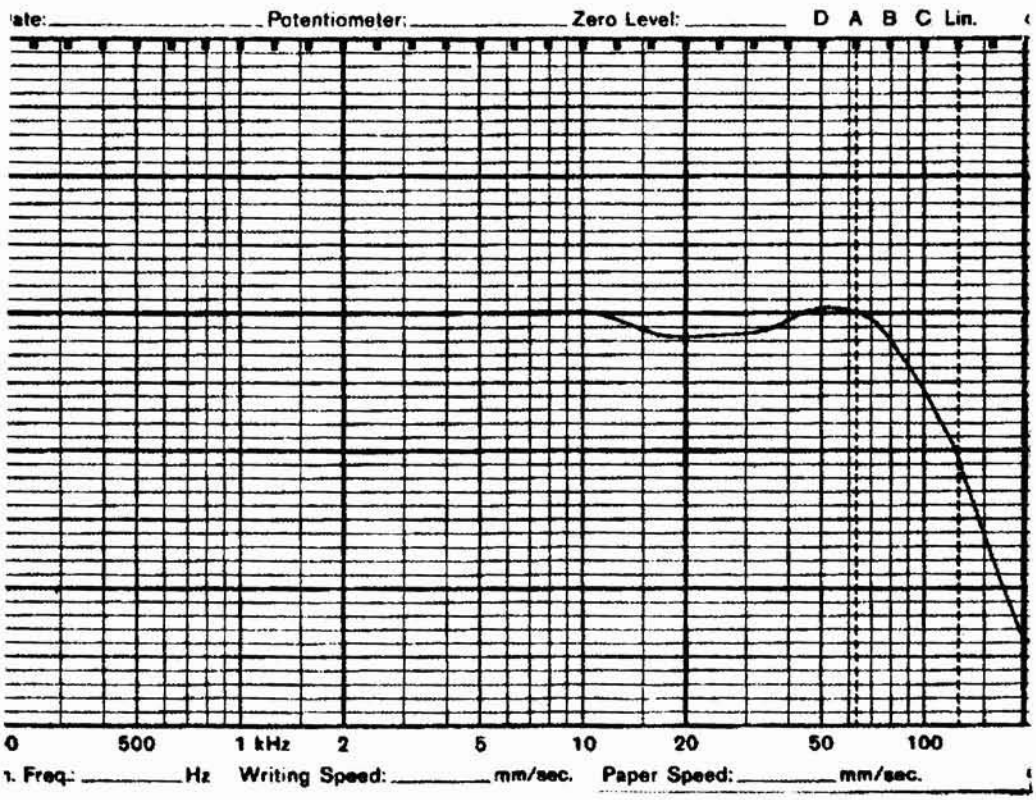

Fig. 4. 1: Response characteristics of B&K 8103 transducer

Since the acoustic spectrum of rain noise extends up to 100 kHz, a wide band flat response hydrophone is selected. At first, experiments were performed with

different hydrophones by immersing them in water and to capture the acoustic noise due to the drop impact. The signals captured by the sensors for water drops falling in water was captured and analysed first. Finally, a B&K hydrophone (B&K 8103) was found suitable because of its small size and flat frequency response (Fig. 4.1).

4.1.1 Initial experiments

Experiments were carried out under laboratory conditions by using container of moderate dimensions. The container is filled with water and a hydrophone is suspended inside to capture the acoustic signal produced, when drops are falling into it. Experiments were conducted by dripping drops of different sizes into the water from different heights.

It was observed that the spectrum of the drop-generated signal contains a predominant low frequency component. The amplitude of this low frequency signal was found to vary with the drop diameter and the height from which the drops are falling. The frequency was found to be stable irrespective of the drop size and the height from which the drop is allowed to fall. Later it was confirmed that the low frequency component in the acoustic spectrum is narrowly tuned and the frequency varies with the size of the container in which the sensor was immersed (Table 4.1).

Table 4. 1: Effect of Physical dimension of the container on the low frequency acoustic signal in the Acoustic noise captured by the sensor

Container details	Frequency	Remarks
PVC 35 Cm Dia round	15Hz	Depth of water = 30cm
PVC 25 cm Dia round	18- 19 Hz	Depth of water = 30cm
PVC 20 cm Dia conical	31 –34 Hz	Depth of water = 20cm

Since the rain capturing area depends on the opening of the container, a chamber having standard 20cm diameter opening was selected for further experiments.

4.1.2 The sensor chamber:

The sensor chamber is responsible for:

(i) Providing sufficient water surface area for the drops to fall

(ii) Providing secure mounting of the sensor assembly

(iii) Preventing the picking up of external acoustic noise.

(iv) Allowing efficient pick-up of the acoustic signals produced by rain.

To make the system rust proof and to reduce the effect due to the change in dimensions due to temperature variations, the material for the chamber is selected as PVC. A schematic of the sensor assembly is shown in Fig. 4.2. It consists of a conical funnel shaped rain-capturing chamber of mouth radius about 20 cm with a narrow nozzle of 15-mm diameter that holds the transducer. The transducer is mounted by using rubber grommets so as to prevent picking up of the vibrations through body of the chamber.

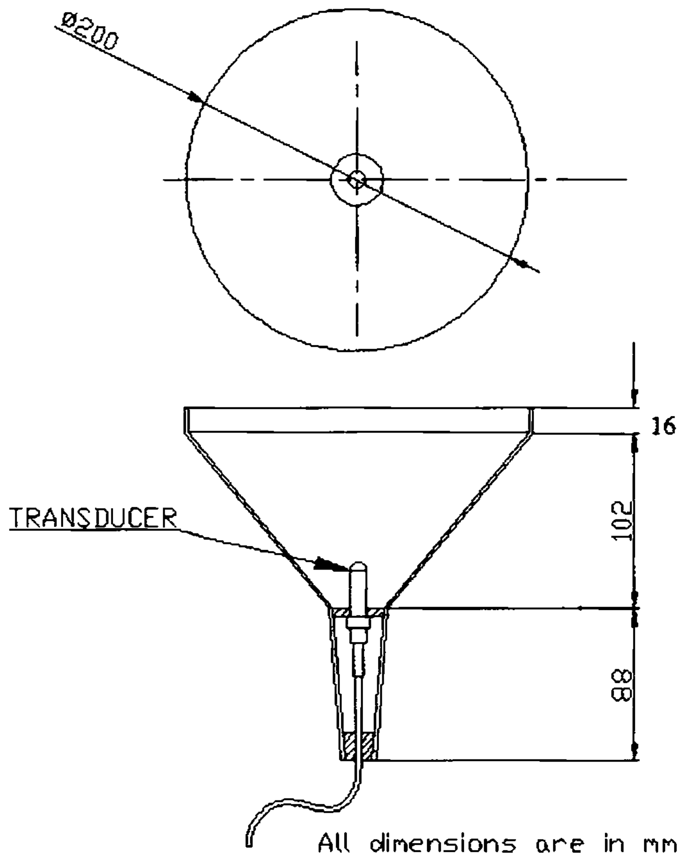

Fig. 4.2: Sensor assembly

4.1.3 Analogue Signal processing

The sensor output voltage is very low and hence need to be sufficiently amplified. Hence a wide band amplifier with flat passband performance in the range of DC to 100 kHz is has to be used. B&K charge amplifier Model 2635 was found suitable for this application. Frequency response characteristics of the 2635 amplifier are as shown in Fig. 4.3. The experimental set up is explained in the next section.

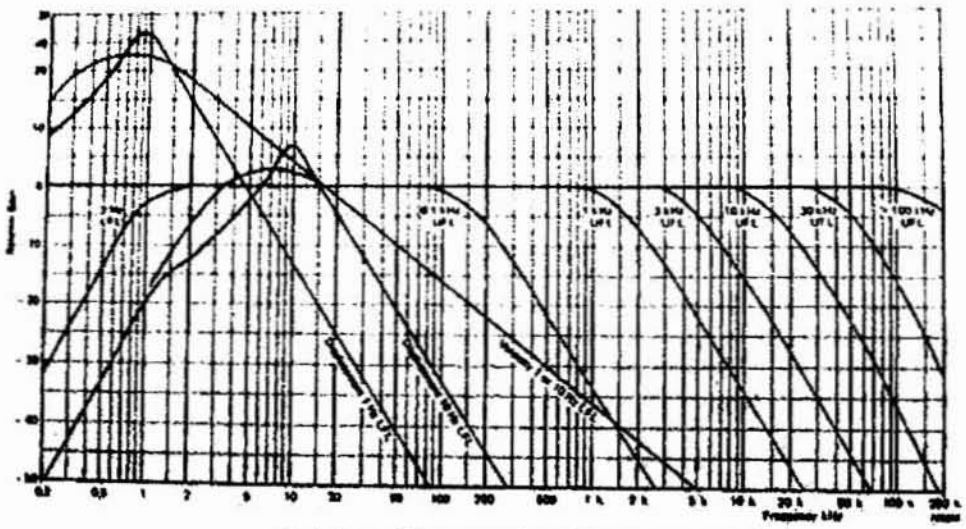

Fig. 4.3: Overall frequency response of the 2635

4.14 Experimental set up

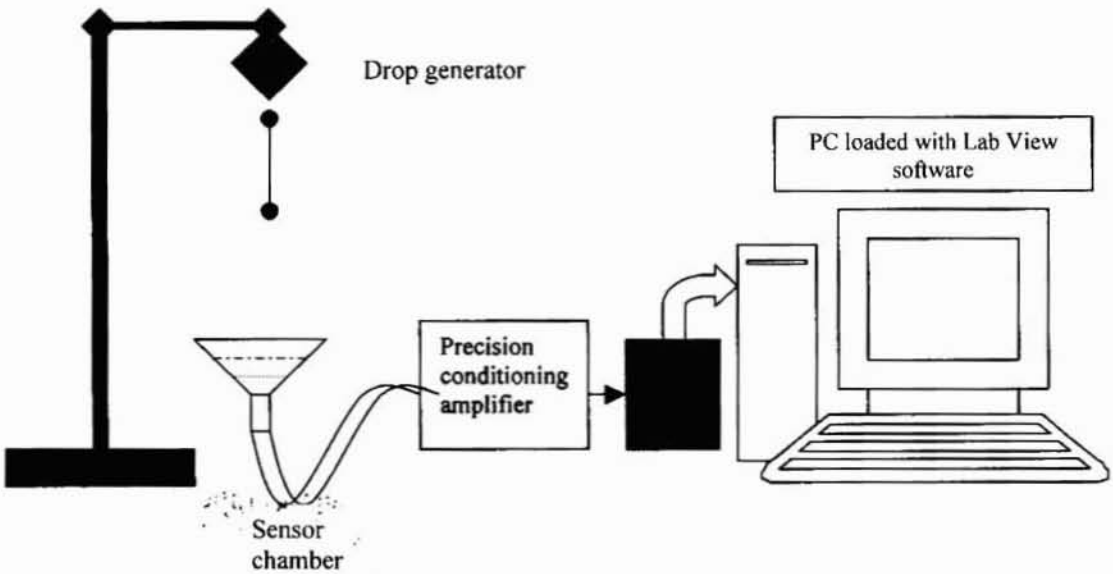

Fig. 4 .4: Experimental set up

The sensor chamber is kept in the upright position to allow raindrops falling into the water surface. As the droplets fall into the chamber, the acoustic signal generated is picked up by the transducer and is converted into electrical signals. The set-up is as shown in Fig. 4.4.

A precision signal conditioning amplifier, 16-bit data acquisition system with 200,000 samples per second alongwith support software has been used for the initial experiments.

4.1.5 Drop generation mechanism

In order to improve the measurement accuracies the set-up should be capable of generating droplets of the desired diameter. Many methods for drop production were tried and the method using syringe together with hypodermic needles was found to yield very accurate and reproducible results. In this method, the syringe is filled with water and by applying controlled pressure on the piston, droplets are released from the tip of the needle. The diameter of the drop produced depends on the nozzle size. The sequence of drop production process is as shown in Fig. 4.5. The liquid at first bulges from the end of the needle then elongates, forming a "neck." As the bulge descends, the neck stretches, depending on the liquid's viscosity and other variables, until it snaps free of the main body of liquid in the capillary. The bulge forms the main drop; the neck, however, forms a much smaller droplet, called a satellite. The satellite drops can cause problems if not carefully applied the pressure on the piston. For all drop experiments, manually released drops are used.

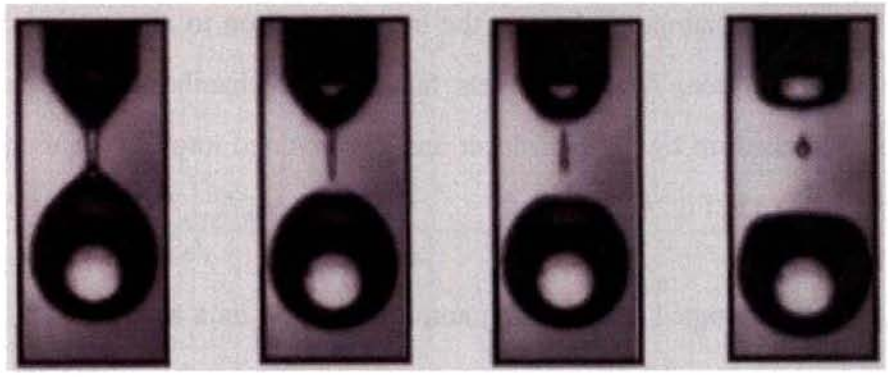

Fig. 4.5: Release of drops from needle

Nine different sizes of drops are produced for the experiments. The effective diameters of the drops are calculated by counting the number of drops produced for 10 ml of water in the syringe.

Table 4.2 Calculation of effective diameter of the drops produced

Number of Drops	Drop diameter (mm)	Number of Drops	Drop diameter (mm)
932/ml	1.2	250/10 ml	4.24
236/ml	1.27	158/10 ml	4.95
117/ml	2.54	108/10 ml	5.62
45/ml	3.48	37/10 ml	8

4.2 Measurements under Laboratory Conditions

The experimental set up described above was used to capture the signal when drops are allowed to fall into the chamber. The sensor chamber is filled with fresh water and drops of different dimensions are allowed to fall into the water surface from various heights. Captured signal is high pass filtered using a digital filter with a cut-off frequency of 500 Hz to avoid low frequency noise signal including the power supply hum. A typical drop generated signal is as shown in Fig. 4.6.

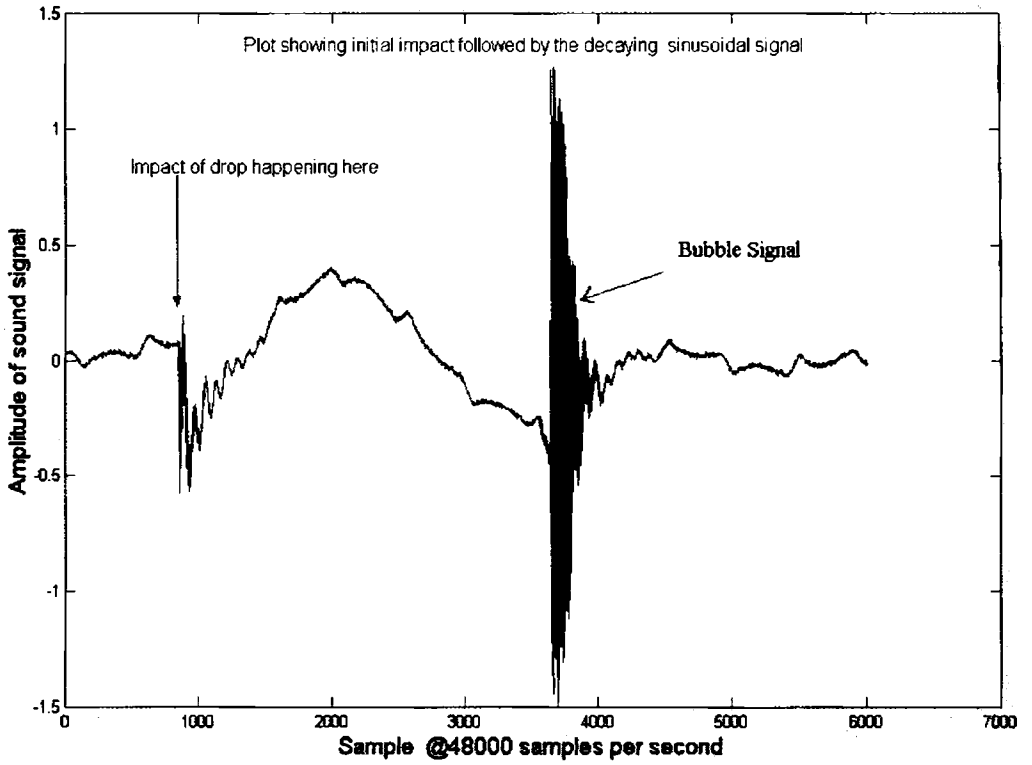

Fig. 4.6: Spectrum of signals produced by droplets of different diameters

It is seen that the impact of drop produces signal with a sharp change in signal level that quickly diminishes (within few hundred microseconds). The impact generates disturbances and the impact energy radiates as a pressure wave. The air trapped inside the water forms an air bubble. This bubble formation takes place few microseconds after the impact. The bubble oscillates producing a high frequency signal (hereinafter this bubble produced signal will be called as the bubble signal and the corresponding frequency as bubble frequency). The bubble signal in Fig. 4.6 is occurring after a time interval of few microseconds, which is confirming to the theory explained in the previous chapter.

The bubble signal was observed to be purely sinusoidal and sharply tuned to a narrow frequency band, The dependence of the frequency of the bubble signal on the drop sizes was studied using different drop sizes. It was observed that the bubble frequency increases with decrease in drop size that produces the bubble as evident from Fig. 4.7. The absence of low frequency components in the Fig. 4.7 is because of the high pass filtering employed whose lower cut off frequency is 500 Hz. It is also observed that the bubble signal strength also varies with the height from which the drop is falling.

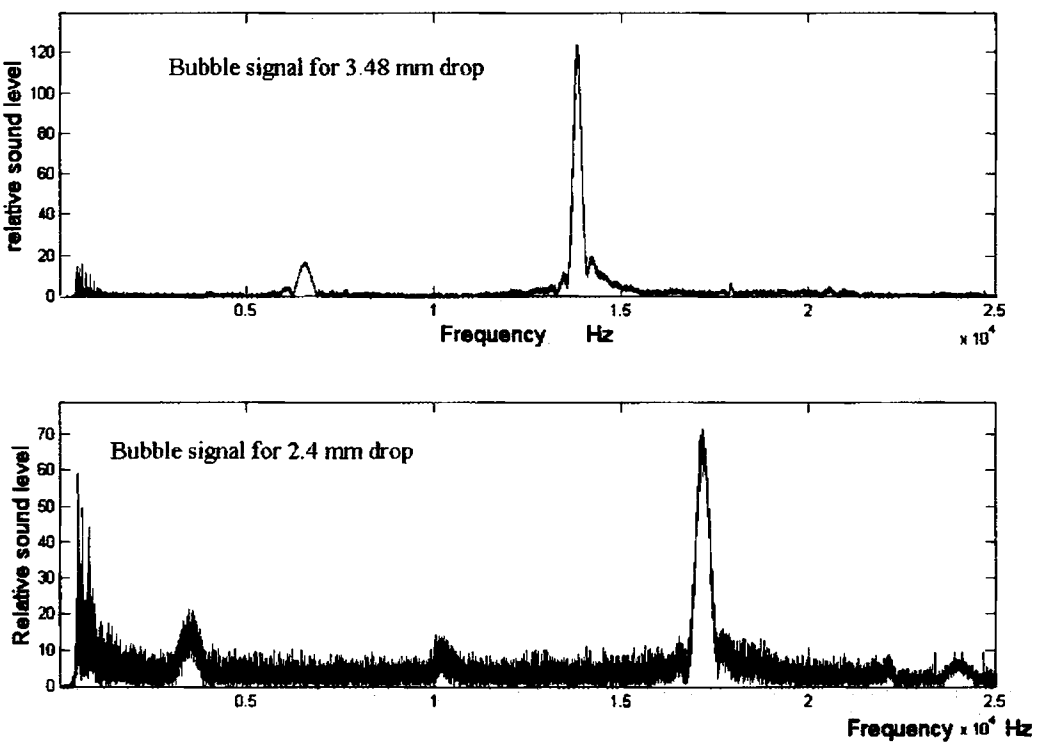

Fig. 4.7: Spectrum of signals produced by drops of different diameters.

Elaborate observations were performed under laboratory conditions as well as in controlled environment outside the laboratory, to study the drop impact at various

impact velocities including the terminal velocity of drops. Laboratory studies included the effect of salinity of the water in the acoustic noise produced by the droplets [T.K. Mani and PRS Pillai, 2002].

4.3 Field Experiments

In order to acquire terminal velocity for the drops released by the drop generation mechanism, the drops must be released from a height of more than 20 meters. A twelve-storied tall building was identified for this purpose. The initial experiments conducted at this building were unsuccessful, due to the presence of turbulent air in the drop passage. This turbulence was found to be due to the updraft of the air and the problem was solved by performing the experiments in the closed chamber constructed for the purpose of installing lift car for this building.

4.4 Observations

The following observations were made that confirmed the effectiveness of the sensor assembly in capturing the acoustic signal generated by the droplets falling in water:

i. The sensor assembly is very efficient in capturing the acoustic pressure variation produced by the falling drops.

ii. Acoustic spectrum obtained agrees with the results published in open literature.

iii. Effect of ambient noise is negligibly small.

iv. It was noticed that the sensor assembly captured the blasting sound produced by the lightening thunder.

v. The bubble signal was not always present confirms the fact that certain droplets does not produce the bubble.

vi. There is a very strong, sharply tuned low frequency component in the drop-generated noise. A detailed study of this phenomenon is attempted in the proposed work.

4.5 Low Frequency Spectrum

One of the most important inferences gathered from the results of the drop experiments using the sensor assembly is the observation of the low frequency component in the acoustic signal, which was not reported earlier. Research findings reported in open literature describe the spectral behaviour of the rain-generated noise in the range of 500 Hz to 50 kHz [Pumphery et al (1989); Medwin et al. (1992); Quartly et al. (2000)]. One of the drawbacks of this method is that all the drops do not produce a bubble and hence some drops are categorized as "silent," which introduce errors in rain rate estimation.

However, few studies have been reported at frequencies below 600 Hz. It has been observed that the spectral energy of the acoustic signal captured by the sensor assembly mainly lies within this low frequency region. Hence, studies were confined on this low frequency behaviour of the drop generated signals. It was observed that the amplitude and duration of the low frequency signal in water at the impact site is related to the kinetic energy of the droplet producing the wave.

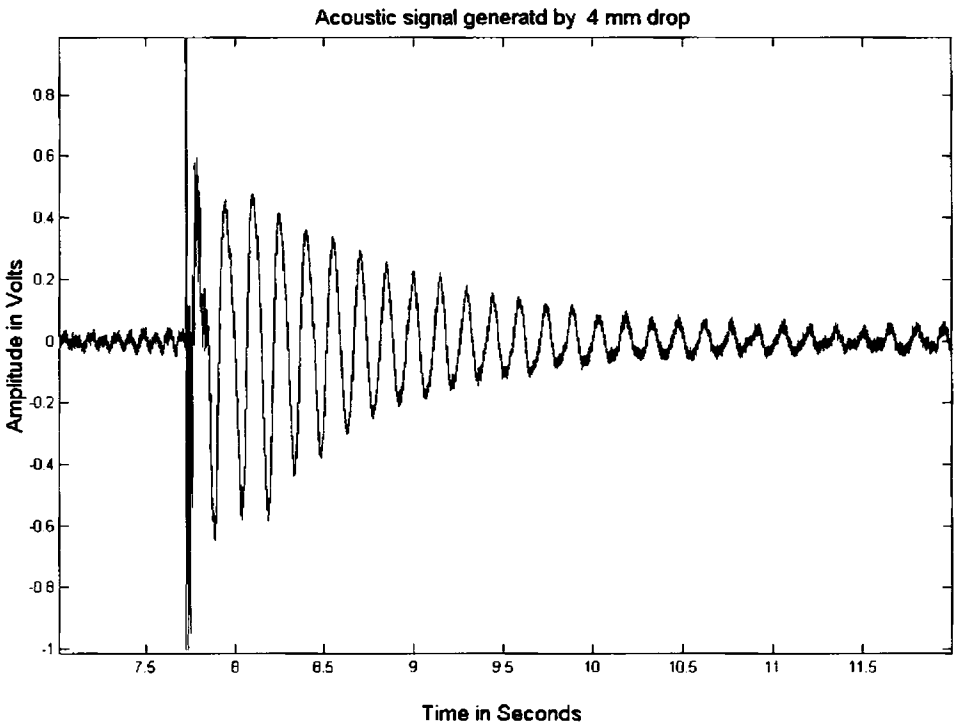

Fig. 4.8: Acoustic signals generated by a single drop (at the output of the amplifier)

Figure 4.8 shows a typical signal captured when a drop hits the water surface in the sensor chamber. The signal is sharply tuned to a low frequency that slowly damps out. A detailed discussion on the nature of the signal is carried out in the forth-coming chapters.

4.6 Summary

A sensor assembly capable of capturing the pressure variations near the impact site has been developed. It has been observed that the sensor assembly captures the near field hydrodynamic pressure variations, the impact sound as well as the bubble sound. The sensor assembly has yielded repeatable and reproducible results. It was observed that the low frequency signal present in the acoustic spectrum is related to the kinetic energy of the drops.

Chapter 5

Experimental Results and Discussions

Measurements were carried out with the experimental setup described in chapter 4. The experimental measurements were conducted under laboratory conditions as well as in the field. A series of experiments were conducted (over a period of three years) during the monsoons and the signals were analysed. Experimental determination of the rainfall rate and DSD of rain were carried out and the results of measurements were compared with the standard rain gauge measurements. Relationship between the rain kinetic energy and the energy of the low frequency component in the rain has been established. Based on the analysis, a method for measuring the rain parameters from this low frequency acoustic signal has also been developed. Results and analysis of these experiments are presented in this chapter.

5.1 Kinetic Energy of Raindrops

It was already reported by various researchers [Pumphery et al (1989); Laville et al, (1991)] that the initial impact pulse produced by the droplet consists of two components, the first being a sharp leading edge, which is the true radiated sound that exists only for a short duration of about 10 to 40 μsec., while the second component is a damped pressure wave. The pressure variation that follows the leading edge is a near field hydrodynamic effect related to the flow established near the impact site. Consider a single drop falling into the sensor chamber. The energy delivered to water in the chamber is given by

$$E = \tfrac{1}{2} m V_i^2 \tag{5.1}$$

where m is the mass of the drop and V_i is the velocity with which it is impinging on water.

Under stable atmospheric conditions, a raindrop of diameter D falling to the earth will attain the terminal velocity before it impinges on the water surface. Several factors influence the speed of raindrops falling through the atmosphere. For very large drops, the terminal velocity, V_T is proportional to D^2 [H. Sauvageot, 1992]

5.1.1. Terminal velocity of drops

When hydrometeors fall, equilibrium is quickly established between the gravity force acting downwards and aerodynamic drag acting upwards. The resulting velocity is called the terminal velocity, or fall speed, V_T. In 1949, Gunn and Kinzer empirically determined a relationship between the velocity of water drops and its diameter in stagnant air at sea level [Gunn and Kinzer 1949]. The relationship is mathematically expressed as

$$V_T(D) = 9.25\left[1 - e^{\left(-6.8D^2 - 4.88D\right)}\right] \text{m/sec} \tag{5.2}$$

where D is in cm. This formula is valid for diameters ranging from 0.5 to 6 mm for an acceptable fit. This formula must be corrected to account for the air density decrease as the altitude increases. Several other relationships have been developed as the ones of Atlas (1973), Beard (1976) and Atlas-Ulbrich (1977) which is valid over a range of drop sizes. Widely accepted Terminal velocity - drop size relationships are as shown:

$$V_T(D) = 9.65 - 10.3e^{(-0.6D)} \tag{5.3}$$

$$V_T(D,P_0)=\begin{cases}0;\Rightarrow D\le 0.03mm\\ 4.323(D-0.03mm);\Rightarrow 0.03mm<D\le 0.6mm\\ 9.65-10.3\exp(-0.6D);\Rightarrow D>0.6mm\end{cases} \quad (5.4)$$

$$V_T(D)=.0561D^3-0.912D^2+5.03D-0.254 \quad (5.5)$$

The equation 5.5 closely agrees with the other more complex equations and with experimental data available.

Since it is easy to compute the terminal velocity of drops using the Eq. 5.5 and it also closely agrees with the measured values, this equation is selected for computing the terminal velocity of drops, throughout this work. The Fig. 5.1 Shows the variation of the Terminal velocity with drop size.

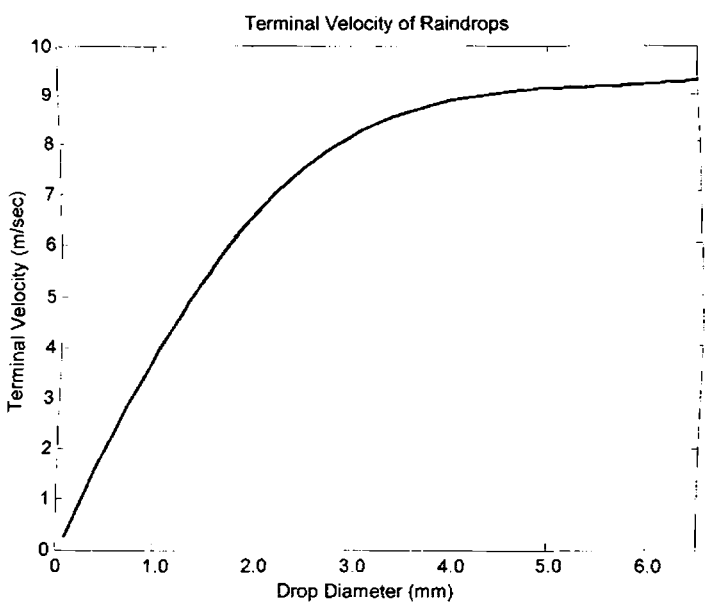

Fig. 5.1: Terminal velocities of raindrops drops (Eq. 5.5)

5.1.2 Kinetic energy computation

Kinetic energy attained by the drops at the time of impact can be computed from Eq. 5.1 by substituting the expression for terminal velocity in Eq. 5.5. This results in a 9^{th} order polynomial relationship. Figure 5.2 shows the computed energy variation with respect to the drop size. It should be noted that the 9^{th} order relationship with the drop diameter is not noticeable because of the fact that the coefficient of the higher order terms are very small.

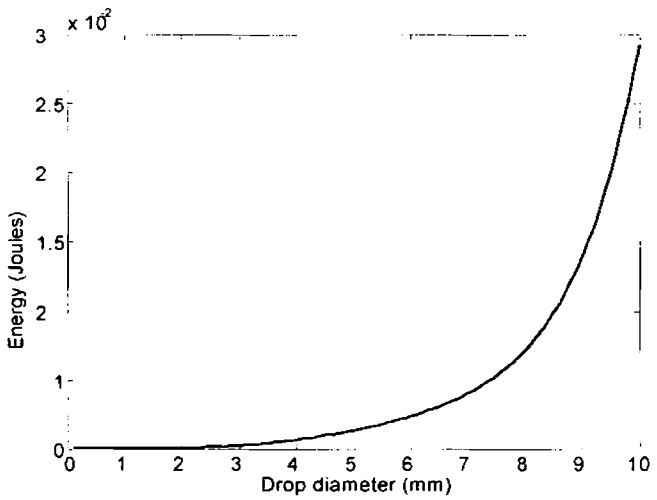

Fig. 5.2: Kinetic energy of raindrops (computed)

5.2 Drop Generated Signal and Acoustic Spectrum

The experimental set-up for generating the drops of desired sizes as explained in chapter 2 (see Fig. 4.2) was used to conduct laboratory experiments with water droplets. It was observed that the spectrum of the signal captured has a predominant low frequency component. Figure 5.3 shows the signal captured and its spectrum for a single drop falling in water. The time domain plot (Fig. 5.3a) of the signal shows

that the amplitude of the signal shoots up at the instants of impact followed by a slowly damping sinusoidal wave. The spectrum of the signal is split into two, the low frequency (from 0 Hz to 600 Hz) and high frequency spectrum (> 600 Hz), as shown in Fig. 5.3b and 5.3c respectively. The frequency spectrum of the signal shows a sharp peak at a frequency of about 32 Hz, which might be the resonant frequency of the sensor assembly. This frequency is found to vary with the dimensions of the sensor chamber of the sensor assembly. The spectral peak around 64 Hz is a harmonic of mechanical resonance frequency. It is also observed that maximum spectral energy lies below 600 Hz. Spectral peaks in the frequency range 13 kHz to 15 kHz due to bubble are negligibly low compared to the low frequency spectrum as evident from Fig. 5.3c. The underwater acoustic noise produced by the drops dies out quickly. The duration of existence of the signal generated by a single droplet depends on the damping effect of the sensor assembly. The damping action is mechanically adjustable with the clamping mechanism of the sensor assembly to the mounting bracket. Low damping causes the signal to diminish at a slow rate and is useful in observing single droplet generated noise while considerable damping is needed to decrease the *response* time in order to separate out the signals produced by a series of droplets falling into the sensor assembly.

It was also noticed that for certain drops the bubble signal [M. Minnaert, (1933)] was not observed, which confirms the fact that not all the drops produce air bubbles underwater. It was also observed that the low frequency spectrum is found to retain its shape with all drop sizes while the signal energy of each frequency component increases with increase in drop size.

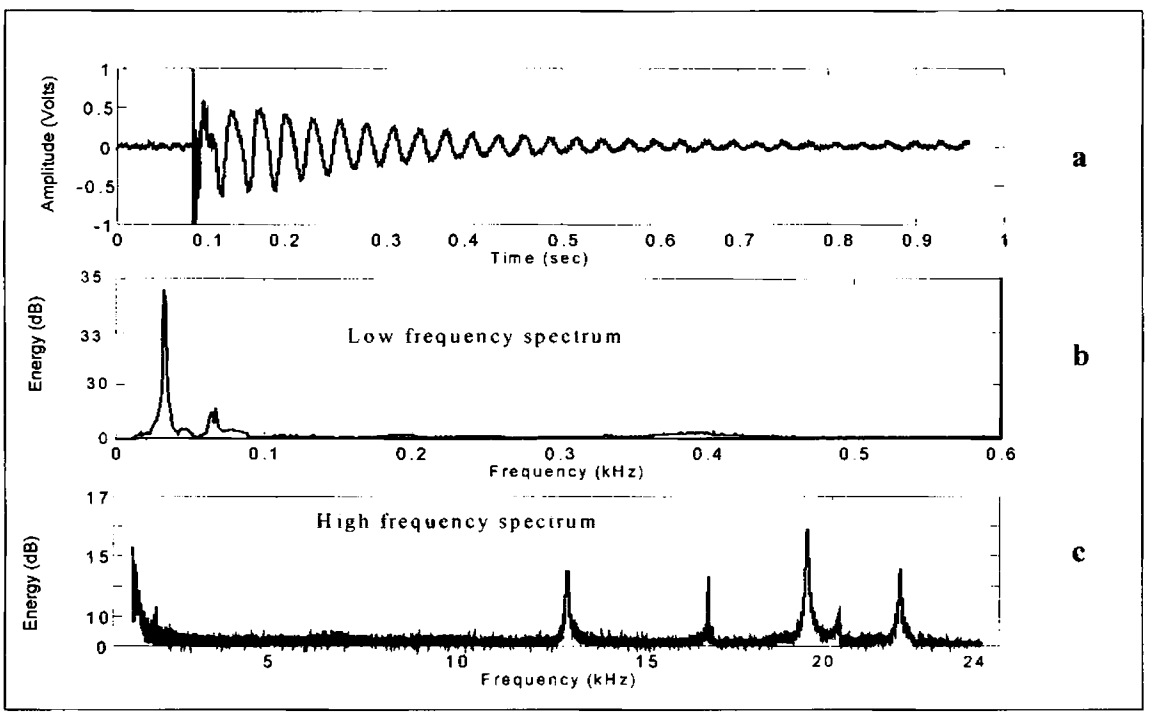

Fig. 5.3: (a) Rain generated noise, (b) Low frequency spectrum over the range of 0 to 600 Hz, (c) Spectrum beyond 600 Hz.

5.2.1 Impact generated noise signal amplitude

The peak amplitude of the acoustic noise captured by the sensor assembly was found to vary with the height from which the drop is allowed to fall. It was also observed that the noise amplitude also changes in accordance with the size of the drops. The Fig. 5.4 shows the effects of drop size as well as the height from which the drop is released, on the acoustic noise peak amplitude.

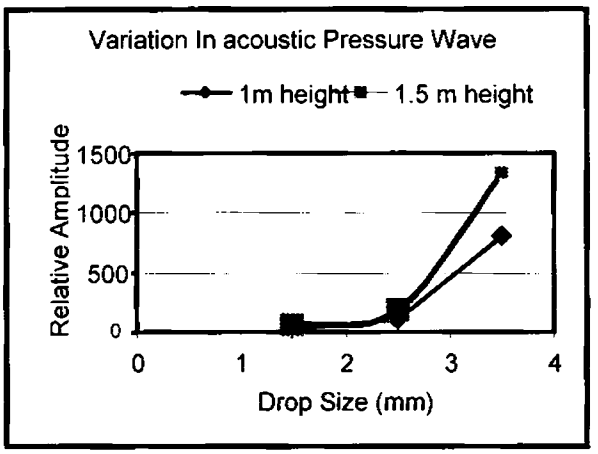

Fig. 5.4: Variation in amplitude of low Frequency pressure wave with drop size

5.2.2 Effect of salinity

Another important observation made was the effect of salinity of the water. The experiment was carried out with water of known salinity poured into the sensor chamber. Figure 5.5 shows that the acoustic energy captured by the sensor assembly decreases with the increase in salinity.

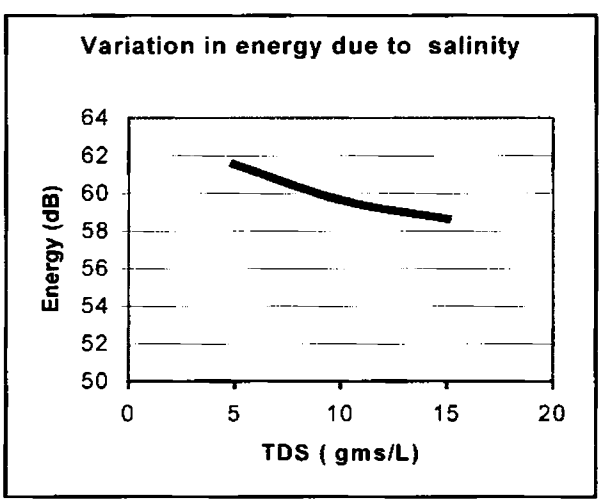

Fig. 5.5: Reduction of energy of acoustic noise due to salinity

5.3 Kinetic Energy of Drops Vs Rain Noise Energy

Experiments were carried out, by allowing the drops of different dimensions to fall into the water in the sensor chamber. Drop sizes and corresponding acoustic energy were tabulated. Acoustic energy was correlated with the computed kinetic energy of drops using the Eq. 5.1 and Eq.5.5.

A plot as shown in Fig. 5.6 indicates the correlation between the kinetic energy of the drops and corresponding noise spectral energy of the signal.

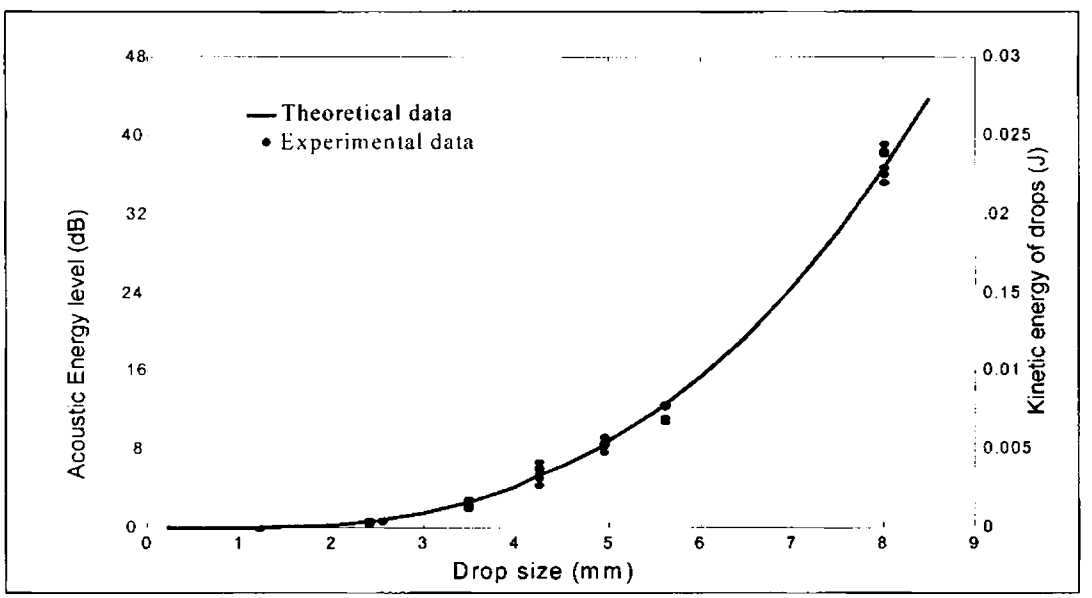

Fig. 5.6: Variation in energy of low frequency pressure wave with drop size

5.4 The Low Frequency Spectrum

As described in chapter 4, the low frequency content in the drop generated acoustic signal captured by the sensor assembly is very stable in frequency and this frequency depends on the physical dimension of the sensor assembly. This frequency

does not change with the drop size or with the terminal velocity of the drops. If the sensor assembly is not damped, then this low frequency is purely sinusoidal in nature where as if it heavily damped, then waveform becomes distorted that generates higher order harmonics of the fundamental frequency. Hence in order to accommodate the energy in the harmonic contents, the signal bandwidth up to 600 Hz is used for calculations. Similarly, to avoid the effect of drift, DC offset, etc., of the signal conditioning stage, frequencies below 10 Hz is avoided. Hence, the acoustic signal in the frequency range of 10 Hz 600 Hz is considered for computing the signal energy.

5.5 Rain Generated Signals

It is possible to estimate the size of the drops falling into the sensor chamber by analysing the acoustic signals captured by the sensor assembly. Hence, it is possible to measure the rainfall by capturing acoustic noise due to the rain by using the sensor assembly. In order to analyse the rain noise, the sensor assembly was exposed to the rain and the acoustic signal generated by the rain is measured. Raindrops falling into the chamber are in random and the time gap between the impacts of drops is of the order of a few milliseconds. To distinguish the signal produced by individual drops, the signal contributed by a drop should not be contaminated with signal produced by another drop, It was experimentally observed that if the signal due to one drop attenuates and vanishes within 20 milliseconds, then the effect of overlap of between two closely timed drops is minimum.

5.5.1 Analysis of rain generated noise

Various rainfall events were captured and recorded for analysis. Intensity of rainfall was also measured by using a standard tipping bucket rain gauge (TBR). The acoustic recording was synchronised and time marked with the tipping instants of the

TBR. A typical time domain plot of the rain noise for two rainfall rates is shown in Fig. 5.7.

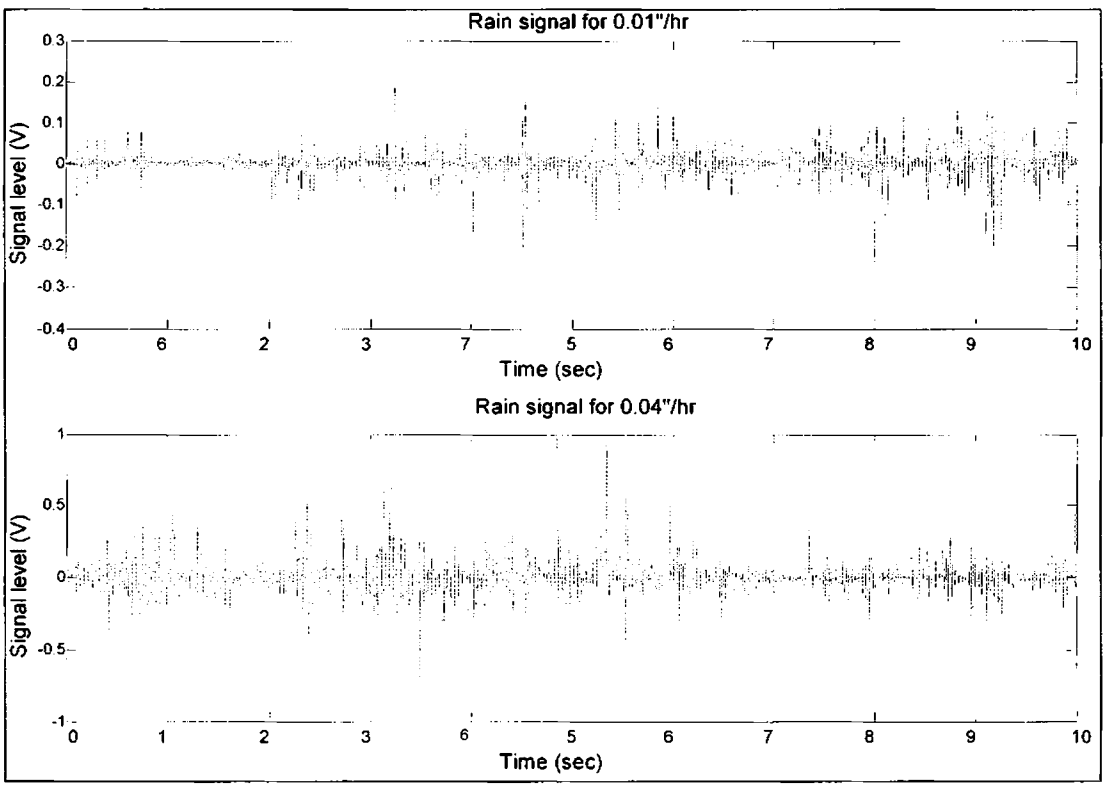

Fig. 5.7: Rain signal captured by the sensor assembly

The rain signal captured contains the low frequency sinusoidal pressure variations, high frequency bubble signal and the wide band impact noise. Figure 5.8 gives an in sight into the significant acoustic components in the rain signal. Figure 5.8(a) shows a portion of the rain signal in which contribution of drop impacts are distinguishable. A portion of the signal in between the time duration in between 0.38 seconds and 0.56 seconds are shown in an expanded time scale in Fig. 5.8(c). It clearly shows the impact; the low frequency pressure variation and the small duration bubble signal 0.4 seconds after the impact. This bubble signal is again shown in

Fig. 5.8(b). It is apparent from Fig. 5.8 that the energy contributed by the bubble signal is too low compared to that of the low frequency signal and can be neglected in computing the energy of the acoustic noise for the purpose of detection of raindrops.

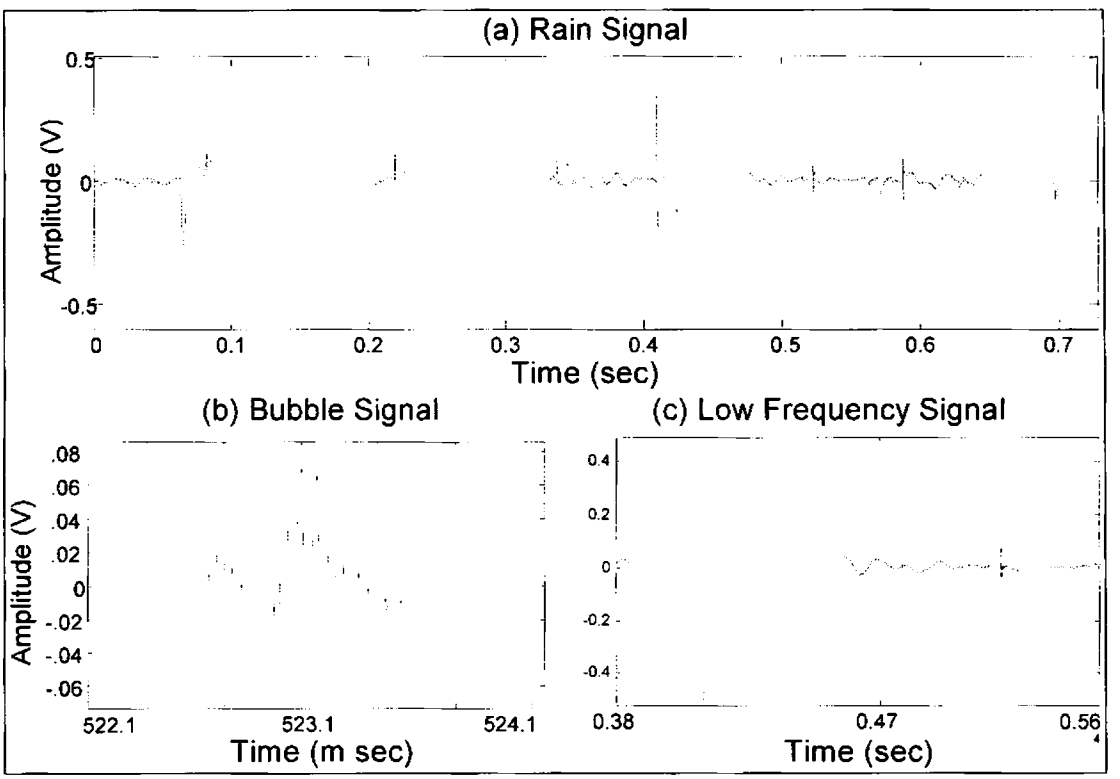

Fig. 5.8: (a) Rain signal captured by the sensor assembly; (b) Zoomed low frequency pressure signal after impact; (c) Bubble generated signal.

5.6 Drop Detection

It is seen that each drop impact produces signal with a clearly defined shape having a sharp rise in signal level at the impact instant that can be easily detected. Since it is essential to compute the drop size distribution for estimating the rain intensity, an algorithm has been developed for detecting individual drops. One important parameter for drop detection is the 'threshold level'. A drop is detected

when there is rapid change in signal level that is greater than the threshold value from its neighbouring samples. This threshold value helps to avoid false drop detection in the presence of noise. A higher threshold value will eliminate the possibility of false detection. When the threshold value is increased, it leads to certain undesirable effects, as smaller droplets will escape the observation of the drop detection system. Such a situation can be handled amicably by setting the threshold value adaptively depending on the average value or median value of the signal level over a selected period. In doing so, small droplets will be ignored during heavy rain. The error introduced is negligible as the rain intensity in heavy rain is mainly due to larger drops. However, for light rain, small drops will be detected as the threshold is proportionately lowered. Drop sizes as low as 0.5 mm in light rainfall typically (less than 14.1 mm h^{-1}) have been detected with this algorithm, while drops of sizes less than 0.5 mm from heavy rain, typically greater than 120 mm h^{-1} escaped detection by the adaptive system.

5.6.1 Drop detection algorithms and determination of DSD function

Two types of drop detection algorithms have been developed to detect and estimate the rain drops in natural rain. Following assumptions and facts are considered for this purpose:

(i) Raindrops of size less than 1.0 mm do not contribute much to the rain fall especially when rainfall rate is moderate and hence negligible.

(ii) Rain drops of size less than 1 mm need to be considered only when the average rainfall intensity is very less (for example, drizzle).

(iii) Equivalent diameter of a raindrop of maximum size is around 6 mm and drop size greater than 6 mm is seldom present in the rain.

(iv) Maximum response time due to drop impact is around 20 milliseconds.

(v) Simultaneous drops will be detected as a single large drop.

A simplified flow chart for the drop detection is shown in Fig. 5.9. The signal is low pass filtered using a low pass filter whose upper cut off frequency is just above 600 Hz. Simple second order Butterworth filter is sufficient for this purpose. A thresholding operation is performed after filtering to eliminate any samples whose value is less than the threshold value. This avoids false detection of drops due to noise present in the signal at very low rainfall intensity.

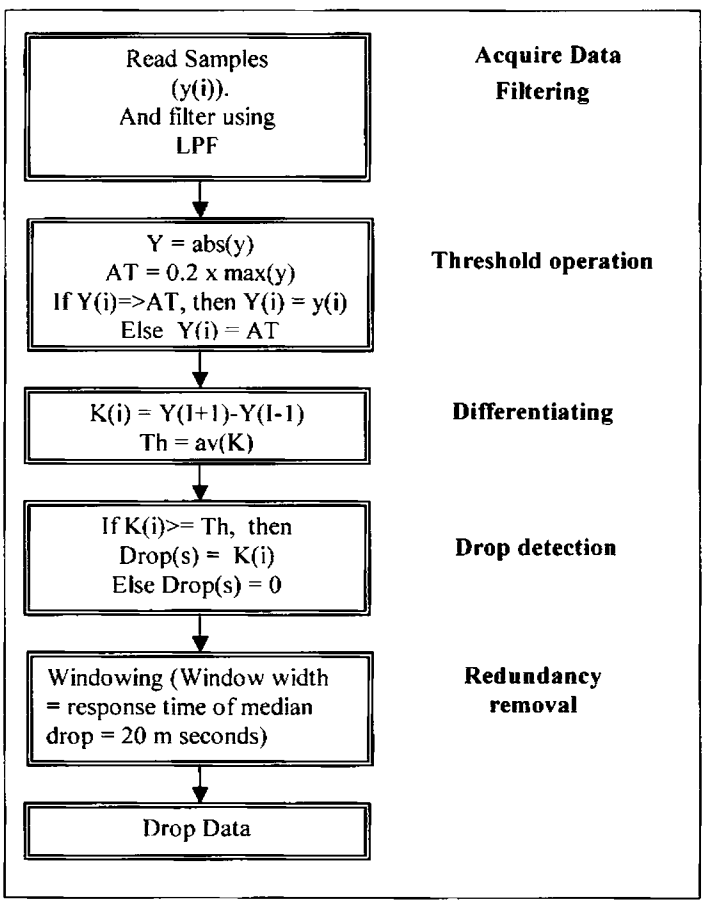

Fig. 5.9: Drop detection algorithm I

It is easy to locate the starting point of a drop-generated signal that is characterized by a sharp rise in amplitude from its previous sample values. After identifying the start of the drop-generated signal, the energy of the signal contributed by this drop is computed using the samples of the signal lying within a response window. Response window width is set by trial and error. If the window is too wide, there is a possibility of overlapping of the window with that for the neighboring drops, which may cause measurement error. In this scheme, simultaneous drops or multiple drops within a single window are detected as a single larger drop. It is assumed that this detected drop size is equivalent to the drop size that produces the sum of the kinetic energy of the simultaneous drops. A lookup table has been prepared to determine the size of the drop from its kinetic energy.

The drop detection algorithm has been implemented in MATLAB 5.3. Figure 5.10 shows the MATLAB plot showing the detection of raindrops and the rain generated noise amplitude. The signal from which this drop extraction was performed is one of the worst-case signal, where the noise contamination and low frequency drift were present. Noise and low frequency drift can cause error in drop estimation and hence to be dealt carefully. False drop detection due to noise has been reduced here by taking the derivative of the signal as suggested in the paper by Friesen *et al. (1990).*

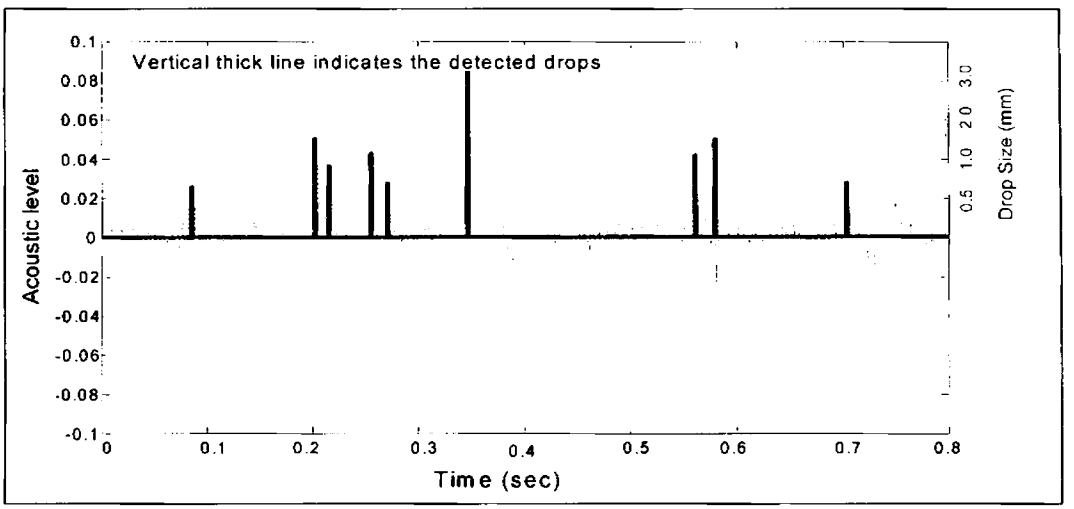

Fig. 5.10: Drop detection

The results of these studies were compared with the drop size measurement results by the filter paper method. The results of comparison show that the estimated drop size closely agrees with the measured dimensions using the filter paper method. It was also noticed that the accuracy of estimation of drops depends on threshold level as explained in section 5.5.

The computations needed for this method was carried using a PC. However, this method of drop estimation is not computationally very efficient and hence not recommended for standalone application where it uses general-purpose digital processor. A much more simpler algorithm was developed to so as to implement it using a low cost DSP processor with limited resources (memory size and speed). Simplified flow chart for this improved algorithm is as shown in Fig. 5.11.

The Acoustic energy of a drop generated underwater signal is determined by calculating the energy contributed by signal after low pass filtering. Low pass filtering eliminates the bubble signal and other high frequency noise present in the signal. Energy computation is done by squaring and adding every consecutive sample

in the signal. While doing so, it is checked if there is a considerable increase in energy than a threshold value after adding a squared sample. If there is no considerable increase in energy even after squaring and adding many consecutive samples (the number of samples to be considered depends on the 'distance' selected), then it is assumed that the acoustic energy due to a single drop is completely added and the cumulated energy up to this point represent the drop energy. This value is stored and the process is initialised for detecting and estimating the next drop present in the signal. Two important parameters defined for these algorithms are the *threshold* value and the *distance*. These two parameters help to avoid false detection of drops due to ambient noise and bubble noise. *Threshold* value and *distance* value are experimentally determined. A distance of two milliseconds (about the span of 100 samples) and a threshold of 1% of the average signal level is a good approximation.

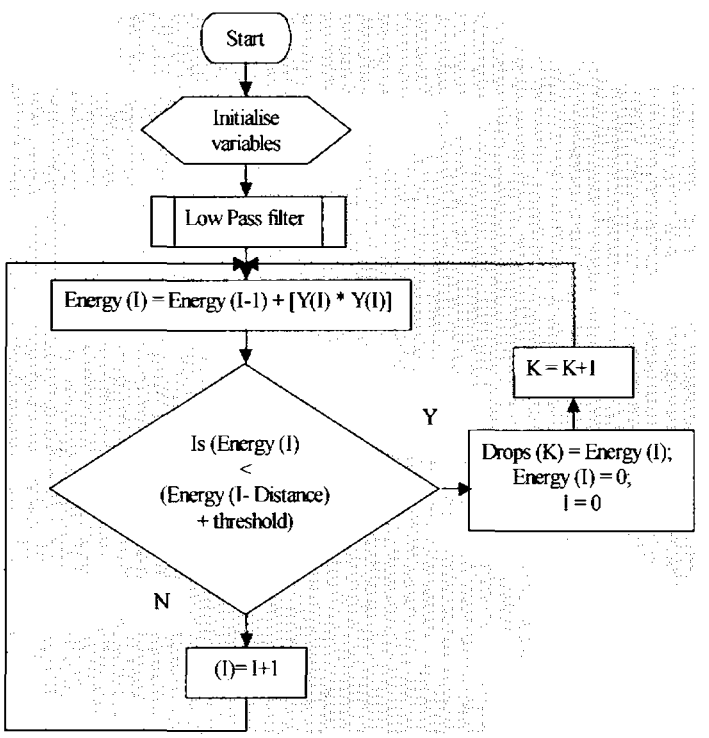

Fig. 5.11: Drop detection algorithm II

5.6.2 Merits and demerits of drop detection algorithms

Drop detection algorithm I is slightly complex and it tries imitate a human being who tries to identify the drop by visually observing the drop signal pattern. This is possible because of the unique pattern of the drop-generated signal (Fig. 5.8a). The determining factor is to identify the start and stop of a drop signal. The start of a drop signal is characterised by a sharp rise in signal level. Once this is detected, then the end of drop signal is searched within a window of width approximately equal to the maximum expected response time due to a drop. This method is easy for manual determination, but fails if tried to detect automatically, due to noise contamination. This method is useless if proper corrective measures are not employed. A redundancy removal process is incorporated in this algorithm to counteract against false drop detection. Altogether this process is complex and requires more intensive mathematical computations. Window width and threshold values are to be adaptively changed for this algorithm to work.

Algorithm II is more straightforward. The total energy contributed by a single drop is computed by determining the start and end of the signal due to this drop. **Start** is determined by the sudden rise in strength of the signal (squared value of the amplitude of signal). From there onwards squaring and adding the subsequent samples compute the energy until there is no further increase in energy. The end of the drop signal is at the point from there onwards there is no additional energy contributed by the subsequent samples of the signal. One serious drawback of this algorithm is that two closely timed drops cannot be detected and will be treated as single larger drop. However, it has been found that Algorithm II gives much better results for measurements of low to moderate rainfalls. Also the computations required are lesser than the algorithm II.

5.6.3 DSD computation

From the *drop energy* computed from any of the algorithm, the actual drop size is computed using the 9th degree polynomial relationship as shown in Eq. (5.6).

$$0.0016D^9 - 0.0268D^8 + 0.7310D^7 - 4.818188D^6 + 13.4901D^5 - 1.3379D^4 + .0338D^3 = Ke(D) \qquad (5.6)$$

The drop concentration thus computed looks like the one shown in Fig. 5.12. To simplify the computation all drop sizes of the range 0.2 to 6mm that may be present in rain were grouped into 30 bins'

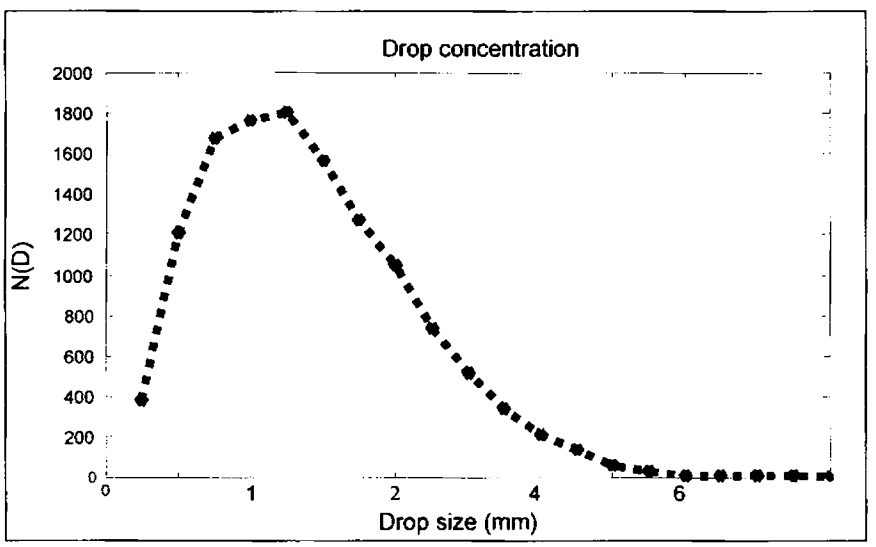

Fig. 5.12: Drop concentration for duration of 8.3 seconds (Intensity = 45.72 mm/hr)

DSD function is then represented by,

$$N(D) = \sum_i \frac{N_i}{V_T(D) A \times t} \qquad (5.7)$$

where N_i is the number of drops in every bin , A the area of the sensor opening, and t is the time duration of measurement in seconds. The DSD function obtained is as

shown in Fig. 5.13. The experimental data obtained for different rain events were evaluated using this method and the drop size distribution and DSD function were computed.

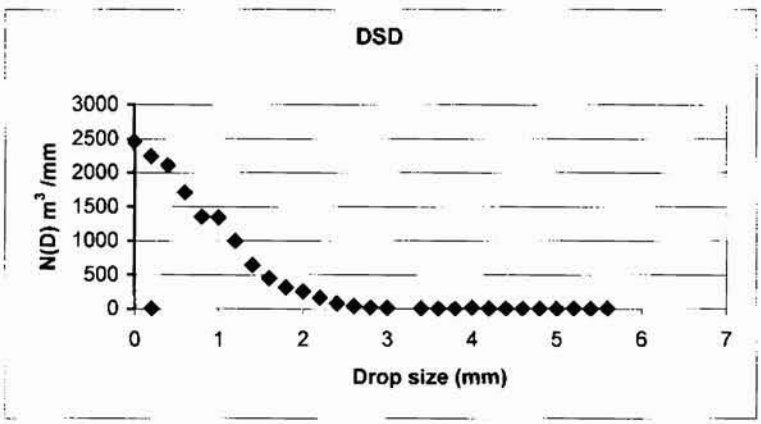

Fig. 5.13: A typical DSD function computed for the rainfall event

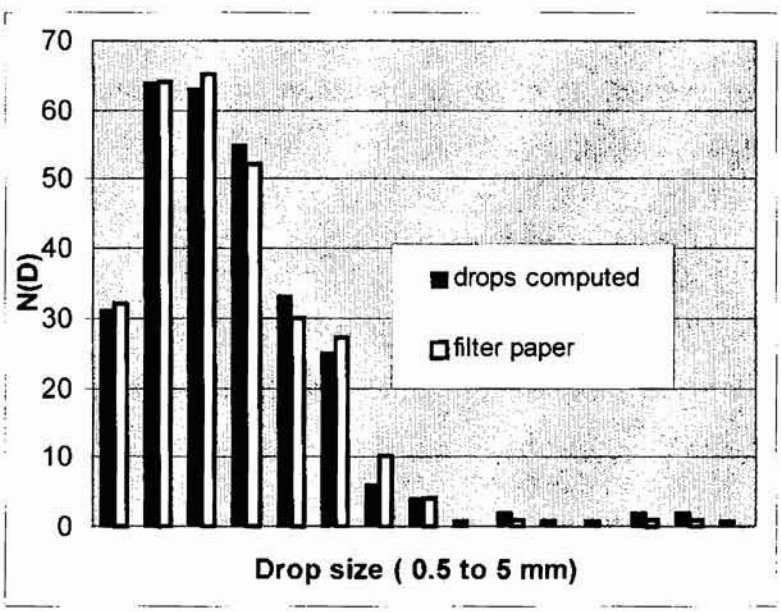

Fig. 5.14: Comparison of computed drop size concentration with concentration that obtained from Filter Paper method (R= 15.24 mm/hr)

Size of the drops computed with the acoustic technique is compared with that obtained by filter paper method and observed that it closely agrees with each other (refer Fig. 5.14). Since filter paper method is a manual process, this type of comparison was practically very difficult for heavy rainfall rates.

As explained earlier, the threshold level setting and the damping property of the sensor assembly plays an important role in the useful rain intensity range for which the device can give good accuracy of measurement.

Higher damping causes smaller response time for the drop signal. Lower damping causes increased response time and produces good sensitivity, which is suitable for detecting light rains like the drizzle. On the other hand, increased response duration causes overlapping of drops that cause error in estimation of drop sizes, especially for heavy rainfall rates.

Experiments were performed by adjusting the damping such that the response duration for the signal for a drop size of 3 mm diameter is about 20 to 25 milliseconds. This response provides fairly good sensitivity and at the same time avoids overlapping of drop-generated signals for closely timed falling drops. The threshold was set as 1 to 2 % of the full-scale output voltage.

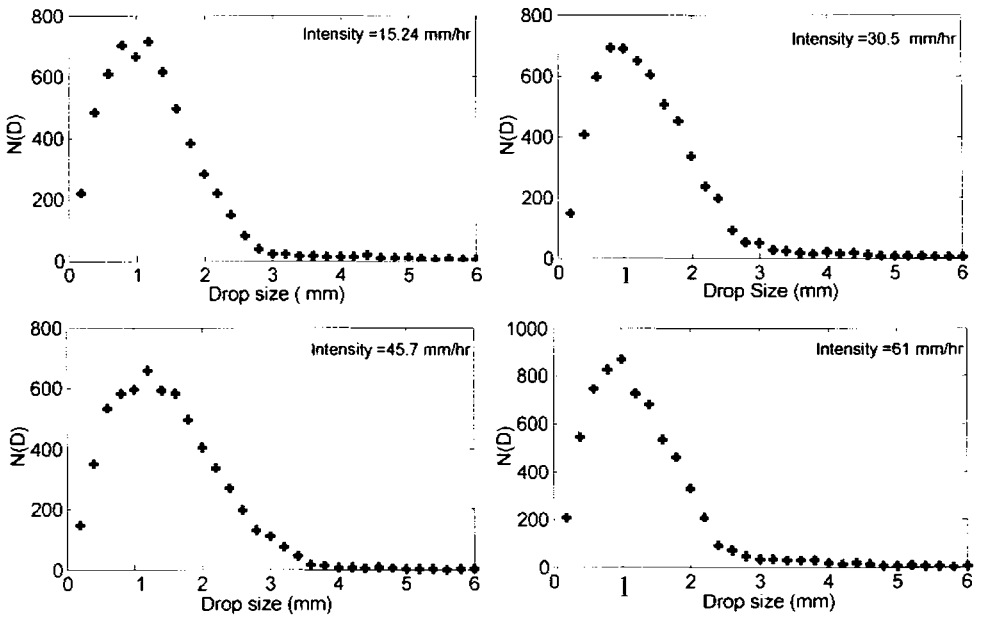

Drop concentration in various rainfall events

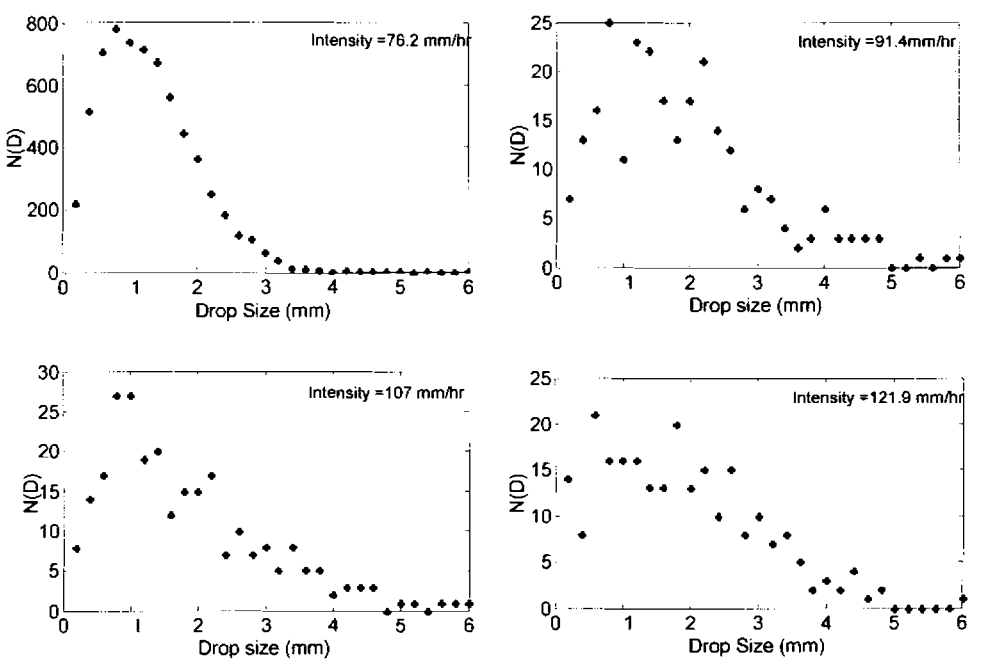

Fig. 5.15: Drop concentration obtained for various rain intensities

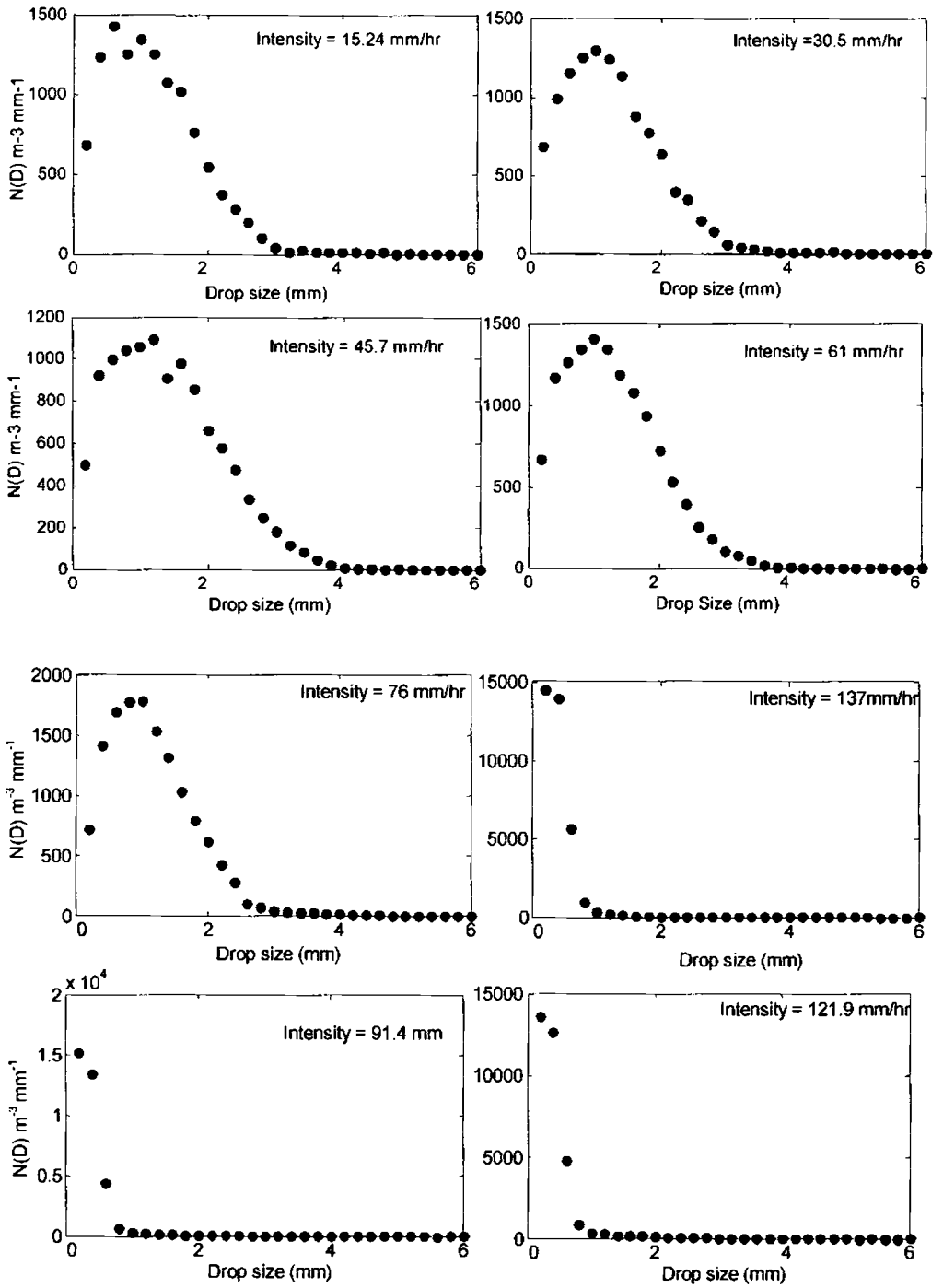

Fig. 5.16: DSD of various rainfall events computed using the signal captured by the sensor assembly.

The Figs 5.15 and 5.16 show the results of the measurements. The results show that the estimation of DSD is possible with this method and gives excellent results when the rain rate is low or medium. However, it was noticed that for heavy rainfall, the performance of the sensor assembly deviates from what was expected. The settings of the sensor assembly were found suitable to measure the DSD in rainfall up to 80 mm/hr.

For very heavy rainfall, drop signal contributed by the individual drops will be mixed up together and hence the detection mechanism may not be working properly.

5.7 Rain Intensity Computation from DSD.

Once the raindrops are estimated in a rain, the rain intensity can be calculated by using the formula,

$$R = \frac{\pi}{6} \sum_i \frac{NiD_i^3}{At} \tag{5.8}$$

Rainfall rate computed using Eq. (5.8) for different rainfall intensities were validated with the rainfall measured by using a standard tipping bucket rain gauge. Figure 5.17 shows that the rain measurement method based on the proposed techniques closely agrees with the rainfall rate measured by using the TBR. However, it is noticed that the error increases if the rainfall rate increases beyond 80 mm/hour. Total rainfall indicated by TBR and the rainfall computed by using Eq. (5.8) agreed fairly, within the limits of experimental errors and theoretical approximation. The differences were seen to be within 2 to 5% of the TBR reading. The ARG reading obtained was always higher than the TBR reading. In this context, it is important to note that the inherent disadvantage of TBR is that it always tends underestimate rainfall.

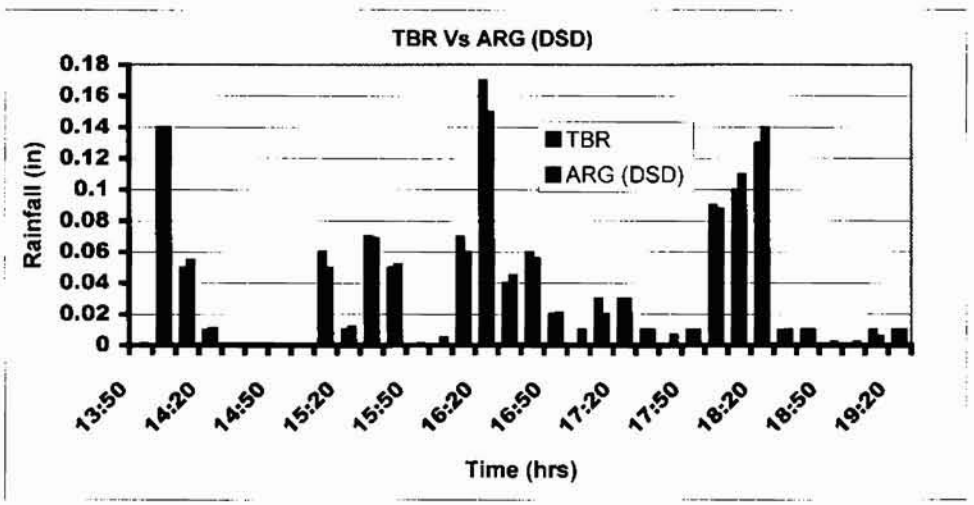

Fig. 5.17: Computed rainfall (ARG -DSD) versus Tipping Bucket Rain gauge reading for the rain event on 22-8-2003

5.8 Kinetic Energy of Rain

Various researchers have carried out studies based on kinetic energy of rain over the years. One reason for the importance of the rain kinetic energy (KE) is that KE is a widely used indicator of the potential ability of the rain to detach soil. Empirical and process based model soil erosion models [Elwell, 1978; Moran et al, 1998a, b; Renard et al., 1997] often use KE as the rain erosivity index.

The rain kinetic energy is the sum of kinetic energy of each individual drops in rain that strikes the ground. DSD measurement and the fall velocity measurement allows one to calculate the rain kinetic energy. Empirical laws linking the terminal velocity V_T and drops size D are also useful in computing the rain kinetic energy. Even though direct measurements of rain kinetic energy using energy sensors are available, these are not widely used for measuring the kinetic energy. Due to the availability of DSD measurements, it is possible to establish the empirical relationships between KE and Rain intensity (I). KE can then be computed directly from any rainfall event I using the KE-I relationship.

5.8.1 KE – I relationship

Kinetic energy of rain can be expressed by the term 'energy contents', the kinetic energy of rain per unit rainfall depth. Energy content is denoted by e_K(in J m^{-2} mm^{-1}). This term is useful for comparative purposes. The kinetic energy contents associated with a particular drop size distribution is thus given by:

$$e_K = \frac{1}{2}\rho\sum_{i=1}^{K} f_i v_i^2 \tag{5.9}$$

where f_i is the mass fraction,

v_i is the terminal velocity of sizes in class i,

ρ the mass density associated with 1 mm of rainfall in Kg m^{-2} mm^{-1}.

Reports on various studies to determine the relationship between the kinetic energy and the rain intensity were already appeared in open literature. Some of these studies suggest a power law relationship between rainfall rate and kinetic energy [Smith and De Veaux (1992), Uijlehoet and Stricker (1999)] of the form:

$$KE_{time} = aI^b \tag{5.10}$$

where KE_{time} is the time specific kinetic energy and a and b are constants.

Another relationship that, suggested by others is a logarithmic relationship [Laws (1941), Laws and Parsons (1943), Gunn and Kinzer (1949), Wischmeier and Smith (1958)] of the form:

$$KE_{mm} = a + b\log_{10} I \tag{5.11}$$

where, KE_{mm} is the volume specific kinetic energy, a and b are constants derived through regression.

A number of *KE-I* relationships have been reported so far and table 5.1 summarises some of the representative relationships that are widely used. An extensive review of the same is made by Christian Sallas [Sallas C et al. (2001)]. The equations in table 1 are being widely used in finding the rain erosivity.

Table 5.1: Some of the relationship between the time specific kinetic energy and Intensities of rain from reported literature [Sallas C et al. (2001)]

Authors	***KE – I relationship***	**Range of I (mm h^{-1})**
Bollinne et al., 1984	$12.32I + 0.56I^2$	0.27 to 38.6
Brandt, 1990	$I(8.95 + 8.44\log_{10} I)$	N A
Brown and Foster, 1987	$29I\left(1 - 0.72e^{-0.05I}\right)$	0 to 250
Carter et al., 1974	$11.32I + 0.5546I^2 - 0.509 \times 10^{-2} I^3 + 0.126 \times 10^{-4} I^4$	1 to 250
Smith and De Veaux, 1992	$11I^{1.23}$	N A

Power law equation and logarithmic equation indicates that there is no upper bound for the kinetic energy where as experimental evidence shows that there is an upper limit for the Kinetic energy of rain. [C.J. Rosewell (1986), K.V. Beard, (1976)] Rain rate can be calculated from its kinetic energy by using the *KE-I* relationship. For example, the exponential relationship of the rain kinetic energy with intensity can be expressed with the general predictive relation ship [A.I.D.J.M. Van Dijk et al (2002)]:

$$e_K = 28.3[1 - 0.52\exp(-0.042I)] \tag{5.12}$$

From Eq. 5.12, Intensity of rain can be computed from the kinetic energy:

$$I = \frac{-1}{0.042}\left[\log\left(1.923 - \frac{e_K}{14.716}\right)\right] \tag{5.13}$$

Similarly, expressions for computing the rain rate R from other Kinetic energy-Intensity relationship can also be derived.

5.8.2 Rain Kinetic Energy measurement

The acoustic technique for determining the rain kinetic energy is simple with the sensor assembly. For these, one need just to expose it to the rain and capture the signal, pre-process it for removing the unwanted noise and bubble frequencies, digitise the signal and compute the energy of every sample by just squaring the sample values and add all the energy values together.

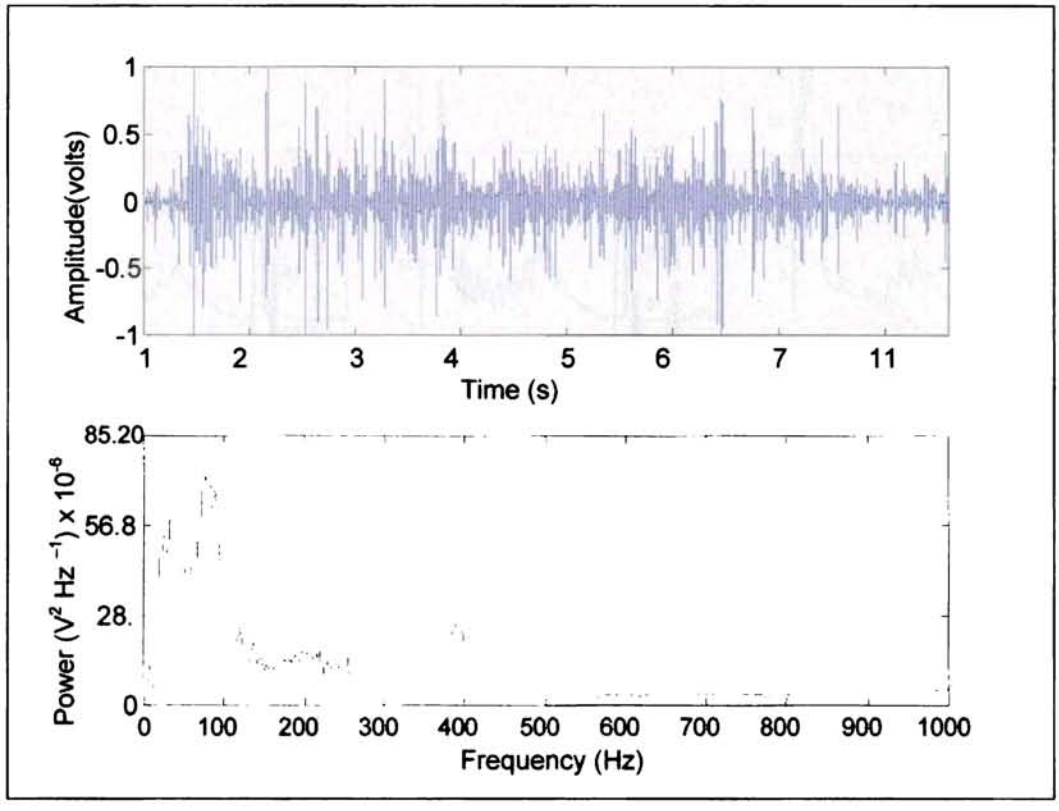

Fig. 5.18: (a) Rain generated acoustic signal. (b) Shape of the low frequency spectrum

It has already been shown that the energy in the acoustic signal due to the impact of raindrops is concentrated more to the lower frequency spectrum (Fig. 5.3).

The spectrum of the rain noise captured by the sensor assembly also shows a similar result.

A sizable percentage of the energy content in the signal lies in the low frequency range. The shape of the spectrum for a typical rain noise is as shown in Fig. 5.18. A detailed study on the low frequency spectrum of the rain noise captured by the sensor assembly was carried out and the Figs. 5.19, 5.20 and 5.21 shows the results of the study for a rainfall of intensity 30.6 mm per hour. Individual graphs in these figures indicate the low frequency spectrum of the signal at different instances.

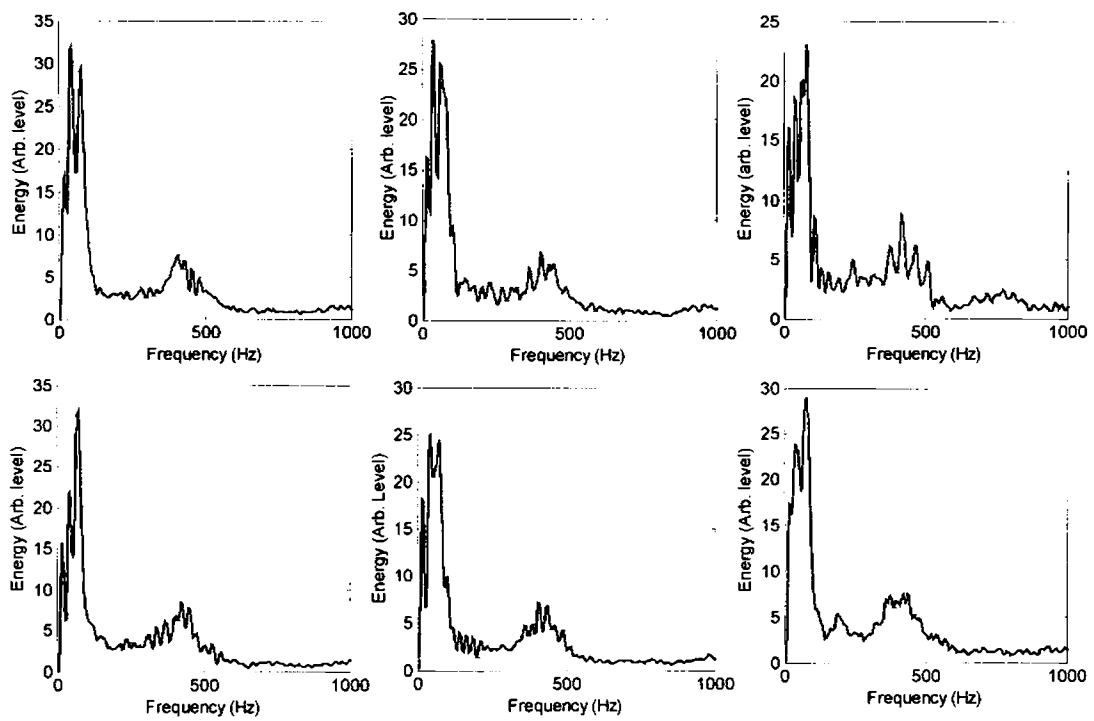

Fig. 5.19: Low frequency spectrum of the rain signal of intensity 30.6 mm/hour for one-second duration

The graphs in Fig. 5. 19 indicate the low frequency spectrum of the rain noise at different instances. Similarly, Fig. 5.20 indicates the low frequency spectrum of the rain noise at different instances for a rainfall event of intensity 45.7 mm/hr.

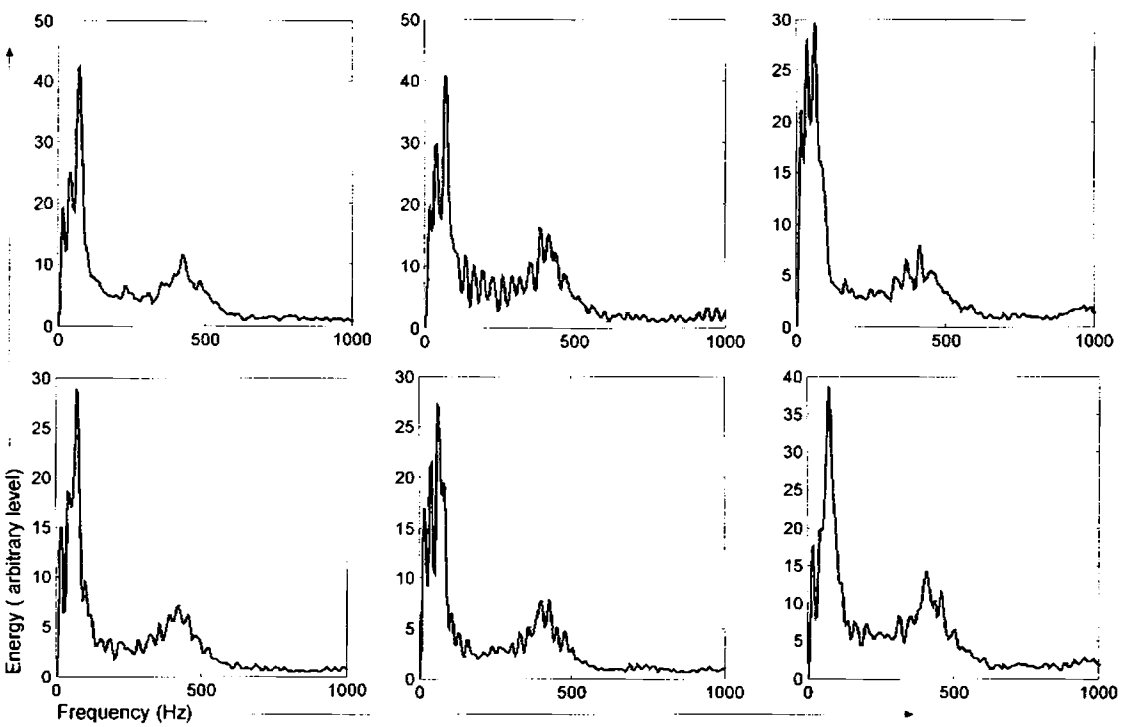

Fig. 5.20: Low frequency spectrum of the rain signal of intensity 15.24 mm/hour (One-second duration)

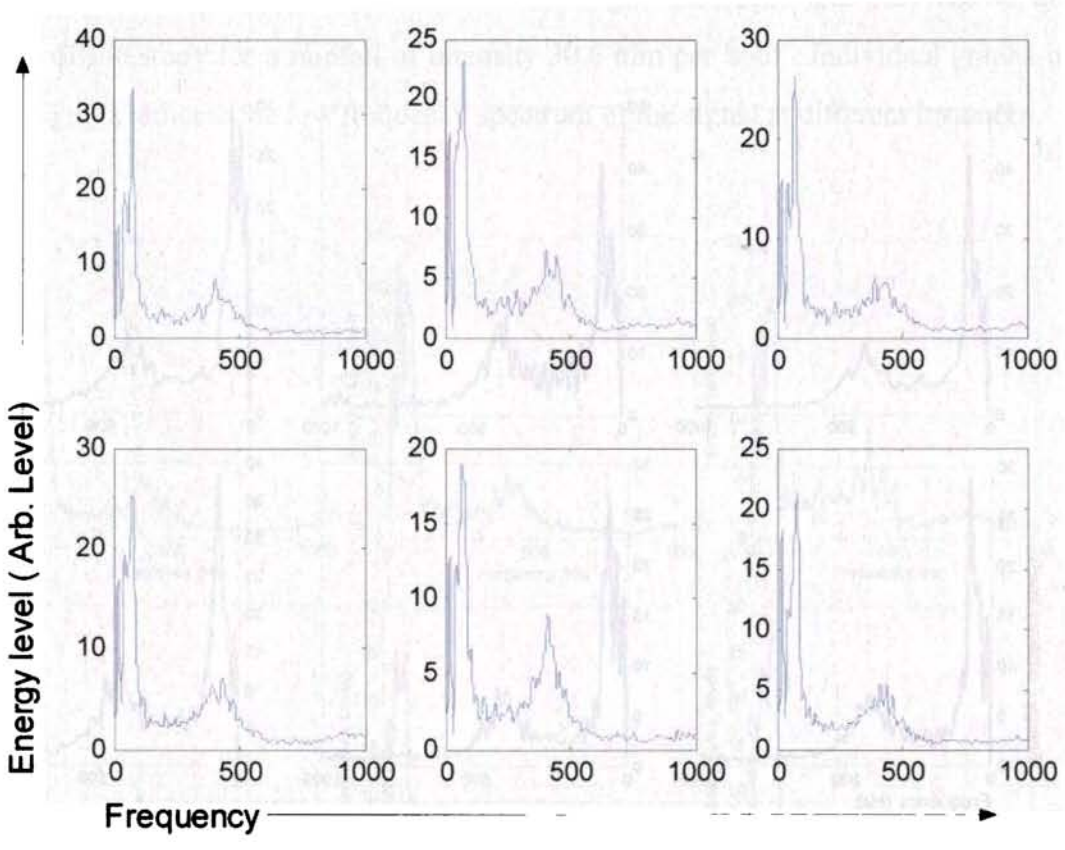

Fig. 5.21(a): Low frequency spectrum of the rain signal of intensity 45.7 mm/hour (one-second duration)

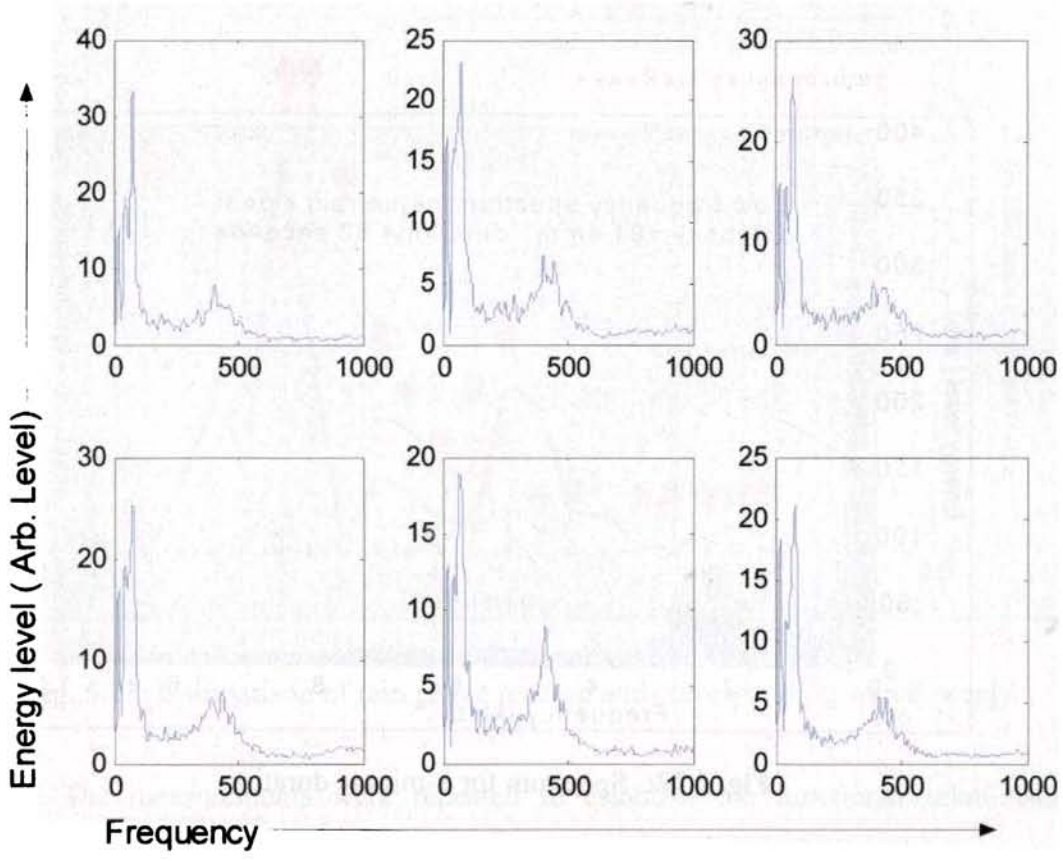

Fig. 5.21(b): Low frequency spectrum of the rain signal of intensity 45.7 mm/hour (one-second duration)

The spectrum of the rain noise averaged over a period of one minute is shown in Fig. 5.22. It has been experimentally found that the shape of the spectrum remains

the same for most of the duration of the rainfall event. The shape of the spectrum mainly depends on the physical parameters of the rain sensor assembly.

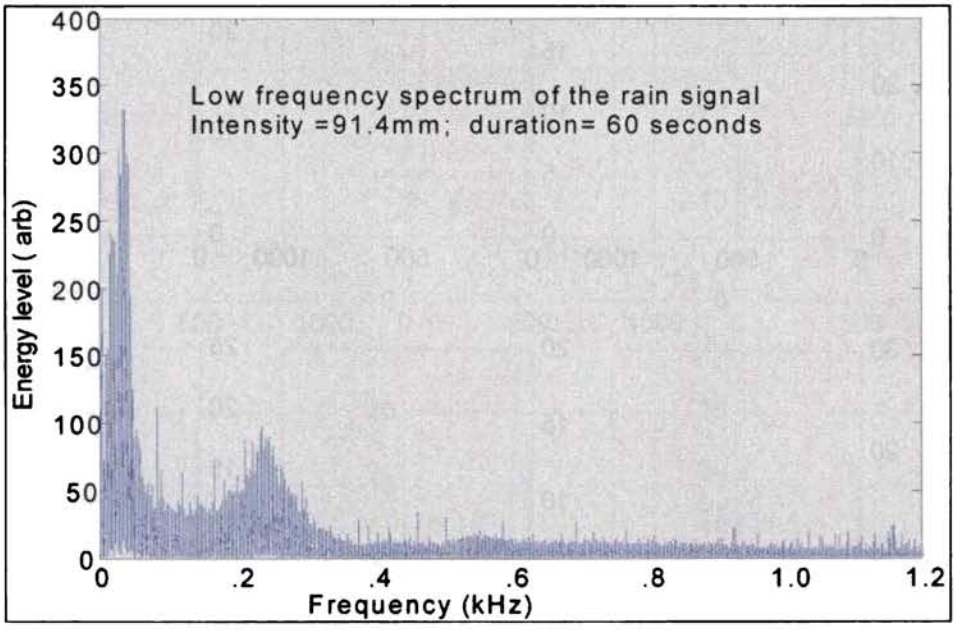

Fig. 5.22: Spectrum for 1-minute duration

5.8. 3 Relationship with the rain intensity

A standard TBR was used to measure the rainfall event and the results of the measurement was compared with the low frequency rain noise energy. It has been noticed that the acoustic signal strength increases with the rain rate. To establish the

fact that the low frequency acoustic energy roughly represents the rain rate, the results of the measurement of TBR reading and rain *KE* are depicted Fig. 5.23.

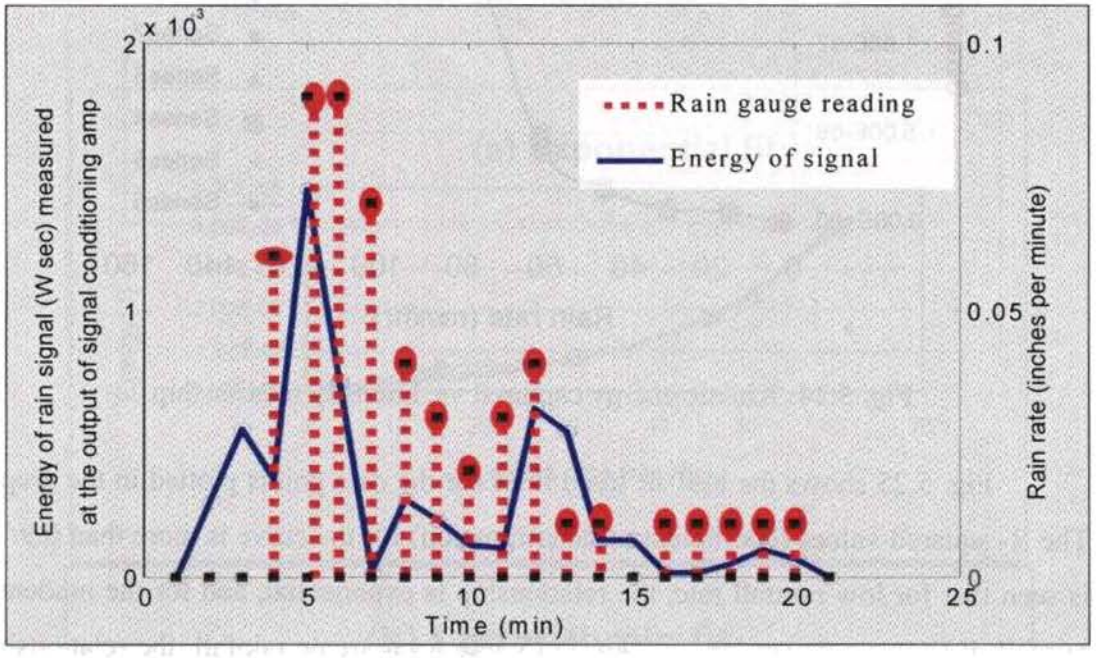

Fig. 5.23: Comparison of rain gauge reading and corresponding signal energy

The measurements were repeated to establish the functional relationship between the rain intensity and the energy computed from the rain-generated noise. It is observed that for low rainfall intensities in the range of 0 to 60 mm per hour, the relationship is exponential and for medium rainfall in the range of 60 to 80 mm per hour, it exhibits a power law relationship while for higher intensities the relationship is logarithmic as shown in Fig. 5.24.

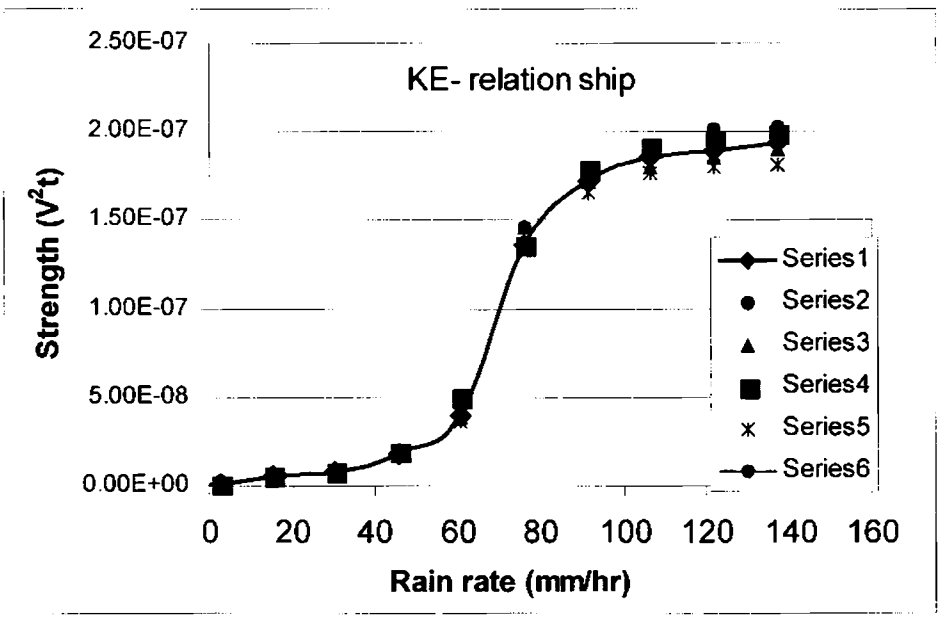

Fig. 5.24: Kinetic energy captured vs. Intensity relationship

Fig. 5.25 shows the best-fit trend lines for the data points plotted in the graph. The R- squared values (coefficient of determination) for the curve is more than 0.9. It is seen that for low rainfall rate, the relationship is exponential, and for the moderate rainfall, it shows a power law relationship while for extreme rainfall, the relationship is found to be logarithmic. The exponential relationship was found to fit for the rainfall rate ranging from 0 to 65mm/hr and the relationship seen to be given by Eq. (5.14)

$$KE_{Low} = 0.887 \times 10^{-9} \times e^{0.068R} \tag{5.14}$$

This equation is very similar to the findings of Rosewell [Rosewell, 1986].

The power law relationship is found to fit for the rainfall rate from 66 mm/hr to 90 mm/hr. This can be seen to relationship and expressed as,

$$KE_{Med} = -6.3896\times10^{-12}R^3 + 1.3302\times10^{-9}R^2 - 8.5586\times10^{-8}R + 1.761\times10^{-6} \quad (5.15)$$

The logarithmic relationship is applicable to heavy rainfall that extends the rainfall rate from 91 mm/hr and above. This relationship best fits with the Eq. 5.16

$$KE_{High} = 0.86\times10^{-7}\log(R) + 0.09\times10^{-7} \quad (5.16)$$

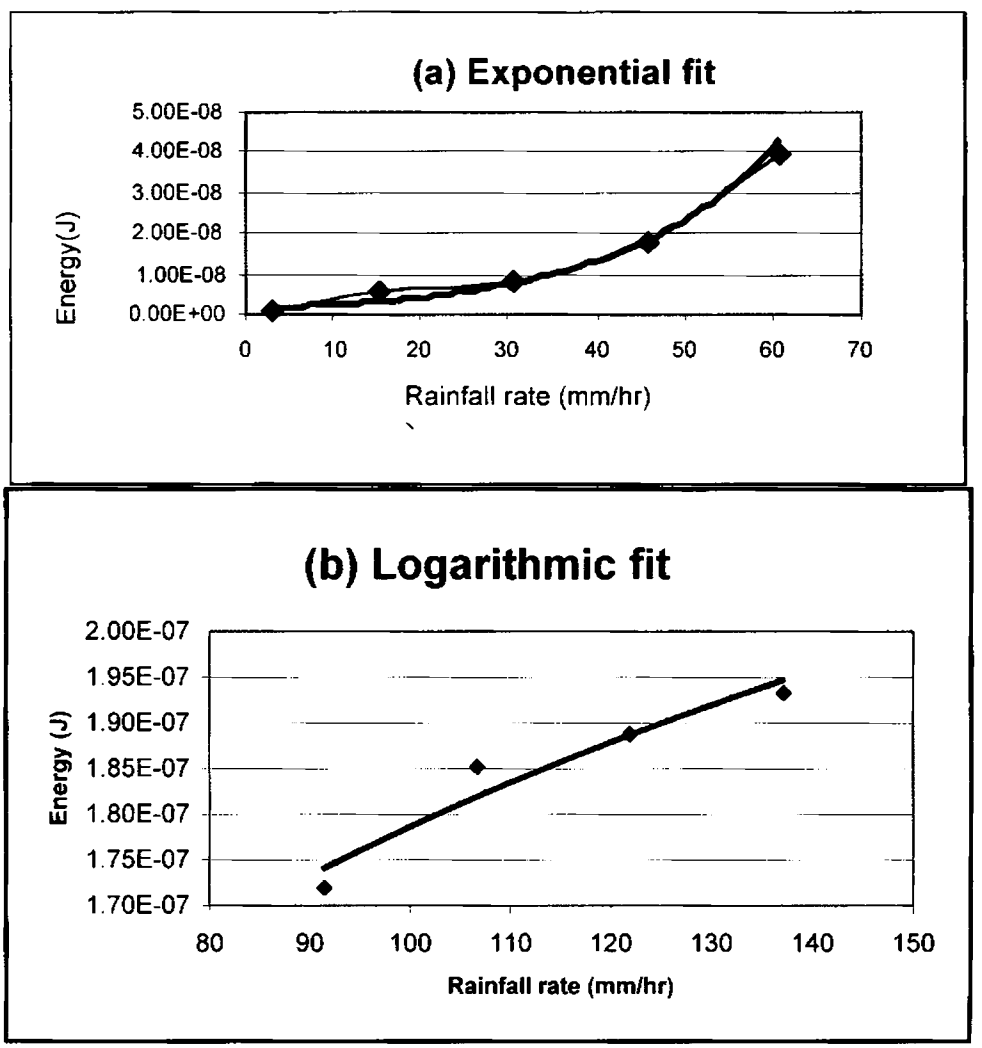

Fig. 5.25: Curve fitting for the Kinetic energy-Intensity relationship

A Single curve showing the relationship between the energy and the rainfall rate ranging from 0 to 150 mm/hr incorporating the three expressions (Eq. 5.15- 5.16) will have a shape as shown in Fig. 5.26. In this figure, energy computed from the signal for one-minute duration. The observed values were found to fit with the curve.

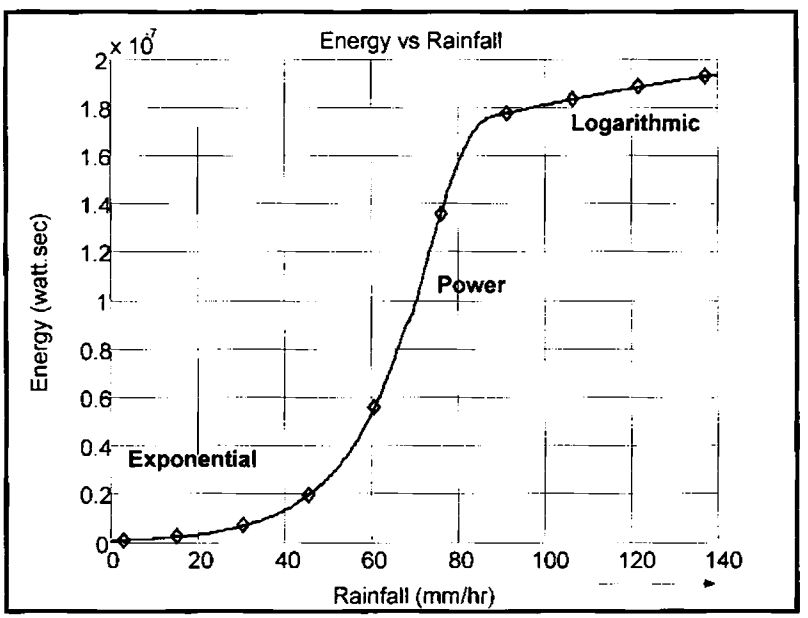

Fig. 5.26: The Kinetic energy-Intensity relationship (mathematical model)

5.9 Acoustic Rain Gauge

The *KE-I* relationship as shown in Fig 5.26 is used to measure the rainfall intensity. This method requires fewer computations compared to the computation of rainfall using DSD measurement. It is rather easy to determine the rain rate from the energy captured by the sensor assembly, by using the curve.

An efficient and easy way of implementing the Acoustic Rain Gauge is by using a lookup table. A look-up table can be made either by using the graph (Fig.

5.26) or by using the equations 5.14 to 5.16. Computations needed for the ARG can be considerably reduced if a lookup table is used. Therefore, the lookup table method is preferred as an efficient way to implement an ARG using a microcontroller or microprocessor.

In order to validate the findings as explained in the previous sections, the rainfall rate for different rainfall events were recorded using TBR and compared with the computed rainfall rate using the proposed acoustic method (*KE-I* relationship). The results are shown in Fig. 5.27.

It is observed that the errors in the measurement tend to increase when the rainfall rate is very high and in a region of the curve where, the rainfall rate shows logarithmic relationship with the kinetic energy. The measurement errors were negligibly low and the results closely agrees with the TBR readings for low to moderate rainfall rates.

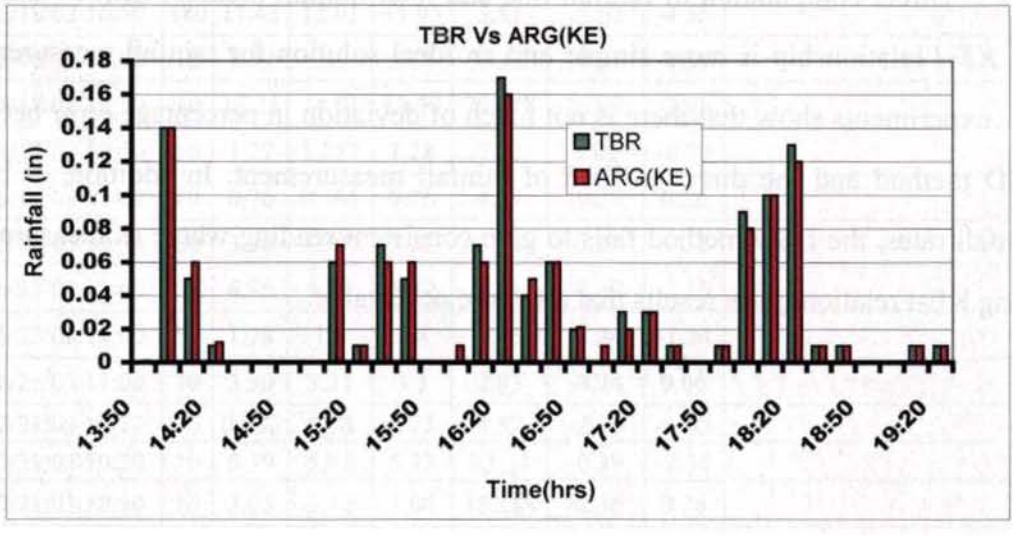

Fig. 5.27: Computed rainfall (ARG -KE) versus Tipping Bucket Rain gauge reading for the rain event on 22-8-2003

The table 5.2 gives an overview of the rainfall measurement based on the DSD techniques and the direct kinetic energy method. These measurements were performed over a period of three years during the monsoon in Kerala. The measurement site was located in the CUSAT campus.

It has been noticed that the sensor is sensitive to acoustic disturbances caused by the environment where the sensor assembly is installed. If the device is not acoustically isolated from the ground, there is a likely chance of picking up vibration of the ground due to movement of heavy vehicles on the road nearby to the measurement site. Other type of noise that is likely to affect the measurement is the thunder sound. During heavy lightening, the blasting sound was always picked up that yielded incorrect rain rates.

Direct computation of rainfall rate and total rainfall measurement by utilizing the *KE-I* relationship is more simple and an ideal solution for rainfall measurement. The experiments show that there is not much of deviation in percentage error between DSD method and the direct method of rainfall measurement. In addition, at heavy rainfall rates, the DSD method fails to give consistent reading where as measurement using KE-I relation gives results that are more acceptable.

Table 5.2: Rainfall rates measured with TBR and Acoustic method.

	Date/time & Duration (min)		Rainfall in mm			I mm/hr	% Error		Remarks
			TBR	R (DSD)	R (KE)		I(DSD)	I(KE	
1	5/17/02 11:30	10	0.76	.763	.76	4.57	-0.13	0.26	
2	5/17/02 13:10	10	3.81	4.01	6.05	22.86	-5.25	-58.79	Contaminated with thunder sound
3	5/17/02 13:20	10	3.30	3.303	3.31	19.81	-0.03	-0.24	
4	5/17/02 14:30	10	5.59	5.586	5.59	33.53	0.04	-0.04	
5	5/17/02 14:40	10	2.03	2.03	2.034	12.19	0.10	-0.10	
6	5/17/02 15:50	30	6.35	6.357	6.4	12.70	-0.11	-0.79	
7	5/17/02 18:50	200	0.25	0.23	0.4	0.08	9.45	-57.48	TBR error due to evaporation
8	5/18/02 15:30	10	2.54	2.545	2.54	15.24	-0.20	0.00	
9	5/18/02 16:50	80	3.81	3.816	3.82	2.86	-0.16	-0.26	
10	5/18/02 17:40	10	5.59	5.612	5.62	33.53	-0.43	-0.57	
11	5/18/02 17:50	10	13.21	13.22	13.22	79.26	-0.08	-0.08	
12	5/18/02 18:00	10	20.17	16.26	21.33	121.02	-31.18	-5.75	DSD error
13	5/18/02 16:50	180	11.43	12.01	11.95	3.81	-5.07	-4.55	
20	5/18/02 17:40	10	5.59	5.6	5.61	33.53	-0.21	-0.39	
21	5/18/02 17:50	10	13.21	14.01	13.48	79.248	-6.07	-2.06	
14	6/14/03 10:50	10	1.27	1.257	1.28	7.62	1.02	-0.79	
15	6/14/03 11:00	10	0.76	0.765	0.76	4.57	-0.39	0.26	
16	6/18/03 10:30	60	3.30	3.295	3.32	3.30	0.21	-0.55	
17	6/21/03 11:00	100	6.35	6.38	6.42	3.81	-0.47	-1.10	
18	6/23/03 18:00	50	1.78	1.8	1.8	2.13	-1.24	-1.24	
19	6/25/03 11:00	70	3.30	3.31	3.3	2.83	-0.24	0.06	
20	7/31/03 10:10	10	0.762	0.78	0.77	4.57	-2.36	-1.05	
21	7/31/03 10:20	10	5.59	5.61	5.72	33.53	-0.39	-2.36	
22	7/31/03 10:30	10	3.05	3.12	3.04	18.288	-2.36	0.26	
23	7/31/03 10:40	10	0.25	0.25	0.26	1.524	1.57	-2.36	
24	8/21/03 17:50	10	0.25	0.28	0.267	1.524	-10.24	-5.12	
25	8/21/03 17:54	10	0.25	0.25	0.25	1.524	1.57	1.57	
26	9/21/2003 21:10	20	11.00	8.49	12.25	33	22.82	-11.36	DSD error

5.9.1 Comparison with conventional ARG.

The proposed method of measuring rain rate has many distinct advantages compared to the conventional multichannel ARG. The table 5.3 summarises the results of the comparison of the proposed method with the conventional ARG.

Table 5.3: Comparison of the conventional ARG and the proposed method

Proposed method	**ARG based on high frequency signals**
Narrow band signals.	Wideband signal.
Cost-effective transducer can be employed.	Need wide band transducer and hence costly.
Signal processing complexity is moderate	Multi channel and complex signal processing is needed
Continuous measurement possible	Sampled processing and hence discrete.
Special sensor assembly is needed	No special sensor assembly is needed
Can be adopted for land based measurement and suitable for other applications	Only suitable for oceanic measurement

5.9.2 Factors affecting the accuracy of measurement

There are various factors that may introduce errors in the measurement. Remedial measures have to be taken into consideration for better measurement accuracy.

5.9.2.1 Problem with sensor chamber

One serious problem that must be taken care of while designing the rain gauge is that the drops hitting the wall of the sensor chamber can cause errors in measurement. Suitable masking arrangement is to be provided to prevent drop from

hitting the wall of the sensor chamber. Driving rain causes hitting of drops on the body of the sensor chamber. This will cause disturbances that will be picked up by the sensor assembly. Suitable masking can avoid this problem also. It is also desirable to have a layer of sound absorbing material lined inside the chamber wall. This will ensure proper damping of the drop-generated noise to prevent overlapping of a drop signal from the other.

5.9.2.2 Problem with driving rain

Another problem that often encountered in measurement of rain is the driving rain. Driving rain is the raindrop splashes carried into the measurement system by wind. Driving rain often cause errors in measurement. Driving rain correction one method to compensate for the error in measurement. Since driving rain is contributed by wind, this correction is related to wind speed. Another popular method is to use masking the driving rain by the use of suitable masks. A typical masking arrangement is shown in Fig. 5.28.

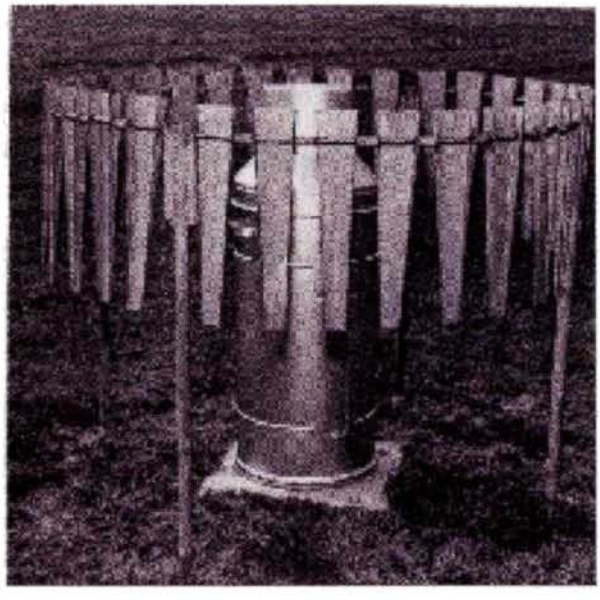

Fig. 5.28: Driving rain masking

5.10 Summary

A new method for detection of rain parameters from the acoustic noise produced by the rain has been suggested. The important findings that guided to this goal is that the low frequency signal strength present in the rain generated acoustic noise is related to the kinetic energy of the drops. Since kinetic energy of the drops is a function of the drop diameter, it is feasible to extract the drop size from the acoustic noise. Two algorithms to measure the DSD are also proposed. A correlation between the energy of the acoustic noise and the rain intensity is established, which will be a valuable aid in determining the rainfall rate from rain generated acoustic noise. Experimental verification of the proposed technique was conducted successfully. This method is well suited for automatic and remote measurement of rain parameters.

Chapter 6

Acoustic Rain Gauge

Based on the techniques as explained in the previous chapter, an acoustic rain gauge has been designed. Hardware and software design aspects of the acoustic rain gauge is explained in this chapter. The design is centred on a cost effective DSP controller chip that contains a DSP core and a microcontroller core. Accuracy considerations and performance comparisons with a standard tipping bucket rain gauge are also studied. This Acoustic rain gauge can be used for DSD estimation, rain detection, and rain rate measurement.

6.1 Practical Design of a Rain Gauge

In situ measurement of rain parameters over a wide area can be measured only by using a large clusters of rain gauges. Even though macro scale monitoring is possible with radar and satellite methods, they actually fail to detect the *ground truth.* In addition, it is always needed to verify the correctness of the indirect methods of rain measurement, which can be carried out with the use of ground-based rain gauges. Automatic rain gauges based on different principles of operation are widely available and were discussed in chapter 2. Most of the precise instruments are very costly and

hence not economical for applications that employ large number of rain gauges whereas the affordable low cost instruments are not accurate or not suitable for the environment. The technique of rain measuring as explained in chapter 5 can be adopted for designing cost effective and reliable instrument. Automatic measurement, remote measurement and automatic calibration features can be easily implemented. It is even practical to deploy irrecoverable instrument suitable for measurement at a remote or inaccessible locations.

6.1.1 Block schematic of acoustic rain gauge

A prototype rain gauge is developed to study the feasibility of using it in practical applications. All the signal processing functions were first simulated using MATLAB and verified the results. The block schematic of the rain gauge is shown in Fig 6.1.

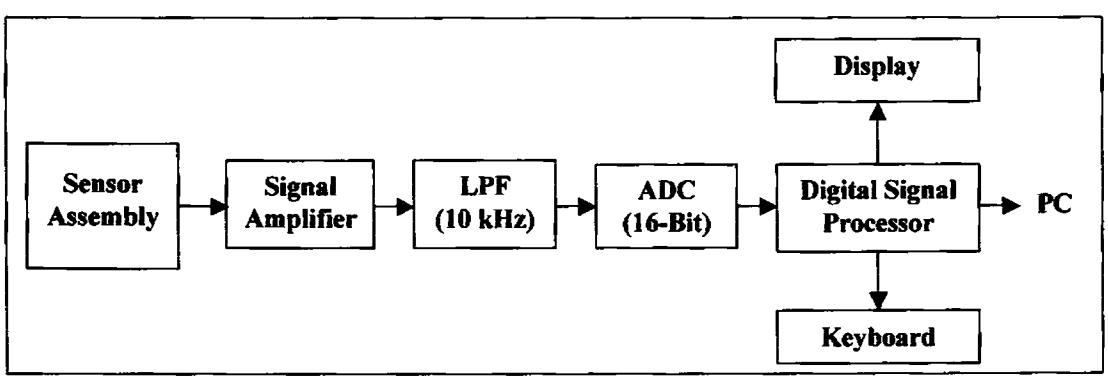

Fig. 6.1: Block schematic of the rain gauge

The design is very straightforward. The Sound card ADC of in a personal computer was found suitable to capture the acoustic signal. The signal was sampled at 48 kHz and digitised with 16 bits per sample. This signal is processed in the PC. A simplified flow chart for computing the rainfall from the signal captured by the sensor

assembly is furnished in Fig. 6.2. This has been implemented in MATLAB and experimented. The results obtained are correctly coincides the data obtained by other measurement methods.

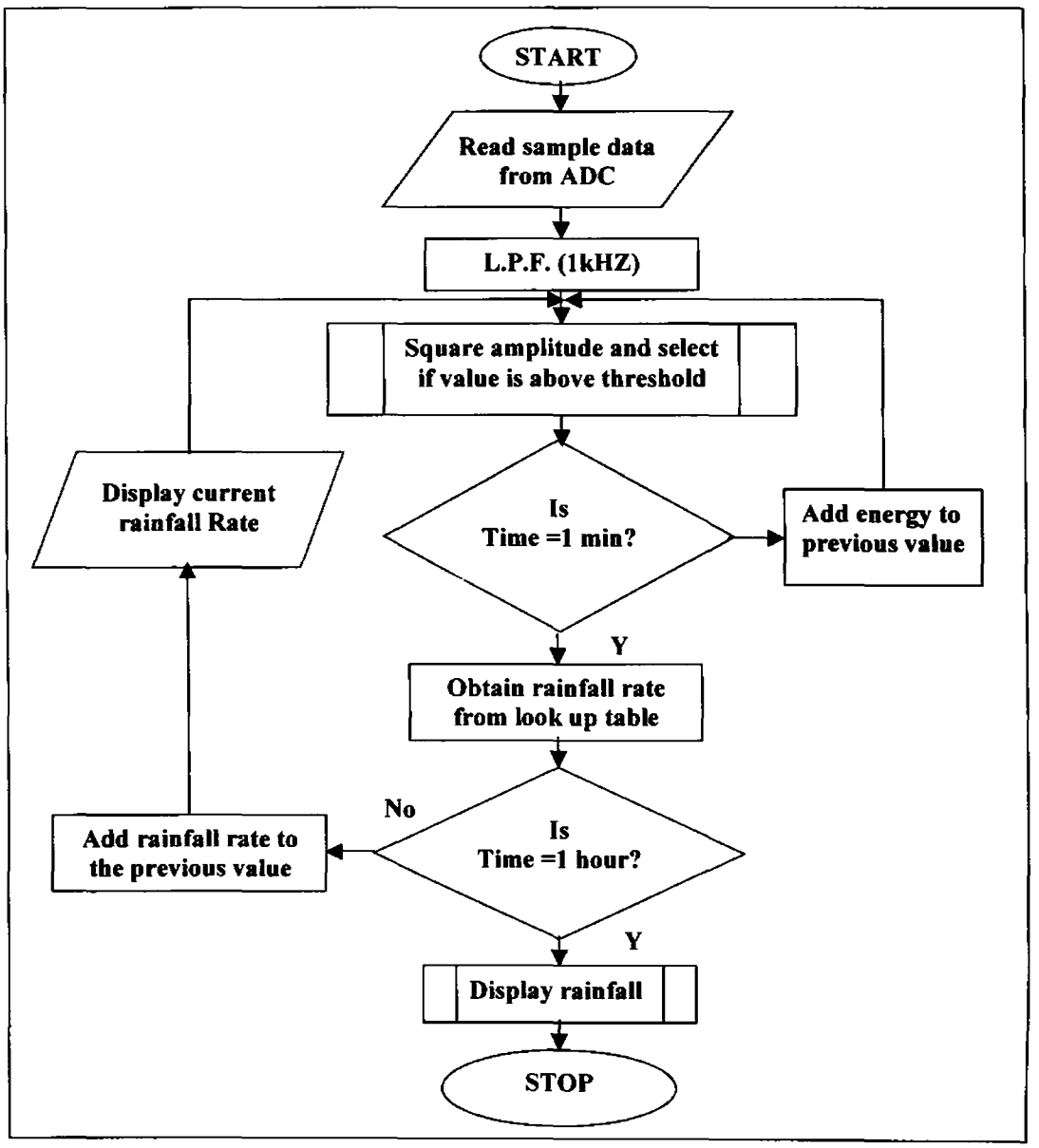

Fig. 6.2: Flow chart for estimating the rain

6.2 A Disdrometer Based on Kinetic Energy

An acoustic disdrometer is also built by using a DSP controller chip developed by Microchip Inc, USA, the block diagram of which is shown in Fig. 6.3. The rain sensor assembly is connected to a programmable gain amplifier (PGA) so as to have a sufficient level for the signal.

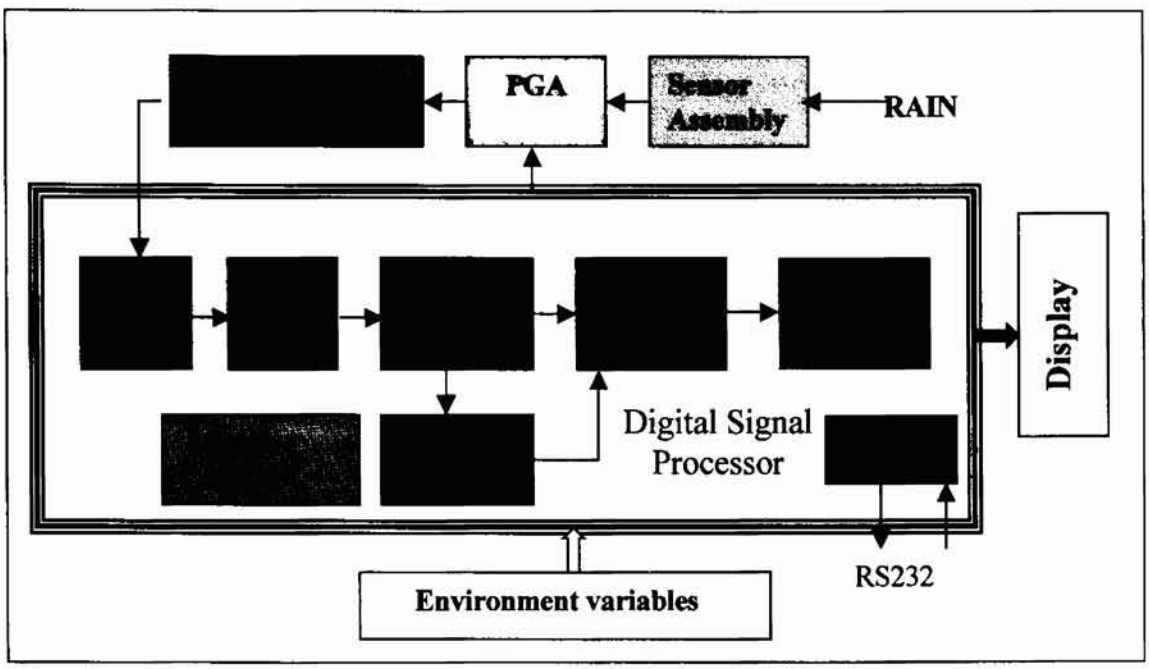

Fig. 6.3: Block schematic of the DSPIC based Rain gauge

6.2.1. Detailed block level explanation

PGA: Since rain noise has wide dynamic range, it is required to control the gain of the signal-conditioning amplifier. For lower rainfall events, higher gain is preferred and for heavy rain, gain is to be reduced to avoid saturation of the output. Circuit diagram

of the Programmable Gain Amplifier (PGA) is shown in Fig. 6.4. A digital potentiometer controls the gain of this stage. The first stage is a programmable gain differential amplifier. A dual digital potentiometer chip MCP 42100 performs gain adjustment. Microchip data sheet available in pdf format (Microchip Data sheet, MCP41XXX/42XXX Single/Dual Digital Potentiometer with SPI™ Interface, Microchip 11195c.pdf,) provides detailed information on this.

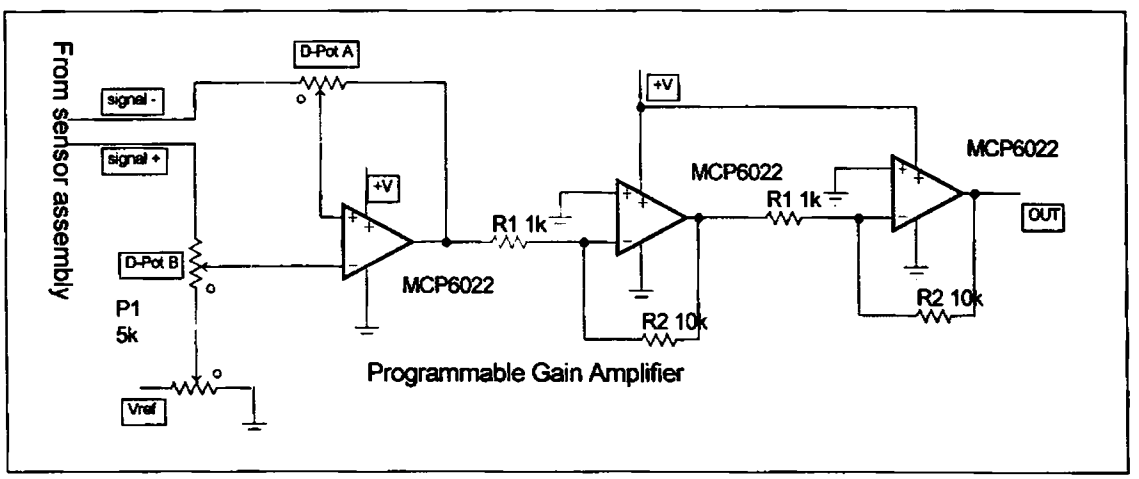

Fig. 6.4: Programmable gain amplifier

Second and third stage provides total gain of 100. MCP6022 dual op-amp having gain bandwidth product of 10 MHz is selected for this circuit. [Microchip data sheet, Single/Dual Digital Potentiometer with SPI™ Interface, 21733d.pdf].

The over all gain of the PGA can be set by the Digital signal controller manufactured by Microchip (commercially knows as "dsPIC") through the SPI Interface. Since the ADC of dsPIC cannot accept negative voltages, an offset voltage is added to the PGA so that the zero reference will be shifted to +2.5 volts. Now the signal level in the range of –2.5 to +2.5 Volts will be shifted to the range of 0 to 5

Volts at the output. Corrective measures are taken in the software to compensate this offset. The PGA output is fed to an anti aliasing filter, with a cut off frequency of 25 kHz. The circuit diagram of the antialiasing filter is shown in Fig.6.5. Here a three pole Butterworth design is adopted to provide sufficient high frequency rejection with good flat pass band characteristics. The filter characteristics are shown in Fig. 6.6.

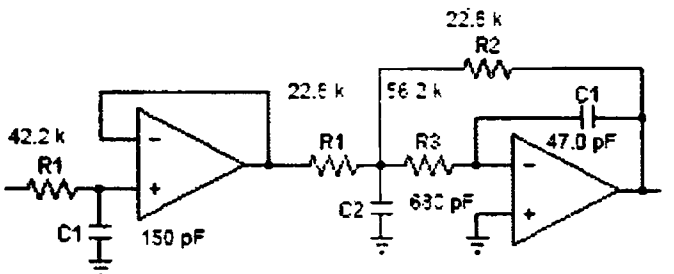

Fig. 6.5: Three pole Anti aliasing filter (cut off frequency 25 kHz design)

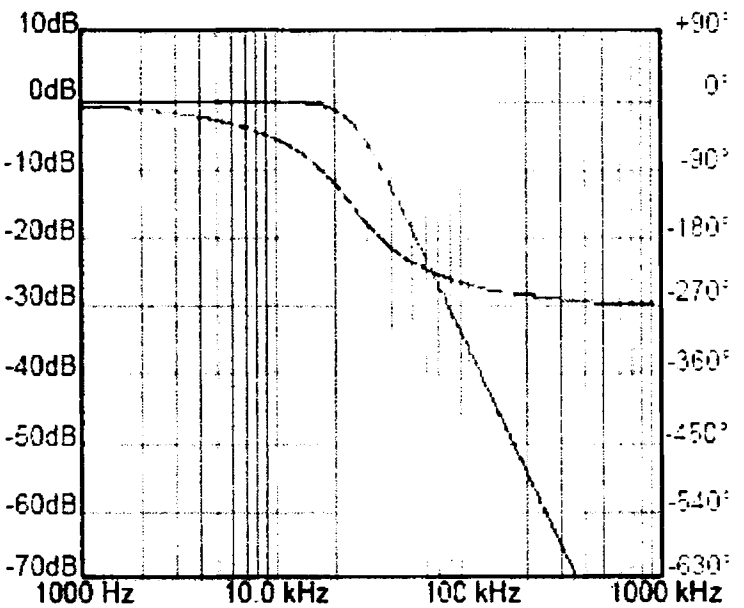

Fig. 6.6: Phase response (red) and gain (green) characteristics of the anti aliasing filter

ADC: The ADC is configured as 12 bits that can convert the input samples at every 10 microseconds. The conversion is initiated by the timer interrupt routine that gives "start of conversion" to the ADC every 10 microseconds.

6.2.2. Processing

Signal processing involves filtering, down sampling and energy computation. The digitised signal from ADC is read and low pass filtered. Filtered output is free from high frequency noise, especially that due to the bubble [M. Minnaert, 1933]. This filter is implemented using dsPICfdLite software. The Filter Reponses are shown in Figs. 6.7 and 6.8.

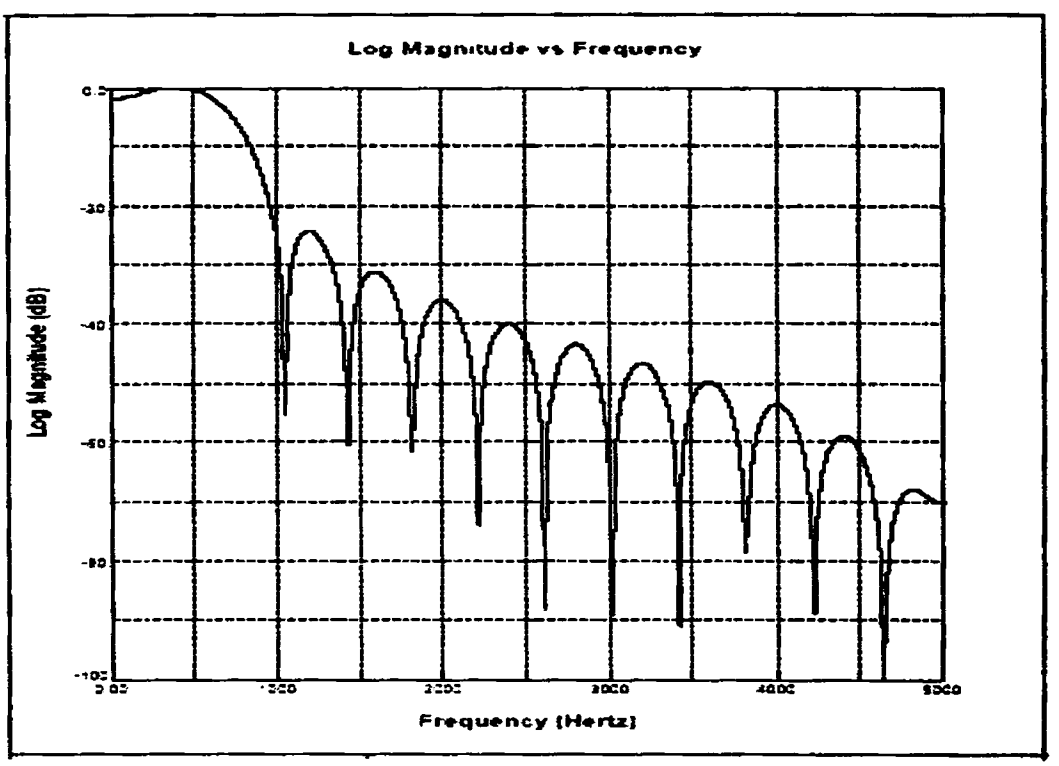

Fig. 6.7: Log magnitude plot of the LPF

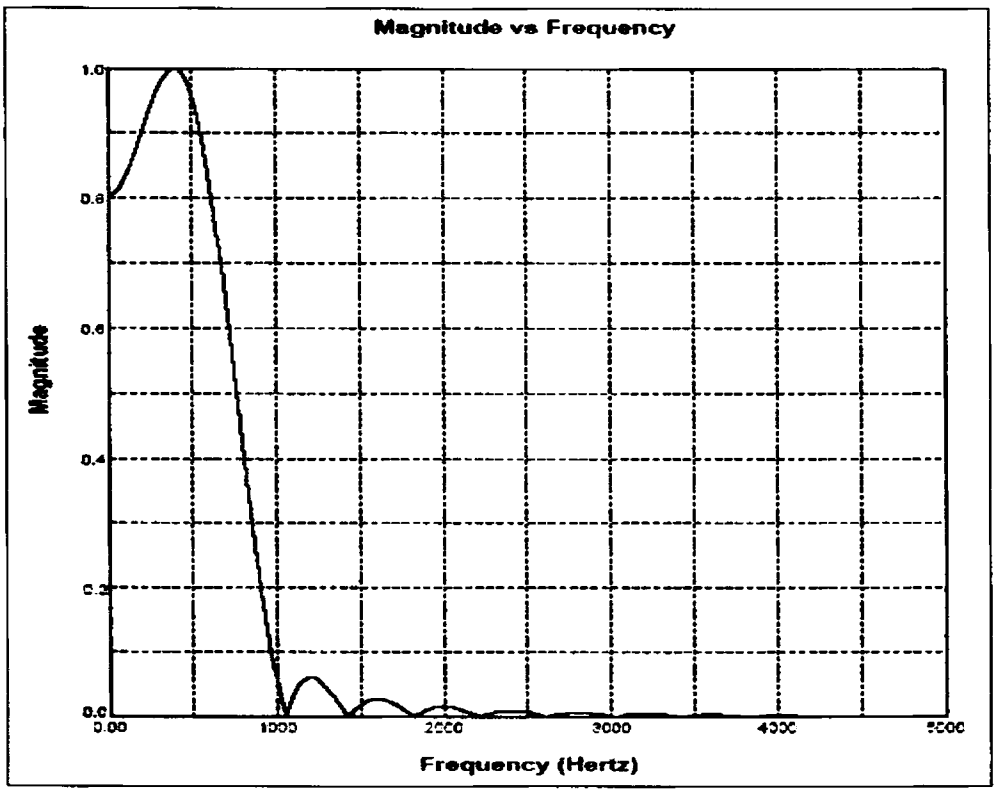

Fig. 6.8: Magnitude plot of the filter

To reduce the storage space and the processing overhead, the filtered data are down sampled by a factor of 5. Filtering and down sampling operations are performed in a single function. The technique used in this function actually performs convolution once in every 5th sample from ADC.

The dsPICfdLite was used to generate the filter coefficients. Filter routine is called whenever a new sample is available. Down sampling is also performed to reduce the sampling rate to 1/10.

Rainfall computations: Rainfall rate is computed for every one-second interval of time. This operation is performed by squaring and adding every sample for a duration

of one second. The resultant value is scaled down by multiplying it with a constant, determined by the over all gain of the analogue signal path and the digital filter characteristics. This constant needs to be calibrated (trimmed) for better accuracy. The scale down value is a 10-bit number and is used to address the "rain_rate_lookup_table" for getting the corresponding rainfall rate.

DSD estimation: The DSD computation is the most complex operation that is performed in the proposed system. The drop size is estimated from the signal energy contributed by the individual drops. For this, one needs to find out the significant portion of the signal contributed by the pressure variation due to the drop impact. The energy samples are accumulated in one of the 32-bit registers. This operation continues until the end of the response of a drop is reached. This operation is explained as shown below:

Let TE_n be the accumulated energy by taking sample values up to the nth sample from the start of a drop and $E_{n+distance}$ be the accumulated value after accumulating the energy samples up to $n+distance$. The distance was selected by trial and error. Now *TEn* represents the energy contributed by the drop, if $TE_{n+distance} < (TE_n + threshold)$. This comparison operation is also performed every time a new sample is input to the DSD estimation routine. TE_n is then scaled down to 10 bits and is used to address the "drop_lookup_table" and to retrieve the drop size corresponds to this energy.

Main Program: The flow chart of the main program shown in Fig.6.9 is self-explanatory. Processing and updating is done every seconds. The system is connected to the computer through the serial link (RS232 interface). User can communicate with the DsPIC processor using serial link and can send commands to the DSP processor. These commands include, creation of lookup-table, updating of processing variables like *threshold, distance*, etc. Data from the dsPIC (rain rate, DSD, etc) can also be sent to the computer by the DsPIC using the serial link.

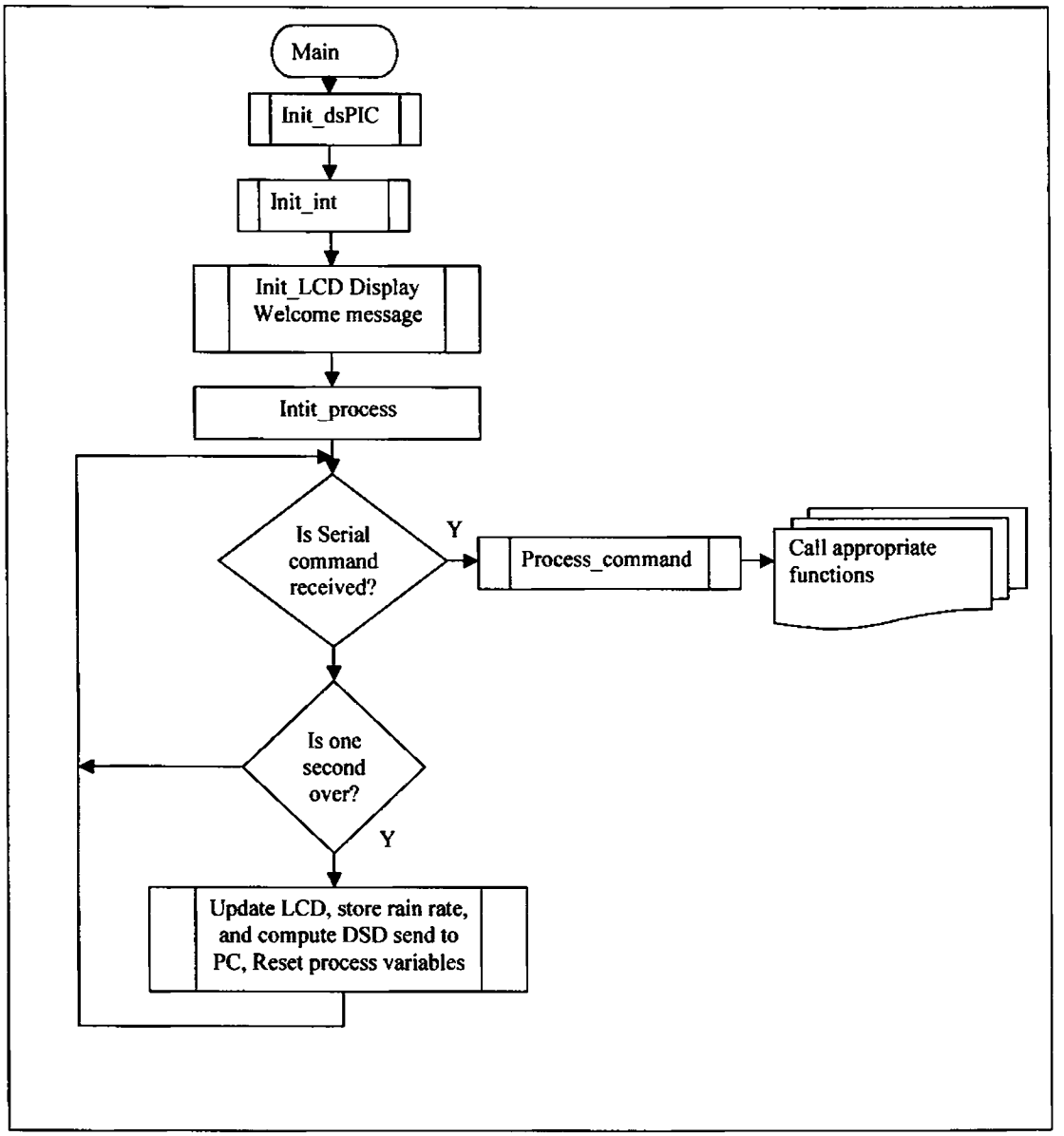

Fig. 6.9: Flow chart- Main Program

Drop detection routine: One of the very important routines is the implementation of the drop detection algorithm as explained in section 6.2.2. The flow chart for this routine is shown in Fig. 6.10.

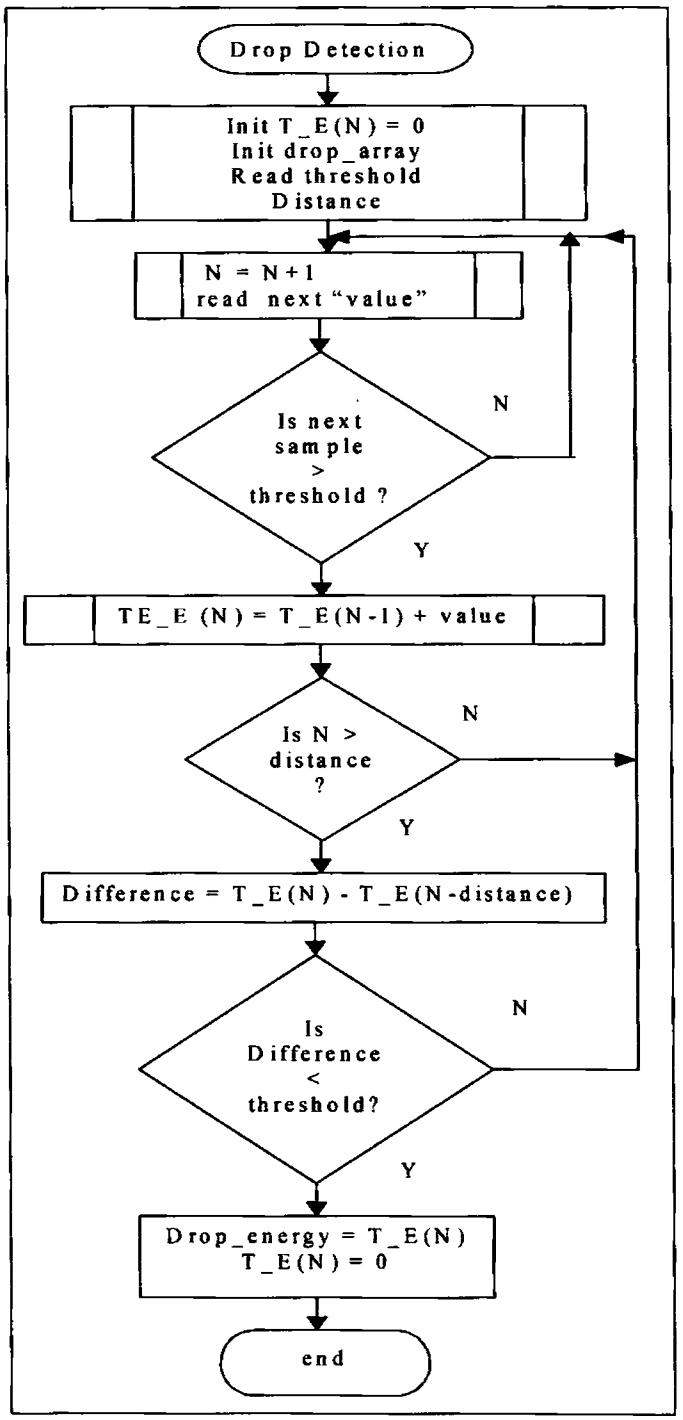

Fig. 6.10: Flowchart- drop detection

6.3 Accuracy and Resolution Considerations

Measurement accuracy of acoustic rain measurement system depends on many factors, which will be discussed in this section. The high sensitivity of the system enables one to detect and classify light rain like a drizzle. However, there are some ill effects due to the high sensitivity: The system will be overloaded with heavy rain or when a bigger drop is present in the rain. In addition, there is a chance of picking up noise from the wiring or from external sources like a power distribution transformer situated in the nearby place. A dynamically configurable gain setting of the amplifier in the sensor circuit can greatly reduce the noise problems. Better shielding of the sensor wiring and mounting of the sensor assembly will minimise the noise and electromagnetic interference (EMI) problems.

6.3.1 Lookup table creation

For the rain gauge to perform satisfactorily, the lookup table must be constructed carefully. Since the Intensity- acoustic energy relationship is not linear and depends on the energy accumulation period, separate lookup tables are needed for different duration of observations. Even though it is possible to construct the lookup table for higher time resolution of say 10 seconds, duration of less than 60 seconds measurement interval is seldom needed. Two lookup tables have been developed for rainfall accumulation for 1 minute and 10 minutes duration. Equations (5.14), (5.15) and (5.16) are used to construct the lookup table. The numerical constants of the expressions depend on the sensitivity of the hydrophone and overall gain of the analog processing circuits. The number of entries in the lookup table depends on the resolution of measurement. The total number of entries has to be limited due to the

finite word length and the memory capacity of the processing circuit. In most practical cases, higher measurement resolution is needed to measure lower rainfall rate than the resolution needed at higher rain intensity to be measured.

6.3.2 Dynamical configuration of gain setting

If the rainfall measurements at locations where one can expect wide variations in intensity are to be carried out, then it is always required to adjust the gain of the signal-conditioning amplifier. This warrants an adaptive gain setting for the system. This modification can be easily adopted in software. Adaptive gain setting will definitely improve the performance of the ARG.

6.4 Selection of Suitable Transducer

The performance of the ARG was validated with the wide band transducer manufactured Brüel & Kjaer. This transducer is intended for scientific research. Since the cost of the transducer is very high, and since the ARG does not require such a wide band transducer, a cost effective transducer can be used. A transducer with low frequency response of 1 kHz is less costly than a wide band transducer.

6.5 Advantages and Disadvantages

A critical analysis of the proposed method reveals its advantages and disadvantages. However, many of the distinct and desirable features of the system make it attractive for various applications. The features and disadvantages will be discussed in the following sections.

6.5.1 Advantages and features

The cost of the system is comparable to that of a TBR. So the ARG can be compared with TBR for its features and measuring accuracy. It is true that many of the facilities available with the ARG are not available with many of the existing conventional rain gauges. These features are discussed below:

6.5.1.1 A low cost disdrometer

As explained in the previous sections, this system is suitable for measuring DSD. Experimental result shows that it can be used as a low cost disdrometer. Better accuracy is obtained if the system is calibrated at the environment where it is to be installed. However, detailed tests and evaluation methods are to be adopted for calibration. When used as a Disdromter, its cost will only be a fraction of the cost of the most accurate Disdrometers (eg: the 2D video disdrometer) presently available in the market.

6.5.1.2 Automatic rain gauge

Rainfall accumulation will be automatically acquired more accurately with this system than with a TBR. Since there are no moving parts, mechanical errors are eliminated. Rain intensity measurements at regular intervals are possible and there is no delay in the measurement whereas TBR gives a reading only when its bucket is filled and tipped. Resolution of measurement of TBR is only 0.01" whereas more than 10 times resolution is possible at lower rainfall rates with the proposed design. Remote measurement is possible by acquiring and transmitting the acoustic signal directly to the processing site where all the processing systems are installed. At the monitoring sites, only the sensor assembly and minimum hardware required for amplifying, modulating and transmitting the signals are needed. The processing

system installed at the processing site can be simultaneously used to process signals from many such measurement sites.

Table 6.1 shows a performance comparison of a standard tipping bucket rain gauge with the proposed ARG.

Table 6.1. Comparison of ARG with TBR

TBR	ARG
Delay in the measurement	Real time measurement
Mechanical errors present	No moving parts and hence no mechanical errors
Under estimation error due to evaporation	No error
Under estimation of higher rainfall rates	No appreciable error until the upper measurement limit is reached
Stationary and plane platform is needed.	Positioning is not very critical.
Not effected by atmospheric acoustic noise	Can cause error due to acoustic noise from other sources and vibrations.
Design is simple and no signal processing or electronics needed	Needs electronics circuit and signal processing circuits
Very low power consumption	Power consumption is more than that of a TBR

6.5.1.3 Rain detector

One simple alternate application for the system is to use it as a rain detector, where one needs to know only the presence of rain. The sensor assembly with minimum hardware as shown in Fig. 6.11 can be used as a rain detector that eliminates the chance of false triggering.

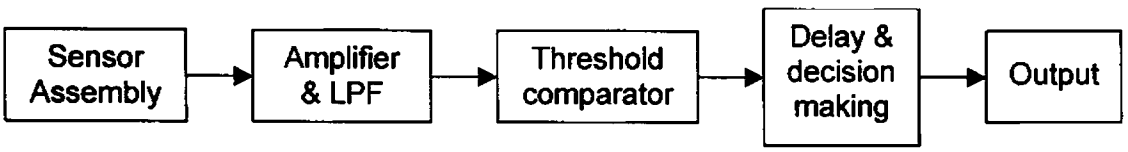

Fig. 6.11: Rain detector

Since the drop impact generated signal contains a low frequency around 32 Hz, depends upon the geometry of the sensor assembly, the detection of rain is possible simply by measuring the signal level at 32 Hz in the acoustic noise. Rain is detected if the 32 Hz signal is continuously present.

6.5.1.4 Alternative uses for the proposed rain gauge

Widely used fire protection systems in buildings and warehouses use water spray sprinklers for automatic fire protection. For effective fire suppression, the sprinkler water must reach the burning surface. An optimum sprinkler system is the one that provides the maximum fraction of water delivered by the sprinklers to the burning surfaces and suppresses the fire in the shortest time after its initiation. The design of such a sprinkler system depends on the geometrical relationship between the sprinklers and the fire source and its heat release rate, the geometry of the room and its ventilation conditions and the sprinkler spray characteristics.

Field measurements are needed to ascertain the drop size distribution, drop velocity, sprinkler induced flows, and the actual delivery density. A number of standard techniques and instruments are available for measuring drop size distributions such as Phase-Doppler Interferometry (PDI) [W.D. Bachalo (1994); Widmann, J.F. (2000)] and the Optical Array Probe (OAP) by Particle Measuring Systems [C.R. Tuck et al., 1997. Putorti, A.D. et al., 1999]

The acoustic method is a suitable technique to provide the drop size distribution and drop velocity data of sprinklers. Arrays of sensors are to be used to determine the sprinkler DSD as well as the sprinkling pattern.

6.5.2. Drawbacks

Some of the inherent disadvantages of the ARG are as follows:

1. The system can only be used to measure the liquid precipitation, whereas many of the automatic rain gauges can be used to measure solid precipitation by adding attachments (heater) so as to transform the solid precipitation. Since the drops have to fall into the sensor chamber with terminal velocity, this method cannot be adopted for ARG.
2. Calibration requirement is more complex than the cost effective automatic measurement systems. Factory set-up is needed for full calibration. However, It is possible to develop a calibration procedure with the use of personal computer and knowledge of DSD function of the expected rainfall.
3. The most important component of ARG is the sensor and the sensor assembly. The availability of the small size, low cost and reliable transducer is to be designed and developed.
4. Sensitivity to noise: The system if not installed properly, can pick up acoustic noise propagated through the ground such as vehicle traffic, power transformer vibrations due to magnetostriction, etc. Since rain gauges are normally installed at convenient places at a calm and quiet place, this is not a serious limitation.
5. One drawback of the ARG compared to the TBR is the power consumption. Since TBR will be active and consuming power only at the

time of tipping the bucket, the power consumed by the TBR is less. The ARG need power to function the signal conditioning amplifiers continuously, which demands more power than the TBR.

6.6 Summary

In this chapter, a discussion of the design and implementation of an acoustic rain gauge capable of sensing the DSD and rainfall rate is presented. Various advantages and shortcomings of the design are also discussed in this chapter. The Acoustic rain gauge can find many applications in real life.

Chapter 7

Summary and Conclusions

This chapter consolidates the measurement techniques, results and inferences gathered from the investigations discussed in this thesis. A comparison of the measurement method suggested on the basis of the findings of this research work with the conventional acoustic rainfall measurement technique is also presented in this chapter. The conventional acoustic technique uses multi channel high frequency signal processing and hence the computational complexity is more, whereas the proposed technique needs only to process the low frequency spectrum of the acoustic noise. Absence of bubble generated acoustic noise for certain drop sizes will contribute errors in the measurement using the conventional acoustic rain gauge. The proposed method is more accurate for ground-based measurement as well as for open ocean measurement. There is no time delay in extracting the rain parameters compared to the other types of rain gauges. The proposed technique can be adopted for various other applications such as sprinkler nozzle calibration, rain detection, etc. These alternate applications are also discussed in this chapter. Improvements possible and the possibilities that can be further investigated to improve the accuracy of measurement are also discussed in this chapter. The thesis concludes with a brief discussion on the future scope of research in this area such as investigations using array of sensors and the development of a low cost transducer for the sensor assembly.

7.1 Highlights of the Thesis

This work has been carried out to determine a simple, cost effective solution to the problems encountered in rainfall measurement by employing the acoustic technique, in which a lot of researches are going on. Most of these works are concentrated on the wideband underwater noise produced by the impact of raindrops onto the water surface. Acoustic rain gauges are already available in the open market as a commercial product that utilises the phenomenon of the ringing sound of bubbles entrapped underwater by the raindrops. These rain gauges are suitable for rainfall measurement over open ocean only and suffers many drawbacks. One of the major drawbacks of this measurement technique is that bubble is not always produced by the falling drops since the bubble production depends on many other variables like surface tension, salinity, temperature etc. Hence, necessary corrections are to be applied for eliminating the errors contributed by the silent drops. Another drawback is associated with the formation of secondary droplets. This was explained in chapter 3.

These issues were addressed in a different way in this thesis. The research work is concentrated on to the kinetic energy of raindrops. At first, investigations are carried out to establish the relationship of the near field pressure variations at the impact site and the kinetic energy of the impacting drop. It was also discovered that there is a low frequency component in the underwater acoustic noise and this has been studied in detail to classify the drops. This was studied in detail and established the relationship between the drop size and the acoustic energy of the underwater noise. Later a sensor assembly was developed to capture this low frequency underwater noise produced by the drops. One of the major highlights of the thesis is the development of the sensor assembly, which facilitates the measurement of rainfall in land as well as in ocean or lakes.

Since the maximum frequency of the rain noise to be dealt with is around 600 Hz only, the processing of the signal becomes simple and efficient. The transducer for the sensor assembly will also becomes simple, as it needs to pickup only low frequency signals. Thus, cost effective realisation of the measurement systems using the technique proposed in this thesis is very much practically motivated.

The effectiveness of the sensor assembly in capturing and analysing the underwater noise with an aim to detect raindrops and to classify the rainfall was experimentally established.

A rain gauge was developed by employing the outcome of the approach and verified the measurement results. Experiments on rainfall measurement were conducted for almost three years to arrive at the proposed system.

Another highlight of this work is that the technique proposed and the sensor assembly developed can be modified and applied in various other applications such as detection of rainfall, calibration of sprinkler nozzles, drop counting that finds wide application in industry as well as in medical fields.

7.2 Future Scope for Research

The work presented in this thesis has a lot of scope for further research for betterment of the result obtained as well as to perfect the applications of the techniques. Some of the possible threads for research are discussed here:

7.2.1 Developing a suitable transducer

A good transducer with better sensitivity, reliability and low cost is always preferred for the ARG. An innovative transducer design based on conducting

polymers can be adopted for this application. The Department of Polymer Science and Rubber Technology, Cochin University of Science and Technology had developed a conducting polymer material and they are in the process of developing a pressure transducer based on conducting polymers that can be used for these types of applications. Their initial findings show that the transducer developed will be cost effective and reliable.

7.2.2 Experimental studies and comparison with more precise measurement systems

The experiments were conducted in Cochin (south India) and that also for monsoon rain. Experimental verification and proof for the usefulness and accuracy of the measurement for other type of rainfall events that exists in other geographical area can also to be attempted. Similarly, precise equipments like optical disdrometer, etc. may be employed for more accurate verification of the results and calibration of the system.

7.2.3 Better processing algorithms

It is always possible to adopt better algorithms to compute the parameters to be measured to improve the accuracy of the measurement and to reduce the computational complexity. Improvement of accuracy of measurement and increased area of coverage may also be attempted with an array of sensors and a single processing unit.

7.2.4 Use of multiple sensors

Study of the effectiveness of measuring the rain intensity and DSD by using more than one sensor assembly scattered around the same location is yet another aspect that can be explored. An array of sensors can be used to capture and cross compare the values, so that the errors due to noise, instrumental errors, sensor errors, etc. can be minimised.

7.2.5 Other factors affecting the measurement

For very precise measurement, various environmental factors affecting the measurement are to be investigated in detail. The effect of temperature variation on the measurement is an important aspect that has to be investigated in detail.

7.3 Summary

This research work was carried out with an aim of developing a technique to measure the rain parameters using the low frequency signal present in the acoustic signal captured using the sensor assembly. The proposed measurement method has been validated experimentally. This new technique of measurement can be exploited to solve several other problems like sprinkler calibration and Kinetic energy determinations. The proposed method is economical compared to the existing methods of DSD measurement and rain rate measurement.

Appendix A

A1. MATLAB program for Drop Detection
(Algorithm 1 as per Fig. 5.9)

```
clear all;
sig1=wavread('rain.wav'); % read the rain wave file
sig2 = sig1(30000:70000); % ( processing is done part by part to speed up operation)
L = length(sig2);
% window size declaration. The drop fall oscillation range is set to be 1000
% need to be fine tuned.
DURATION = 600;
Y0 = abs(sig2);
AT = .2 * max(Y0): % 40 percent of max amplitude as threshold. Needs modification
for i=1:L
   if (Y0(i) >= AT)
      Y1(i) = Y0(i);
   else
      Y1(i) = AT;
   end;
end;

% find derivative
for i=2:L- 1
  Y2(i) = Y1(i+1) - Y1(i-1);
end;

% plot(sig2):figure; plot(Y2):break;
TH=.005; % set a threshold
% Detect drop fall points
i=1; k=1;

while (i < L)
   if (Y2(i) > TH)
      DROP(k) = i;
      k = k+1;
   end;
   i = i+1;
```

```
end;

Q = DROP;
% Map drop fall points to actual timing
k=1;
for i=1:length(sig2)
  if i == Q(k)
     sig(i) = (sig2(Q(k)));
     k = k+1;
     if k > length(Q)
       break;
     end;
  else
     sig(i) = 0;
  end;
end;

% Remove redundant points caused due to oscillations. Assume that the
% drop range is 2000. Need to be revised ?
i=1;
SL=length(sig);
while i <= SL
  if sig(i)
   if ((SL-i) > DURATION)
     RNG = DURATION;
   else
    RNG = SL-i
   end;
   % A rain drop fall cause oscillations of almost equal range in +ve and
   % -ve directions whereas a bubble break does not cause an equal swing in
   % the -ve range. So, take the ratio of local max and local min to see
   % whether the peak is caused by a rain drop or noise. (Ratio need to be
   % fine tuned )
   Mx=max(sig(i:i+RNG)); % local maximum
   Mn=min(sig(i:i+RNG)); % local minimum
   if (abs(Mx/Mn) > 1)
     Mx = 1000; Mn = 1000; % set to impossible values
   end;
   % check for the local max in the window and set to zero all other peaks
   for k=i:i+RNG
```

```
      if sig(k) ~= Mx
         sig(k)=0;
      end;
    end;
    i = i + RNG;
   else
    i = i+1;
   end;
end;
plot(sig2,'g');hold;
plot(sig,'r');hold;

% END OF PROGRAM
```

A2. MATLAB program for Drop Detection
(Algorithm 2 as per Fig. 5.11)

```
% this program plots the signal and the total
%energy and compares with the that of the previous
% sample. If the previous value is less than present value+ THRESHOLD,
% then present value is set to zero, and a new cycle of drop
% detection begins. The energy sample value just before the zero value
% represents the drop energy.
clear all;
close all;
% read the audio wave file
xx = wavread('E:\Research\RAIN\different_rainrates/01.wav');
N = length(xx); % take suitable lenght of data for computation
ax = [1:N];
threshold1 = 0.0001; % assume threshold values
threshold = 0.001;
[b,a] = cheby1(10, .01, 600/24000);
%x = filter(b,a,x);
Xx = (decimate (xx,8));
Ith =0;
L =3;
A = pi*0.1^2;
t= (L*10000)/48000;
for list =1: L,
  Y =(Xx(1+list*10000:list*10000+ 10000));
%figure:plot(Y); Signal can be pltoed with this command
  N = length(Y)
  %drops(1:N) = 0;
  %Ith = 0;
  axes = [1:N];
  distance = 40;
  % compare distance
  energy(1) = 0;
 %drops(1:N)=0;
 %length(drops);
  nth =1;
      for I = 2:N,
          if (abs(Y(I))> threshold1)  % thresholding operation
             nth = nth+1;
```

```
                energy(I) = energy(I-1)+ (Y(I)*Y(I));
            else
                nth = nth+1;
                energy(I) = energy(I-1); % Energy accumulation
            end
        if (nth>distance)
            diff = energy(I)-energy(I-distance);
        if (diff < threshold)
            Ith = Ith+1;
          drops(Ith) = energy(I);
          energy(I);
          drd(I) = energy(I); %drop energy computed
         energy(I) =0; %Initialise for next drop
         nth = 1;
      end
      end
  end
    length(drd)
    figure; plot(axes, Y,'k'); hold; stem(axes(3:10000),drd);
    %figure; stem(drops(1:Ith));
  % loop='loop begin'
% drop computations by solving the polynomial expression
  Ith

for I = 1:Ith,
    P=[0.0016  -0.0268   0.7310  -4.8188  13.4901  -1.3379   0.0338 0 0 -drops(I)];
   x = roots(P);
  drop_size(I) = x(5);
end

 % intermediate ploting for observation
  message = 'drops computed'

dsd= hist(drop_size,300);
[b,a] = cheby1(2, .1, 100/500);
 % dsd = filter(b,a,dsd);
  %figure; plot(dsd,'.');
  figure; plot(axes,energy*2,axes,Y);
end
 dsd= hist(drop_size,30); % dsd computation in 30 bins
```

```
   for D = 1:length(dsd),
      X = D/5;
      Vt = (0.0561*X^3-0.912*X^2+5.03*X-0.254);
      N(D)= dsd(D)/(Vt*A*t);
   end
   figure; plot(N,'.');
 % different plots are possible withe the following lines:
%    figure; plot(dsd);
  % plotyy(ax,Y, ax,drops);
  % figure;
%subplot(3,1,1), plot(Y,'r');
%subplot(3,1,2), bar(drops,'grouped');subplot(3,1,3), plot(energy,'b');
%subplot(3,1,2), hist(drops,100);
% END OF PROGRAM
```

Bibliography

1 Adami, A. and Da Deppo, L., 'On the systematic errors of tipping bucket recording rain gauges', *Proc. Int. Workshop on the Correction of Precipitation Measurements*, Zurich, 1-3 April 1985.

2 Alexander R and Dusan Z, 'Beamwidth Effects On The Differential Phase Measurements Of Rain', *J. Atmos. and Oceanic Tech.*, Vol. 15, pp. 624, 694, 1998

3 Atlas, D., 'Optical extinction by rainfall', *Journal of Meteorology,* 10, pp 486-488, 1953.

4 Atlas, D., Ulbrich, C. W., 'Path- and area integrated rainfall measurement by microwave attenuation in the 1-3 cm band', *Journal of Applied Meteorology* 16, pp 1322-1331, 1977.

5 Attle et al, 'Applications of Image Analysis', *American Laboratory*, April 1980.

6 Bachalo W.D., 'Experimental Methods in Multiphase Flows', *Int. J. Multiphase Flow,* Vol. 20, Suppl., pp261-295, 1994.

7 Battan L.J., 'Radar Observation of the Atmosphere', Univ. of Chicago Press, Chicago, Illinois, pp. 324, 1973.

8 Beard K.V., 'Terminal velocity adjustment for cloud and precipitation drops aloft', *Journal of Atmospheric sciences,* 33, pp. 851-864, 1976.

9 Beard, K.V, Terminal velocity and shape of cloud and precipitation drops aloft, *Journal of atmospheric Sciences*, 33, pp. 851-864, 1976.

10 Beard, K.V., and C. Chuang, 'A new model for the equilibrium shape of raindrops', *J. Atmos. Sci.,* 44, pp. 1509 – 1524, 1987.

11 Bentley and Wilson A., 'Studies of raindrops and raindrop phenomena', *Monthly Weather Review*, 32, pp. 450-456, 1904.

12 Black, Peter G., Proni, John R., Wilkerson, John C., Samsury, Christopher E., 'Oceanic Rainfall Detection and Classification in Tropical and Subtropical Mesoscale Convective Systems Using Underwater Acoustic Methods', Monthly *Weather Review*, Vol125 (9), pp. 2014-2042, 1997

13 Blanchard, D. C., and A. T. Spencer, 'Raindrop measurement during Project Shower', *Tellus*, 9, pp. 541-552, 1957.

14 Blanchard and Duncan C., 'Raindrop size distribution in Hawaiian rains', *Journal of Meteorology*, 10, pp. 457-473, 1953.

15 Bowen, E. G., 'The formation of rain by coalescence', *Australian Journal of Scientific Research*, A3, pp. 192-213, 1950.

16 Bragg W, The world of sound, *Bell*, London, 1920.

17 Brazier-Smith, P. R., Jennings, S. G., and Latham, J., 'The interaction of falling water drops: coalescence', *Proc. Roy. Soc. Lond.*, A326, pp. 393-408, 1972.

18 Bringi, V.N. and V. Chandrasekhar, *Polarimetric Doppler Weather Radar: Principles and Applications*, Cambridge University Press, 636 pp., 2001.

19 Bühler S., P. Eriksson, W. Haas, N. Koulev, T. Kuhn and O. Lemke, 'ARTS User Guide, Version 1.0.38', Download from http://www.sat.uni-bremen.de/arts/, *University of Bremen*, Aug. 2002.

20 Calder, I.R. and Kidd. C.H.R., 'A note on the dynamic calibration of tipping-bucket gauges, *J. Hydrology*, 39, pp. 383-386, 1978.

21 Campos, Edwin, and Isztar Zawadzki, in preparation: Instrumental uncertainties in Z-R relations, Submitted to the *Journal of Applied Meteorology*.

22 Campos, 'On measurements of drop size distribution', Top. Meteor. Oceanog., 6(1), pp. 24-30,1999

23 Carey, L.D., S.A. Rutledge, and D.A. Ahijevych, 'Correcting propagation effects in C-band polarimetric radar observations of tropical convection using differential propagation phase', *J. Appl. Meteor.* 39, pp. 1405 – 1433, 2000.

24 Cerro, Carlos, Bernat Codina, Joan Bech, and Jeroni Lorente, 'Modeling Raindrop Size Distribution and Z(R) Relations in the Western Mediterranean Area', *Journal of Applied Meteorology*, 36, pp. 1470-1479, 1997.

25 Chan P.W. and Yeung C.L., '*A Study of Drop-counting Rain Gauges*', *Hong Kong Observatory*, February, 2004

26 Collier, C.G., 'Applications of weather radar systems: a guide to uses of radar data in meteorology and hydrology, *Ellis Horwood Limited Publishers. Chichester UK*, pp. 408, 1996.

27 Doviak, Richard J., Zrnić, Dušan S., 'Doppler Radars and Weather Observations', San Diego Academic Press, Second Edition, 1993.

28 Donnadieu, G., 'Comparison of results obtained with the VIDIAZ spectro pluviometer and the Joss-Waldvogel rainfall disdrometer in a 'rain of a thundery type', *Journal of Applied Meteorology*, 19, pp. 593-597, 1980.

29 Eigel J.D., and More I.D, 'A simplified technique for measuring raindrop size and distribution', *TRANSACTIONS of the ASAE* 26, pp.1079-1084, 1983.

30 Elmore P. A., G.L Chahine and H. N. Oguz, 'Cavity flow measurements of reproducible entrainment following drop impacts', *Experiments in Fluids*, 31, pp. 664-673, Springer_Verlog 2001.

31 Elwell, H.A, 'Modelling soil losses in Southern Africa', *J. Agri. Engg*, 23, pp. 117-127, 1978.

32 Fankhauser, R., 'Influence of systematic errors from tipping bucket rain gauges on recorded rainfall data', *Wat. Sci. Tech.*, 37 (11), pp. 121-129, 1998.

33 Feingold, G., and Z. Levin, 'The lognormal fit to raindrop spectra from frontal convective clouds in Israel', *Journal of Climate and Applied Meteorology*, 25, pp. 1346-1363, 1986.

34 Foster G.R., McCool D.K., Renard K.G., and W.C. Moldenhauer, 'Conversion of the universal soil loss equation to SI metric units', *Journal of Soil and Water Conservation*, 36, 6, 1981.

35 Foster, G.R., Modeling the Erosion Process. In: T.C. Haan (ed.), 'Hydrologic Modeling of Small Watersheds', St. Joseph, MI: *American Society of Agricultural Engineers*, pp. 297-380, 1982.

36 Franz, G.J., 'Splashes as source of sound in Liquids', *J. Acoust. Soc. Am*, Vol. 31 (8), 59, pp. 1080-1096, 1959.

37 Frere, M.H. and Leonard R.A, 'Modeling the Quality of Water from Agricultural Land'. In: T.C. Haan (ed.), *Hydrologic Modeling of Small Watersheds*, St. Joseph, MI: American Society of Agricultural Engineers, pp. 381-405, 1982.

38 Fuchs N., and Petrjanoff I., 'Microscopic examination of fog-, cloud-, and rain-droplets', *Nature* 139, pp. 111-112, 1937.

39 Fujiwara, Miyuki, 'Raindrop size distribution in warm rain as measured in Hawaii', *Tellus*, 3, pp. 392-402, 1967.

40 Friesen, G M, Thomas C J, Manal A J, Stanford L Y, Stephen R Qt and Troy H N, 'A comparison of noise sensitivity of Nine RS detection Algorithm', *IEEE Trans. On biomed. Eng.* Vol. 37, No.1, Jan 1990.

41 Gekat, F, P. Meischner, K. Friedrich, M. Hagen, J. Koistinen, D.B. Michelson and A. Huuskonen, 'The State of Weather Radar Operations, Networks and Products', *Weather Radar: Principles and Advanced Applications (*Ed. P.Meischner). Springer monograph series "Physics of Earth and Space Environment", pp. 337, 2003.

42 Gillespie, Daniel, T., 'Three Models for the Coalescence Growth of Cloud Drops', *Journal of the Atmospheric Sciences*, 32, pp. 600-607, 1975.

43 Guifu Zhang, J. Vivekanandan, and Edward Brandes, 'A Method for Estimating Rain Rate and Drop Size Distribution from Polarimetric Radar Measurements', *IEEE Transactions On Geoscience And Remote Sensing*, VOL. 39, NO. 4, pp. 830-841, 2001.

44 Gunn, R., Kinzer, G.D., 'The terminal velocity of fall for water droplets in stagnant air', *J. Meteor*, 6, pp.243-248, 1949.

45 Hall, 'Use of the Stain Method in Determining the Drop-Size Distribution of Coarse Liquid sprays', *Transactions American Society of Agricultural Engineers*, 13, 1, pp. 33-37, 41, 1970.

46 Hauser, D., P. Amayenc, B. Nutten, and P. Waldteufel, 'A New optical instrument for simultaneous measurements of raindrop diameter and fall speed distribution', *Journal of Atmospheric and Oceanic Technology*, N0.1, pp. 256-269, 1984.

47 Hawkins, R.H, 'Effects off rainfall intensity on runoff curve number', *Hydrollogy and Watter Resources off Ariizona and the Sout west* 8, pp. 53—64, 1978.

48 Hawkins, R.H, 'Asymptotic determination of runoff curve numbers from data', *Journal of Irrigation and Drainage Engineering* 119:2, pp. 334-345, 1993.

49 Hawkins, R.H., A.T. Hejlmfelt, and A.W. Zevenburgen, 'Runoff probability, storm depth, and curve numbers', *Journal of Irrigation and Drainage Engineering* 111:4, pp. 330-340, 1985.

50 Hejlmfelt, A.T., 'Empirical investigation of curve number technique', *Journal of Hydraulic Division* 106:HY9, pp. 1471-1476, 1980.

51 Houghton, H.G., 'On precipitation mechanisms and their artificial modification', *J. Appl. Meteorol.* , 7, pp. 851-859, 1968

52 Hu, Z., and R. C. Srivastava, 'Evolution of raindrop size distribution by coalescence, breakup, and evaporation: Theory and observations', *Journal of the Atmospheric Sciences*, 52, pp. 1761-1783, 1995.

53 Hugh C Pumphery and L.A. Crum, 'Under water sound produced by individual drop impacts and rainfall', *J. Acoust. Soc. Am,* 85, (4), pp. 1518-1526, 1989.

54 Illingworth, A. J., and C. J. Stevens, 'An optical disdrometer for the measurement of raindrop size spectra in windy conditions', *Journal of Atmospheric and Oceanic Technology*, 4, pp. 411-421, 1987.

55 Illingworth, Anthony J., Daniele Hauser, and Paul Amayenc, 'A Comparison of Optical Shadowgraph Instruments for Measuring Raindrop-Size Spectra', *Journal of Atmospheric and Oceanic Technology*, 7, pp. 175-176, 1990.

56 Imam, B, 'Nonlinear Uncertainty Analysis of Multiple Criteria Natural Resource Decision Support Systems'. Ph.D. dissertation, School of Renewable Natural Resources, The University of Arizona, 382 pp, 1994.

57 Jacobus P.W., 'Sound radiation from large raindrops', M.S. thesis, Naval Postgraduate School, Monterey, California, 1991.

58 Jiang, H., M. Sano, and M. Sekine, 'Weibull raindrop-size distribution and its application to rain attenuation', *IEE Proceedings-Microwave Antennas Propagation*, 144, pp. 197-200, 1997.

59 Joe, P. I., and R. List, 'Testing and performance of two-dimensional optical array spectrometers with grayscale', *Journal of Atmospheric and Oceanic Technology*, 4, pp. 139-150, 1987.

60 Jones, D. M. A., 'The shape of raindrops', *Journal of Meteorology*, 16, pp. 504-510, 1959.

61 Joss, J. and A. Waldvogel, 'Precipitation measurement and hydrology', *Radar in Meteorology*, D. Atlas (Ed.), AMS, pp. 577-606, 1990.

62 Joss, J., and A. Waldvogel, 'A spectrograph for the automatic analysis of raindrops', *Pure and Applied Geophysics*, 68, pp. 240-246, 1967.

63 Joss, J., and A. Waldvogel, 'Raindrop·Size Distribution and Sampling Size Errors', *Journal of the Atmospheric Sciences*, 26, pp. 566-569, 1969.

64 Joss, Jürg, and Enrico G. Gori, 'Shapes of Raindrop Size Distributions', *Journal of Applied Meteorology*, 17, pp. 1054-1061, 1978.

65 Kitchen, M and P.M. Jackson, 'Weather Radar Performance at Long Range–Simulated and Observed', *J. Appl. Meteor,* **32**, pp. 975-985, 1993.

66 Knisel, W.G, *GLEAMS II, '* Groundwater Loading Effects from Agricultural Management Systems, User Manual', Washington, D.C.: U.S. Department of Agriculture, Agricultural Research Service, 1993.

67 Knollenberg, R. G., 'The optical array: An alternative to scattering or extinction for airborne particle size distribution', *Journal of Applied Meteorology*, 9, pp. 86-103, 1970.

68 Knollenberg, R. G., 'Three new instruments for cloud physics measurement: The 2-D spectrometer, the forward scattering spectrometer probe and the active scattering aerosol spectrometer', Preprints, *International Conference on Cloud Physics*, Boulder, American Meteorological Society, pp. 544-561, 1976.

69 Koistinen, J., R. King, E. Saltikoff, A. Harju, 'Monitoring and assessment of systematic measurement errors in the NORDRAD network', *Proceedings. of the 29th Intern. Conf. on Radar Meteorology, Amer. Met. Soc.*, Boston, pp. 765-768, 1999.

70 Komabayasi, M., Gonda, T., and Isono, K., 'Life times of water drops before breaking and size distribution of fragment droplets', *Journal of the Meteorological Society of Japan*, 42, pp. 330-340, 1964.

71 Koschmieder, H., 'Methods and results of definite rain measurements', *Mon. Wea. Rev.*, 62, pp. 5–7, 1934.

72 La Barbera, P., Lanza, L. G. and Stagi, L. 'Tipping bucket mechanical errors and their influence on rainfall statistics and extremes', *Wat. Sci. Tech.*, 45, (2), pp. 1-9, 2002.

73 Laville F, and Grayson D. A and Matthew J. M, 'Underwater sound generation by rainfall', *J. Acoust. Soc. Am,* 89, (2), pp. 715- 721, 1991.

74 Laws, J. O., and D. A. Parsons, 'The relation of raindrop-size to intensity', *Transactions, American Geophysical Union,* 24, part II, pp. 452-460, 1943.

75 Laws, J.O, 'Measurements of the fall-velocity of water drops and raindrops', *Trans. Am. Geophys. Union,* 22, pp. 709-721, 1941

76 Laws, J.O, Parson, D.A, 'Relation of raindrop size to intensity', *Trans. Am. Geophys. Union* 24, pp. 452-459, 1943.

77 Legates and T.L. deLiberty, 'Precipitation measurement biases in United States', *Water Resour. Bull*, 29, pp. 855-861, 1993.

78 Liebe H.J, 'Modeling attenuation and phase of radio waves in air at frequencies below 1000 GHz', *Radio Sci.* Vol. 16, pp. pp. 1183-1199, 1981.

79 Liebe H.J., G.A. Hufford, and M.G. Cotton, 'Propagation Modeling of Moist Air and Suspended Water/Ice Particles at Frequencies Below 1000 GHz', *AGARD Conference Proc. 542, Atmospheric Propagation Effects through Natural and Man-Made Obscurants for Visible to MM-Wave Radiation,* pp.3.1-3.10, 1993.

80 Lilly D. K, "Cirrus outflow dynamics", *J. Atmos. Sci.*, 45, pp 1594–1605, 1988.

81 List, R., N. R. Donaldson, and R. E. Stewart, 'Temporal evolution of drop spectra to collisional equilibrium in steady and pulsating rain', *Journal of the Atmospheric Sciences*, 44, pp. 362-372, 1987.

82 Locatelli, J.D., and P.V. Hobbs, 'Fall speeds and masses of solid precipitation particles', *J. Geophys. Res.*, 79, pp. 2185-2197, 1974.

83 Longuet M.S, Higgins, 'An analytical model of sound production by raindrops', *J. Fluid Mech.* 214, pp. 395-410, 1990.

84 Low, T., and R. List, 'Collision coalescence and break-up of raindrops with size', *Journal of the Atmospheric Sciences*, 39, pp. 1591-1618, 1982:

85 Lowe, E. J., 'Rain drops', *Quarterly Journal of the Royal Meteorological Society*, 18, pp. 242-245, 1892.

86 Mallock A. , Proc. R. Soc. London, Ser. A.95, pp. 138-143, (1919)

87 Marsalek, J., 'Calibration of the tipping bucket rain gauge', *J. Hydrology*, 53, pp. 343-354, 1981.

88 Marshall J.S, Hitschfiled W., Gunn K.L.S, 'Advances in RADAR weather', *Advances I Geophysics* 2, pp. 1-56, 1955.

89 Marshall, J. S., and W. M. Palmer, 'The distribution of raindrops with size', *Journal of Meteorology*, 5, pp. 165-166, 1948.

90 Marshall, J. S., R. C. Langille, and W. McK. Palmer, 'Measurement of rainfall by radar', *Journal of Meteorology*, 4, pp. 186-192, 1947.

91 Mark New, Martin Todd, Mike Hulmec and Phil Jones, 'Precipitation Measurements And Trends In The Twentieth Century, *Int. J. Climatol.* **21**: pp. 1899–1922, 2001.

92 Matrosov, S.Y., R.A. Kropfli, K. A. Clark, and W. Campbell, 'Multi-parameter Polarimetric estimators of rainfall rate at X-band. Preprints', *30th Int. Conf. on Radar Meteorology*, pp. 609 – 611, 2001.

93 Matrosov, S.Y., R.A. Kropfli, R.F. Reinking, and B.E. Martner, 'Prospects for measuring rainfall using propagation differential phase in X- and Ka radar bands', *J. Appl. Meteor.*, 38, 7, pp. 66 – 776, 1999.

94 May K.R., 'The Cascade Impactor: an instrument for sampling coarse aerosols', *J. Sci. Instr.*, 22(10), pp. 187-195, 1945.

95 May, P.T, T.D. Keenan, D.S. Zrnic, L.D. Carey, and S.A. Rutledge, 'Polarimetric radar measurements of tropical rain at a 5-cm wavelength', *J. Appl. Meteor.*, 38, pp. 750 – 765, 1999.

96 McCool, D.K., G.R. Foster, C.K. Mutchler, and L.D. Meyer, 'Revised slope length factor for the Universal Soil Loss Equation', *Transactions of the American Society of Agricultural Engineers* 32, pp.1571- 1576, 1989.

97 McCool, D.K., L.C. Brown, G.R. Foster, C.K. Mutchler, and L.D. Meyer, 'Revised slope steepness factor for the Universal Soil Loss Equation', *Transactions of the American Society of Agricultural Engineers* 32, pp.1378-1396, 1987.

98 McCool, D.K., 'Personal Communication', USDA-ARS, Agricultural Engineering Department, Washington State Univ., Pullman, 1982.

99 McFarquhar, Greg, and Roland List, 'The Effect of Curve Fits for the Disdrometer Calibration on Raindrop Spectra, Rainfall Rate, and Radar Reflectivity', *Journal of Applied Meteorology*, 32, pp. 774-782, 1993.

100 Medwin, H., Nystuen J.A., Peter W. Jacobusd, Leo H Ostwald and David E. Synder, 'The anatomy of underwater noise', J. *Acoust. Soc. Am,* 92 (3), pp. 1613-1624, 1992.

101 Medwin, H., Kurgan A. & Nystuen J.A., 'Impact and bubble sounds from raindrops at normal and oblique incidence', *J. Acoust. Soc. Am.*, vol. 88, pp. 413-418, 1990.

102 Microchip Data sheet, MCP41XXX/42XXX Single/Dual Digital Potentiometer with SPI™ Interface, Microchip 11195c.pdf,

103 Microchip data sheet, Single/Dual Digital Potentiometer with SPI™ Interface, 21733d.pdf

104 Minnaert M., 'On musical air bubbles and the sounds of running water', *Philos. Mag.* 16, pp. 235–248, 1933.

105 Mokhothu, N.M., 'Field and Catchment Water and Soil Monitoring', *MEMP Internal*, 1994.

106 Molini, A., La Barbera, P., Lanza, L.G. and L. Stagi 'Rainfall intermittency and the sampling error of tipping-bucket rain gauges', *Phys. Chem. Earth*, 26(10-12), pp. 737-742, 2001.

107 Monahan, E.C., & I.G. O'Muircheartaigh, 'Whitecaps and the passive remote sensing of the ocean surface', *International Journal of Remote Sensing,* 7, pp. 627-642, 1986.

108 Moran R.P.C, Quinton, J.N, Smith R.E, Govers G, Poesen J.W.A, Aurswald K, Chisci G, Torri D, Styczen M.E, 'The European soil erosion model (EUROSEM): a dynamic approach for predicting sediment transport from fields and small catchments', *Earth Surf. Process. Landforms*, 23, pp. 527-544, 1998

109 Moran R.P.C, Quinton, J.N, Smith R.E, Govers G, Poesen J.W.A, Aurswald K, Chisci G, Torri D, Styczen M.E, Folly A.J.V., 'The European soil erosion model (EUROSEM): documentation and user guide', *Cranfield University*, 1998.

110 Neuberger, Hans, 'Notes on Measurement of Rain-Drop Sizes', *Bulletin of the American Meteorological Society*, 23, pp. 274-276, 1942.

111 Niemczynowicz, J., 'The dynamic calibration of tipping-bucket rain gauges', *Nord. Hydrol.*, 17, pp. 203-214, 1986.

112 Nystuen J. A, Leo H. Ostwald Jr. Herman Medwin, 'The acoustics of raindrop impact', J. Acoust. Soc. Am. 92, pp. 1017-1021, 1992.

113 Nystuen J.A., 'The underwater sound generated by heavy rainfall', *J. Acoust. Soc. Am.*, vol. 93, pp. 3169-3177, 1993.

114 Nystuen, J.A, C.C. Mc. Glothin and M.S. Cook, 'The underwater sound generated by heavy precipitation', *J. Acoust. Soc. Am.* 93, pp. 3169-3177, 1993.

115 Nystuen, PG Black and J.C Wilkerson, 'A comparison of automatic rain gauges', *J. Atmospheric. Oceanic. Technol.* 13, pp. 62-73, 1996.

116 Nystuen, 'Acoustical rainfall analysis: rainfall drop size distribution using the underwater sound field', *J. Atmos. Oceanic Technol.*, 16, pp. 74-84, 1996.

117 Nystuen J.A and H.D. Selsor, Weather classification using passive acoustic drifters, *J. Atmos. Oceanic Technol.*, vol. 14, pp. 656-666, 1997

118 Nystuen J. A, 'Relative performances of automatic rain gauges under different rainfall conditions', American meteorological society, pp. 1025-1043, 1999.

119 Nystuen, J.A. and Selsor, H.D., 'Weather classification using passive acoustic drifters', J. *Atmos. Oceanic Technol.*, 14, pp. 656-666, 1997.

120 Oguz. H.N. and A. Prosperetti, 'Bubble entrainment by the impact of drops on liquid surface', *J. Fluid Mech.* 218, pp. 143-162, 1990.

121 Pimentel et al, 'Environmental and economic costs of soil erosion and conservation benefits', *Science* 267, 1211-1237, 1995

122 Ponce, V.M. and R.H. Hawkins, 'Runoff Curve Number: Has It Reached Maturity?', *Journal of Hydrologic Engineering*, 1, 1, 1996.

123 Pruppacher, H. R. and K. V. Beard, 'A wind tunnel investigation of the internal circulations and shape of water drops falling at terminal velocity in air". *Quart. J. Roy. Meteor. Soc.*, **96**, pp. 247-256, 1970.

124 Pruppacher H. and J. Klett, 'Microphysics of clouds and precipitation', Dordrecht (NL): Reidel Publishing Company, 1978.

125 Pruppacher, Hans R., and James D. Klett, 'Microphysics of Clouds and Precipitation', II rev. and enl. ed. *Atmospheric and Oceanographic Sciences Library*, Kluwer Academic Publishers, Dordrecht, 1997.

126 Pumphery. H.C., L.A Crum, and L. Bjorno, 'Underwater sound produced individual drop impacts and rainfall', *J. Acoust. Soc. Am,* 85, pp. 1518-1526. 1989.

127 Pumphery. H.C., 'Underwater noise, : the initial impact component', *Proceedings of Institute of acoustic*, Weymouth, England, 1991.

128 Putorti, A.D., Belsinger, T.D., and Twilley, W.H., 'Determination of Water Spray Drop Size and Speed from a Standard Orifice Pendent Spray Sprinkler', NISTFR 4003, 6561, *National Institute of Standards and Technology*, Gaithersburg, MD, May 1999.

129 Quartly, G.D., K.M. Shannon, T.H. Guymer, K.G. Birch & J.M. Campbell, 'Intercomparison of ambient acoustic spectra in inland and coastal waters', *Acta Acustica United with Acustica'* vol. 88, pp. 811-813, 2002.

130 Quartly, G.D., T.H. Guymer and M.A. Srokosz, 'Measuring rainfall at sea; Part 2 — Spaceborne sensors'', *Weather*, vol. 57, pp. 363-366, 2002.

131 Remko Uijlenhoet, Matthias Steiner, And James A. Smith, 'Variability of Raindrop Size Distributions in a Squall Line and Implications for Radar Rainfall Estimation', *Journal Of Hydro Meteorology*, Vol (4), Jan 2003, pp. 43-61, 2003.

132 Renard, K.G. (ed.), 'Predicting Soil Erosion by Water - A Guide to Conservation Planning with the Revised Universal Soil Loss Equation (RUSLE). Washington, D.C', *U.S. Department of Agriculture*, Agricultural Research Service, 354 pp, 1992.

133 Report. Mutchler, C.K., C.E. Murphree, and K.C. McGregor, 'Subfactor method for computing C-factor for continuous cotton', *Transactions of the American Society of Agricultural Engineers* 25, pp.327-332, 1982.

134 Richardson E.G., Proc, Phy. Soc, (London), 68, 541,1955.

135 Rogers, R. R., 'Doppler radar investigation of Hawaiian rain', *Tellus*, 19, pp. 432-455, 1967.

136 Rogers R. R., and M. K. Yau, 'A Short Course in Cloud Physics', III ed. *International Series in Natural Philosophy*, Pergamon Press, Oxford, U.K. 293 pp, 1991.

137 Rosenkranz, P. W, 'Water vapor microwave continuum absorption, 'A comparison of measurements and models', *Radio Science*, 33, pp. 919-928, 1998. Correction, Radio Science, 34, p. 1025.

138 Rosewell C.J., Rainfall kinetic energy in Easter Australia, *Journal of Climate and applied Metrology* 25, pp. 1695-1701, 1986.

139 Sallas C., S, Sempere-Torresm D, Creutin, J.D, 'Characterisation of raindrop size distribution in Mediterranean climate: analysis of the variations of the Z-R relationship', *Proceedings of the29th Conference on Radar Meteorology*, AMS, Montreal, Canada, pp. 671-673, 1999.

140 Sallas C, Poesen J, Sempere-Torres D, "Kinetic energy of rain and it's functional relationship with intensity", *J. Hydrology*, 257, pp. 257-269 2002

141 Sanchez-Diezma, R., I. Zawadzki and D. Sempere-Torres, 'Identification of the bright band through the analysis of volumetric radar data', *J. Geophys. Res.-Atmos.*, **105**, pp. 2225-2236, 2000.

142 Sauvageot H., 'Radar Meteorology', Artech House, Boston, MA, 1992.

143 Sauvageot, Henri and Jean-Pierre Lacaux, 'The Shape of Averaged Drop Size Distributions' *Journal of the Atmospheric Sciences*, 52, pp. 1070-1083, 1995.

144 Schönhuber. M, H.E. Urban, J.P.V. Poiares Baptista, W.L. Randeu and W. Riedler, 'Measurements of Precipitation Characteristics by a New Distrometer, Proceedings of *Atmospheric Physics and Dynamics in the Analysis and Prognosis of Precipitation Fields*, Rome, Italy, November 15 - 18, 1994

145 Schuur, T.J, A.V. Ryzhkov, and D.S. Zrnic, 'A statistical analysis of 2D-video-disdrometer data: impact on polarimetric rainfall estimation', Preprints, *30th Int. Conf. on Radar Meteorology*, pp. 646 – 648, 2001.

146 Scrimger, J. et al. 'Underwater noise due to rain, hail and snow', *J. Acoust. Soc. Am.*, **81**, pp. 79-86, 1987

147 Sempere-Torres, Daniel, Josep M. Porrà, and Jean-Dominique Creutin, 'A General Formulation for Raindrop Size Distribution', *Journal of Applied Meteorology*, 33, pp. 1494-1502, 1994.

148 Serra, Y. L., P. A'Hearn, H. P. Freitag, , and M. J. McPhaden, 'ATLAS self-siphoning rain gauge error estimates', *J. Atmos. Ocean. Tech.*, 18, pp. 1989–2002, 2001.

149 Sevruk, B. 'Reliability of precipitation measurement', ***Instruments and Observing Methods***. Proc. Int. Workshop on Precipitation Measurements. WMO Rep. No 48, p. pp. 13-19, 1989.

150 Shannon K.M., Quartly G.D., Birch K.G., Campbell J.M., Guymer T.H., Jones C.E., 'Gauging the Rain - Comparing Measurements of Rain at Sea', Challenger Centenary Conference, 2002.

151 Sheppard, Brian, 'Effect of Irregularities in the Diameter Classification of Raindrops by the Joss-Waldvogel Disdrometer', *Journal of Atmospheric and Oceanic Technology*, 7, pp. 180-183, 1990a.

152 Sheppard, Brian, 'Measurement of Raindrop Size Distributions Using a Small Doppler Radar', *Journal of Atmospheric and Oceanic Technology*, 7, pp. 255-268, 1990b.

153 Smith, J.A, De Veaux, R.D, 'The temporal and spatial variability of rainfall power', *Envirometrics*, 3 (1), 29-53, 1992.

154 Smith, J.A. and W.F. Krajewski, 'A modeling study of rainfall rate – reflectivity relationships', *Water Resour. Res.*, **29**, pp. 2505-2514, 1993.

155 Spiel D. E., 'On the births of jet drops from bubbles bursting on water surfaces', *J. Geophys. Res.*, 100(C3): pp. 4995–5006, 1995.

156 Steiner, M., Smith, J.A. and R. Uijlenhoet, 'A microphysical interpretation of radar reflectivity – rain rate relationships', J. *Atmos. Sci.*, **61**, pp. 1114-1131, 2004.

157 Telford, J. W., 'A new aspect of coalescence theory', *Journal of Meteorology*, 12, pp. 436-444. 1955.

158 Testud, J, E. Le Bouar, E. Obligis, and M. Ali-Mehenni, The rain profiling algorithm applied to polarimetric weather radar, *J. Atmos. Oceanic Technol.*, 17, pp. 332 – 356, 2000.

159 Thomas B. Greenslade, Jr., 'Experiments with Helmholtz Resonators', *Phys. Teach.*, 34, pp. 228-230, 1996.

160 Tuck C.R., Butler Ellis M.C., and Miller P.C.H., 'Techniques for the measurement of droplet size and velocity distributions in agriculture sprays', *Crop Protection*. Vol. 16 No. 7, pp 619-628, 1997.

161 U.S. Soil and Conservation Service, 'National Engineering Handbook', *Section 4: Hydrolog'*, Washington, D.C.: U.S. Department of Agriculture, 1985.

162 Uijlehoet, R, and Stricker J.N.M, 'A consistent rainfall parameterisation based on the exponential raindrop distribution', *J. Hydrol.*, 218, pp. 101-127, 1999.

163 Ulbrich, Carlton W., 'Natural Variations in the Analytical Form of the Raindrop Size Distribution', *Journal of Climate and Applied Meteorology*, 22, 1764-1775, 1983.

164 Vagle S., W.G. Large and D.M. Farmer, 'An evaluation of the WOTAN technique for inferring oceanic winds from underwater sound', *J. Atmos. Oceanic Technol.*, vol. 7, pp. pp. 576-595, 1990.

165 Valdez, M. P., and K. C. Young, 'Number fluxes in equilibrium raindrop population: A Markov chain analysis', *Journal of the Atmospheric Sciences*, 42, 1024-1036, 1985.

166 Van Dijk A.I.D.J.M., Bruijnzeel L.A, Rosewell C.J., 'Rainfall intensity-kinetic energy relationship: A critical literature appraisal', *Journal of Hydrology*, 261, pp. 1-23, 2002.

167 Van Dijk, A. I. J. M, L. A. Bruijnzeel and E. H. Eisma, 'A methodology to study rain splash and wash processes under natural rainfall', *Hydrol. Process.* 17, pp. 153–167, 2003

168 Waldvogel rainfall disdrometer in a 'rain of a thundery type, *Journal of Applied meteorology*, 19, pp. 593-597.

169 Waldvogel, A., 'The N0 Jump of Raindrop Spectra', *Journal of the Atmospheric Sciences*, 31, pp. 1067-1978, 1974.

170 Widmann, J.F., 'Characterization of a Residential Fire Sprinkler Using Phase Doppler Interferometry', NISTIR 6561, *National Institute of Standards and Technology*, Gaithersburg, MD, August 2000.

171 Wiesner, J., 'Beiträge zur Kenntnis des tropischen Regens, (Contributions to the knowledge of the tropical rain', *Sitz. Ber.Math. Nat. Akad. Wiss. Kl. Wien*, 104, pp. 1397-1434, 1895.

172 Wischemeier W.H., Smith D.D, 'Rainfall energy and it's relationship to soil loss', *Trans. AGU.* 39, pp. 285-291, 1958.

173 Worthington A.M., Philos. Trans. R. Soc. London, A189, pp. 137-148 (1897)

174 Yang, D., B. E. Goddison, J. R. Metcalfe, V. S. Golubev, R. Bates, and T. Pangburn, 'Accuracy of NWS 8" standard nonrecording precipitation gauge: Results and application of WMO intercomparison', *J. Atmos. Ocean. Tech.*, 15, pp. 54–68, 1998.

175 Yolande L. Serra And Patrick A'hearn, Atlas, 'Self-Siphoning Rain Gauge Error Estimates', *J. Atmos. Ocean. Tech.*, 18, pp 1989-2002, 1990.

176 Young, K. C., 'The evolution of drop spectra due to condensation, coalescence and break-up', *Journal of the Atmospheric Sciences*, 32, pp. 965-973, 1975.

177 Yuter, S. E., and R. A. Houze Jr., 'Three-dimensional kinematic and microphysical evolution of Florida cumulonimbus. Part I:Spatial distribution of updrafts, downdrafts, and precipitation', *Mon. Wea. Rev.*, 123, pp. 1921–1940, 1995a.

178 Yuter, S. E., and R. A. Houze Jr., 'Three-dimensional kinematic and microphysical evolution of Florida cumulonimbus. Part II: Frequency distribution of vertical velocity, reflectivity, and differential reflectivity. *Mon. Wea. Rev.*, 123, pp. 1941–1963, 1995b

179 Yuter, S. E., and R. A. Houze Jr, 'Three-dimensional kinematic and microphysical evolution of Florida cumulonimbus. Part III: Vertical mass transport, mass divergence, and synthesis', *Mon. Wea. Rev.*, **123**, pp. 1964–1983. 1995c

180 Zawadzki, I., and M. de Agostinho Antonio, 'Equilibrium Raindrop Size Distributions in Tropical Rain', *Journal of the Atmospheric Sciences*, 22, pp. 3452-3459, 1988.

181 Zawadzki, I., E. Monteiro, and F. Fabry, 'The development of drop size distributions in light rain', *Journal of the Atmospheric Sciences*, 51, pp. 1100-1113, 1994.

182 Zawadzki, I., F. Fabry, R. de Elia, A. Caya and P. Vaillancourt, 'On Quantitative Interpretation of Radar Measurements', *Proceedings. of the 29th Intern. Conf. on Radar Meteorology, Amer. Met. Soc.*, Boston, pp. 784–786, 1999.

183 Zrnic, D.S., and A.V. Ryzhkov, 'Polarimetry for weather surveillance radars', *Bull. Amer. Meteor. Soc.*, 80, pp 389 – 406, 1999.

List of Publications

1. **Mani. T. K** and P. R. Saseendran Pillai, "Measurement and Analysis of Rain Generated Acoustic Noise", *Proceedings of the National Symposium on Ocean Electronics*, p. 115-123, 2001.

2. **Mani. T. K** and P. R. Saseendran Pillai, "The Acoustics of Raindrop Impact on Water Surface", *Journal of Acoustic Society of India*, p. 214-217, 2002 (This paper received the Sir. C. V Raman award for the best paper).

3. **Mani. T. K**, P. R. Saseendran Pillai, James Kurian and M.H. Supriya, "Rain parameter estimation using impact generated low frequency acoustic signals", *J. Acoust. Soc. Am.*, 113(4), pt.2, p. 2278, 2003.

4. **Mani. T. K** and P. R. Saseendran Pillai, "Rain estimation using the energy generated during the drop Impact", *Proceedings of the National Symposium on Ocean Electronics*, p. 162-167, 2003.

5. Anil Kumar C.P., Sajith N Pai, Soniraj, P. R. S. Pillai, James Kurian, M.H. Supriya, C. Madhavan, **Mani T.K.**, "Studies on Geometrical Backscattering Models of Marine Bodies", *J. Acoust. Soc. Am.*, 113(4), pt.2, p. 2236, 2003.

6. **Mani. T. K** and P. R. Saseendran Pillai, "A novel technique for measuring the rainfall from its kinetic energy ", *J. Acoust. Soc. Am.*, 115(5), pt.2, p. 2618, 2004.

7. **Mani. T. K** and P. R. Saseendran Pillai, "Drop parameter estimation from underwater noise produced by raindrop impact", *Acoustic Research Letters On line, Acoust. Soc. Am.*, p. 118-123, June 2004.

Index